UNIVERSITAT
POLITÈCNICA
DE VALÈNCIA

Diseño y aplicaciones de nuevas estructuras difractivas aperiódicas

Memoria presentada por:
Vicente Ferrando Martín

Directores:
Juan Antonio Monsoriu Serra
Walter Daniel Furlan

Febrero, 2017

Dr. Juan Antonio Monsoriu Serra, Catedrático de Universidad del Departamento de Física Aplicada de la Universitat Politècnica de València y Dr. Walter Daniel Furlan, Catedrático de Universidad del Departamento de Óptica de la Universitat de València.

CERTIFICAN que la presente memoria ”Diseño y aplicaciones de estructuras difractivas aperiódicas” resume el trabajo de investigación realizado, bajo su dirección, por D. Vicente Ferrando Martín y constituye su Tesis para optar al título de Doctor.

Y para que conste, en cumplimiento de la legislación vigente, firman el presente certificado en Valencia a 7 de febrero de 2017

Fdo.: Dr. Juan Antonio Monsoriu Serra Fdo.: Dr. Walter D. Furlan

Dedicado a
mi familia

Agradecimientos

Son tantas las personas que me han apoyado de alguna forma que si tuviera que agradecer a todos aquellos que han contribuido a la creación de esta Tesis, este apartado seria tan extenso como el trabajo completo.

Quiero empezar agradeciendo a mis directores de Tesis, Juan A. Monsoriu y Walter D. Furlan, por su dedicación incondicional y su valiosa dirección y apoyo para seguir en este camino.

En segundo lugar, un agradecimiento especial a Enrique Silvestre por abrirme las puertas del emocionante mundo de la investigación. Gracias por tu paciencia.

Cuando empece a trabajar en el grupo de óptica difractiva (DiOG) no podía ni imaginarme lo que iba a encontrar. Tras varios años compartiendo *afición* con tanta gente de este campo, compañeros que han tomado otros caminos y otros que siguen como siempre, se crea un sentimiento especial. Si tuviera que definir la relación que nos une diría que somos una gran familia, una familia en continua expansión. Y entre esta gran familia debo hacer especial mención a ciertas personas que caminan o han caminado a mi lado paso a paso: Debo agradecer a Laura por su inestimable ayuda y mejor compañía, yo de mayor quiero ser como tu, a Arnau por que me enseñaste a arriesgar y afrontar nuevos retos, siempre empujando para ir mas allá, a Manu por esas largas explicaciones sobre ojos y estadística, sabes que en el fondo nos echas de menos, a Federico por compartir tantas horas día a día y hacer que no sean tan largas, a Clara por alegrarnos los días, se te hecha de menos

y, finalmente, a Pedro y Amparo porque siempre están ahí para ayudar en todo, sois un gran ejemplo a seguir.

Entrar en esta gran familia no hubiera sido posible sin dar los pasos previos, y que mejor forma de llegar hasta aquí que ir acompañado de la mejor gente allá donde estés.

Desde mis estudios de Física me ha acompañado gente espectacular que me han aportado muchísimo a nivel académico y, lo que es más importante, a nivel personal. Atrás quedan los ratos libres en la cafetería, en el césped o donde nos pille, discutiendo las probabilidades de ser un cuervo o generando calamares infinitos, las interminables clases a primera hora, los estresantes periodos de exámenes confinados en la biblioteca y las risas ante un reconfortante café, pero siempre nos quedarán las cenas de navidad y una amistad que va mucho mas allá del espacio y el tiempo. Gracias por ser tan grandes.

No puedo olvidarme de los amigos que me ha visto crecer, porque junto a ellos aprendí a ser quien soy. En particular, quiero dar las gracias a Pablo, Héctor y Germán por su paciencia y por estar ahí cuando se les necesita.

Por último y más importante quiero dar las gracias a mi familia, porque a ellos les debo valores tan importantes como la capacidad de estudio y el espíritu de superación. Quiero agradecer a mis padres por apoyarme en cada paso que doy y levantarme cuando me caigo, gracias por enseñarme a andar solo. A mi hermano Abel porque, aunque tenemos nuestras diferencias, es un gran pilar en mi vida. A mis abuelos por ser el mejor ejemplo que se puede tener. A mis tíos por todo el apoyo y los consejos que me han llevado hasta aquí. Y un agradecimiento muy especial a M^{a} Carmen por ser la mejor compañera, amiga, consejera y mi complemento hacia la felicidad. Esta tesis ha de ir dedicada a todos vosotros porque nadie la puede apreciar más. Esta tesis es vuestra.

Resumen

Los elementos ópticos difractivos han ganado importancia en las últimas décadas debido al avance de la tecnología que permite su construcción y al aumento de la potencia de cálculo computacional que permite predecir, con un coste mínimo, su comportamiento en función de los múltiples parámetros que definen su estructura. La periodicidad constituye un factor clave a la hora de entender su funcionamiento y estudiar las propiedades y aplicabilidad de los diferentes tipos de elementos difractivos. Ahora bien, esta periodicidad también introduce ciertas limitaciones en el diseño de los elementos y en sus propiedades, como por ejemplo una alta aberración cromática al ser utilizados como elementos formadores de imagen. Para superar estas limitaciones se propuso la aplicación de secuencias aperiódicas deterministas al diseño de los elementos ópticos difractivos. En este trabajo de Tesis se han estudiado diferentes secuencias aperiódicas y sus efectos en el diseño de nuevas estructuras difractivas. En particular, se ha utilizado la secuencia fractal de Cantor, la serie de Fibonacci y la serie de Thue–Morse en el diseño de dispositivos difractivos con diferentes finalidades.

A lo largo del desarrollo del trabajo de Tesis se han generado nuevos elementos difractivos que superan ciertas limitaciones, abriendo nuevos campos de aplicación a tecnologías preexistentes. Entre ellos, podemos destacar los sistemas de alineación óptica, la generación de vórtices ópticos, la reducción de la aberración cromática y el aumento de la profundidad de foco en elementos formadores de imagen.

Resum

Els elements òptics difractius han guanyat importancia les últimes dècades degut a l'avanç de la tecnología que permet la seua construcció y a l'augment de la potència de càlcul computacional que permet predir, amb un cost mínim, el seu comportament en funció dels diferents parámetres que defineixen la seua estructura. La periodicitat constitueix un factor clau a l'hora d'entendre el seu funcionament y estudiar les propietats y aplicabilitat dels diferents tipus d'elements difractius. Ara be, aquesta periodicitat tambe introdueix certes llimitacions en el disseny dels elements y les seus propietats, com per exemple una elevada aberració cromàtica quan actuen com a elements formadors d'imatges. Per superar aquestes llimitacions es va proposar l'aplicació de diferents sequencies aperiòdiques deterministes al disseny dels elements òptics difractius. En aquest treball de Tesi estudie diferents sequencies aperiòdiques y els seus efectes en el disseny de noves estructures difractives. En particular, s'han utilitzat la secuencia fractal de Cantor, la serie de Fibonacci y la serie de Thue–Morse en el disseny de dispositius difractius amb diferents finalitats.

Al llarg del desenvolupament del treball de Tesi s'han generat nous elements difractius que superen certes llimitacions, obint nous camps d'aplicació a tecnologies preexistents. Entre ells, podem destacar els sistemes d'alineació òptica, la generació de vòrtex òptics, la reducció de l'aberració cromàtica y l'augment de la profunditat de fòcus d'elements formadors d'imatges.

Abstract

The diffractive optical elements have enhanced his importance in the last decades due to the improvement of the technology which allows its construction and the greater computing power that helps predicting the behaviour of the diffractive structures in function of the design parameters without en extra cost. The periodic symmetry become a key factor in order to understand the performance of these elements, and it allows to study the properties and the applicability of the different diffractive elements. However, this periodicity also introduces certain limitation in the design of the elements and their properties, such as high chromatic aberration when they are used as image forming elements. To overcome this limitations it was proposed the use of deterministic aperiodic sequences in the design of the diffractive optical elements. In this Thesis work I study different aperiodic sequences and their effect in the design of new diffractive structures. In particular, we use the Cantor fractal set, the Fibonacci sequence and the Thue–Morse series in the design of devices with different purposes.

Along the development of the Thesis there have been generated new diffractive elements which overcome some limitations, opening new field for the application of pre-existing technologies. Between them, they can be highlighted the optical alignment systems, the generation of optical vortex, the reduction of the chromatic aberration and the enhancement of the focal depth in image forming elements.

Índice general

Agradecimientos VII
Resumen IX

1 Introducción general **1**
1.1 Antecedentes y objetivos de la investigación 1
1.2 Estructura de la Tesis 8

2 Publicaciones **13**
2.1 Fractal square zone plates 15
2.2 Cantor dust zone plates 27
2.3 Twin axial vortices generated by Fibonacci lenses . . . 41
2.4 Imaging properties of kinoform Fibonacci lenses . . . 55
2.5 3D printed diffractive terahertz lenses 67
2.6 Bifractal focusing and imaging properties of Thue–Morse Zone Plates 81

3 Discusión general de los resultados **97**

4 Conclusiones **101**
4.1 Cumplimiento de los objetivos 101
4.2 Aportaciones realizadas 103
4.3 Lineas de investigación futuras 103

Bibliografía general **105**

Capítulo 1

Introducción general

En este capítulo se revisa en primer lugar el estado del arte y los conceptos básicos sobre los que se fundamenta esta Tesis. A continuación se definen los objetivos que se persiguen. Finalmente, se expone la estructura general que sigue este trabajo de Tesis presentada en formato de compendio de publicaciones.

1.1 Antecedentes y objetivos de la investigación

En las últimas décadas, los Elementos Ópticos Difractivos (EODs) [Ojeda-Castañeda96] se han aplicado en áreas muy diversas que abarcan desde la microscopia con rayos X para la observación de nanoestructuras [Wang03, Sakdinawat07], hasta la formación de imágenes tomográficas con óptica de THz [Wang02, Siemion12]. Las Placas Zonales (PZs), en su forma más sencilla, son EODs formados por un conjunto de zonas anulares concéntricas transparentes y opacas alternadas de igual área. Esto implica que el radio de las diferentes zonas es proporcional a la raíz cuadrada de los números naturales. De esta forma, podemos escribir la transmitancia de estos elementos como una función

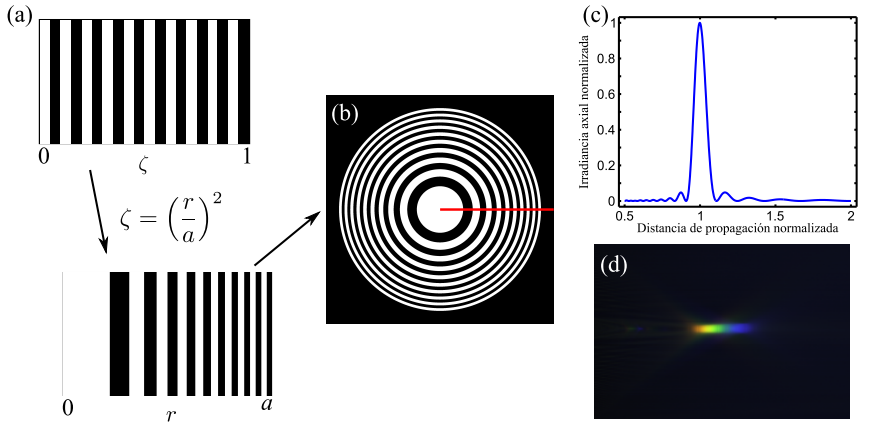

Figura 1.1: Diseño y caracterización de una PZ convencional: (a) Obtención de la función de transmitancia radial a partir de la una secuencia periódica, (b) transmitancia en la pupila de la PZ, (c) irradiancia axial normalizada bajo iluminación monocromática y (d) árbol de irradiancia bajo iluminación policromática en el que destaca la alta aberración cromática.

periódica $p(r^2)$, siendo r la variable radial (Fig. 1.1(a-b)). Si iluminamos una PZ de radio a y N zonas con una onda plana monocromática de longitud de onda λ esta produce una serie de focos situados a las distancias $f_n = \frac{a^2}{n\lambda N}$ de la PZ, donde $n \in \mathbb{Z}$. En la Fig. 1.1(c) se muestra la irradiancia axial normalizada alrededor del foco de orden $n = 1$. Debido a la dependencia de la distancia focal con la longitud de onda, las PZs convencionales presentan una alta aberración cromática (ver Fig. 1.1(d)).

Con el objetivo de modificar los perfiles de focalización de estos EODs se ha sustituido la secuencia periódica por distribuciones aperiódicas basadas en diferentes secuencias matemáticas deterministas. Para entender la naturaleza de estas distribuciones repasaremos los conceptos de orden periódico y aperiódico que aparecen originalmente en cristalografía [Maciá06].

Los cristales se definen como materiales cuyos átomos presentan

simetría de traslación 3D, esto es, están ordenados periódicamente. En cuanto a la simetría de rotación alrededor de cualquier átomo de la red, según el teorema de restricción cristalográfica [Bamberg03], esta solo puede ser de orden 2, 3, 4 y 6. Si estos materiales son iluminados con un haz de rayos X se observa que los cristales presentan un patrón de difracción discreto y periódico que depende fuertemente de los parámetros geométricos de la distribución. Por otra parte, en el otro extremo tenemos los materiales amorfos, cuya distribución de átomos es completamente aleatoria. Si iluminamos con un haz de rayos X un material amorfo no encontraremos picos de difracción, sino una distribución continua.

Entre ambos extremos podemos encontrar lo que se define como cuasicristales. Los átomos de estos materiales siguen distribuciones que no presentan simetría de traslación 3D de forma estricta, aunque su distribución pueden conservar otras simetrías como la auto-similitud (fractalidad) y simetrías de rotación. Es mas, la eliminación de la restricción periódica otorga la posibilidad de generar distribuciones con simetría de rotación prohibidas por el teorema de restricción cristalográfica. Bajo iluminación con un haz de rayos X estos materiales presentan patrones de difracción discretos, pero no periódicos.

En los años 80, Shechtman descubrió unas aleaciones metálicas de Al-Mn cuyo patrón de difracción discreto presenta simetrías de rotación de orden 5 y 10 [Shechtman84], lo que dio lugar a la revolución de los materiales cuasicristalinos y, por extensión, al estudio de las distribuciones aperiódicas que definen su estructura, así como un aumento de sus ámbitos de aplicación.

De entre estas estructuras cuasicristalinas existe un tipo, cuya distribución se replica a diferentes escalas, que tienen especial interés. A esta propiedad la llamamos auto-similitud y es la que define los fractales. Su característica principal es que se construyen por sustitución iterativa a diferentes escalas de una estructura básica, lo que matemáticamente les confiere dimensiones no enteras. La irregularidad de estas estructuras impide que estas puedan ser descritas en términos geomé-

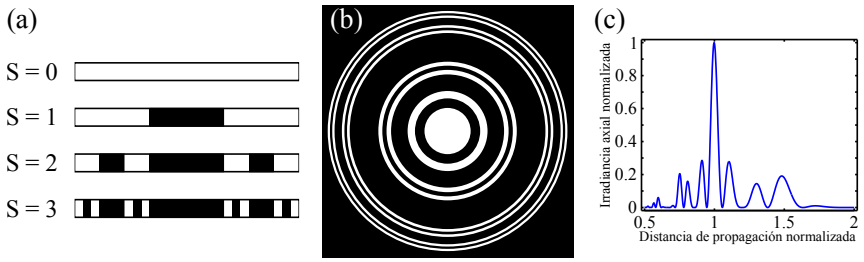

Figura 1.2: (a) Construcción geométrica del fractal triádico de Cantor hasta orden $S = 3$. (b) Transmitancia de la PZF de orden $S = 3$. (c) Irradiancia axial normalizada producida por una PZF bajo iluminación plana monocromática.

tricos tradicionales, pero utilizando la descripción matemática de este tipo de estructuras se pueden modelizar, de forma estadística, objetos tales como montañas, rayos, nubes, lineas de costa, etc...

Placas zonales fractales

A partir de las PZs convencionales y teniendo en cuenta las propiedades de estos elementos aperiódicos, se diseñó un nuevo tipo de estructura formadora de imágenes: las Placas Zonales Fractales (PZFs) [Saavedra03] cuya distribución de zonas se basa en el conjunto fractal de Cantor unidimensional (Fig. 1.2(a)). Se puede probar teórica y experimentalmente [Davis04] que, bajo iluminación plana monocromática, una PZF produce múltiples focos a lo largo del eje óptico. La estructura interna de cada foco muestra una estructura fractal característica que reproduce la auto-similitud de la PZF originaria (Fig. 1.2). El número de focos y su amplitud relativa puede ser modificada mediante los parámetros de diseño de la PZF [Monsoriu04, Hai-Tao05, Remón13b]. Se ha demostrado que esta propiedad puede ser utilizada en sistemas formadores de imagen con el objetivo de aumentar la profundidad de foco [Furlan07, Remón13a, Ge12].

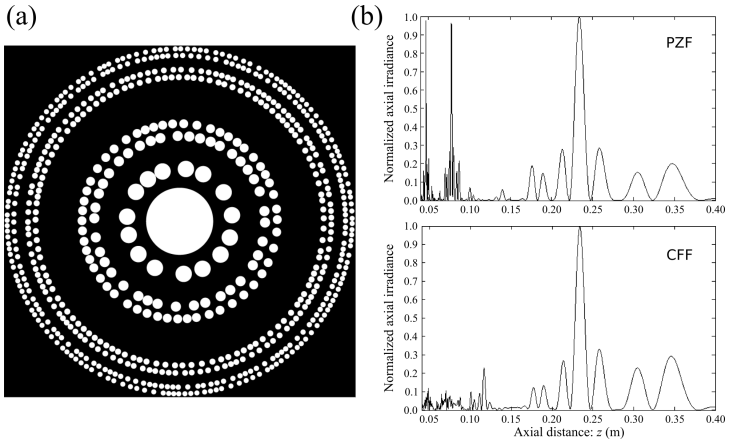

Figura 1.3: (a) CFF de orden $S = 3$. (b) Irradiancia axial normalizada proporcionada por una CFF de orden $S = 3$ y la PZF equivalente.

Criba de fotones

La Criba de Fotones (CF) [Kipp01] es un nuevo tipo de EOD desarrollado para focalizar y formar imágenes con rayos X blandos en aplicaciones de alta resolución. Una criba de fotones convencional consiste en una PZ de Fresnel en la que se han sustituido las zonas transparentes por un conjunto de agujeros no superpuestos de diferentes tamaños. A partir de la primera aparición de este elemento difractivo, han sido desarrollados numerosos trabajos, tanto teóricos como experimentales, estudiando sus propiedades desde distintos puntos de vista [Cao02, Cao03] y mostrando su utilidad en diferentes aplicaciones [Andersen05, Menon05]. A partir de este escenario, Giménez et al. presentaron una nueva modificación de este elemento basada en el conjunto fractal de Cantor: la Criba de Fotones Fractal (CFF) [Giménez06] (Fig. 1.3). Frente a las PZFs, la CFF mejoraba la eficiencia en difracción, apodizando los focos de orden superior.

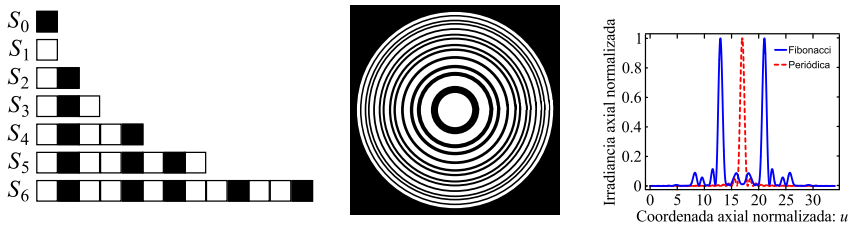

Figura 1.4: (a) Construcción geométrica de la secuencia de Fibonacci hasta orden S_6. (b) Distribución de fase de la lente de Fibonacci. (c) Irradiancia axial normalizada de la Lente de Fibonacci y su PZ periódica equivalente.

Placas zonales basadas en la secuencia de Fibonacci

La observación de la naturaleza ha permitido a los científicos percibir diferentes tipos de orden morfológico, siendo la secuencia de Fibonacci uno de los modelos matemáticos mas recurrentes. Es bien conocido que la razón entre dos números consecutivos de la serie de Fibonacci se aproxima asintóticamente a un número irracional conocido como número áureo. Este número ha sido asociado frecuentemente a conceptos subjetivos como el equilibrio o la armonía. La serie de Fibonacci y la razón áurea pueden encontrarse abundantemente en la naturaleza, desde la distribución helicoidal de las semillas de algunas plantas [Fleming02] hasta sistemas dinámicos que muestran un comportamiento caótico [Linage06]. La fotónica es un potencial campo de aplicación para nuevos dispositivos diseñados y construidos a partir de la secuencia de Fibonacci [Maciá12]. Uno de los recientes estudios consiste en el diseño y caracterización de la lente de Fibonacci [Monsoriu03], cuya irradiancia presenta un desdoblamiento del foco difractivo principal en dos focos cuyas distancias a la lente mantienen la razón áurea (Fig. 1.4).

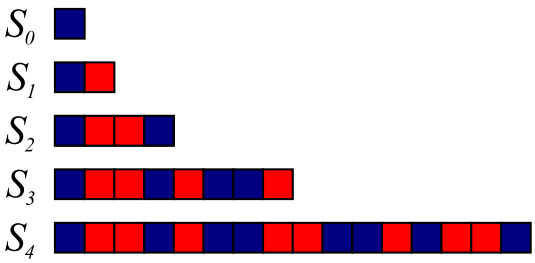

Figura 1.5: Construcción geométrica de la secuencia de Thue–Morse hasta orden S_4.

Serie de Thue–Morse

Otra de las secuencias aperiódicas que aplicamos en este trabajo de Tesis es la serie de Thue–Morse. La serie de Thue–Morse unidimensional se construye iterativamente concatenando en cada iteración el orden anterior con su complemento booleano. En la Fig. 1.5 se construye geométricamente la secuencia de Thue–Morse hasta orden S_4. Esta secuencia ha sido aplicada en múltiples ramas de la física como cristales fotónicos [Tsao14], pozos cuánticos [Hsueh14], metamateriales [Monsoriu07] y superredes de grafeno [Huang13].

Objetivos

Así pues, en esta Tesis Doctoral se propone el diseño y caracterización de diferentes estructuras diffracticas cuya distribución de amplitud y/o fase sigue patrones aperiódicos. En particular, estudiamos estructuras basadas en el conjunto fractal de Cantor, en la secuencia de Fibonacci y en la serie de Thue–Morse. Con estas premisas se identifican los siguientes objetivos para la investigación:

- Diseño y caracterización de un elemento óptico difractivo multifocal con geometría cuadrada que genere un patrón de referencia aplicable al alineamiento y calibración de sistemas ópticos tridimensionales.

- Diseño y caracterización de un elemento óptico difractivo que genere secuencias de vórtices a lo largo del eje óptico, susceptibles de ser utilizadas como trampas ópticas.
- Optimización de la eficiencia de difracción de una lente difractiva bifocal basada en la secuencia de Fibonacci mediante un diseño de tipo kinoform.
- Estudio de las propiedades multifocales de las estructuras difractivas basadas en la secuencia aperiódica de Thue-Morse.

1.2 Estructura de la Tesis

En primer lugar cabe destacar que se trata de una Tesis por compilación de artículos científicos. Cada uno de ellos puede ser leído autónomamente al tener los aspectos necesarios para su comprensión (marco teórico, objetivos, resultados y conclusiones), pero es importante recalcar que la unión de todos ellos constituye un solo trabajo con un claro hilo argumental. Así pues la Tesis se estructura en 4 capítulos:

1. Introducción general
2. Publicaciones
   - 2.1. Fractal square zone plates
   - 2.2. Cantor dust zone plates
   - 2.3. Twin axial vortices generated by Fibonacci lenses
   - 2.4. Imaging properties of kinoform Fibonacci lenses
   - 2.5. 3D printed diffractive terahertz lenses
   - 2.6. Bifocal focusing and imaging properties of Thue–Morse zone plates
3. Discusión general de los resultados

4. Conclusiones

En el **capítulo 1** de introducción se define el marco en el que se desarrolla la Tesis. Como hemos visto, en el primer apartado se muestra el estado del arte sobre placas zonales periódicas y aperiódicas. Se presentan las bases de la teoría escalar de la difracción y su aplicación en el estudio de los EODs que nos sirven como punto de partida para la elaboración de esta Tesis. Además, se exponen los objetivos perseguidos y seguidamente se detalla la estructura de la Tesis, el hilo argumental que siguen los artículos, así como su impacto en la consecución de los objetivos planteados.

El **capítulo 2**, que recoge seis artículos publicados en revistas científicas indexadas, forma el cuerpo principal de la Tesis. En los dos primeros artículos se presentan nuevos elementos difractivos de geometría cuadrada y basados en la serie fractal de Cantor. En el tercer y cuarto artículos se estudian las propiedades de generación de vórtices y formación de imágenes, respectivamente, de lentes basadas en la secuencia de Fibonacci. En el quinto artículo se presenta el diseño y caracterización de placas zonales fabricadas mediante impresión 3D y aplicadas a la focalización de ondas en el rango de THz. En el sexto artículo se aplica la serie de Thue–Morse al diseño de una placa zonal binaria de amplitud, cuyas propiedades policromáticas son interesantes en sistemas difractivos formadores de imágenes. Veamos con detalle las publicaciones de que consta esta Tesis:

El **primer artículo** se titula “Fractal square zone plates” [Calatayud13a]. Este artículo se publicó en la revista Optics Communications en 2013. En esta revista se recogen trabajos relacionados con la óptica, tanto teórica como experimental. El factor de impacto de esta revista en el año 2013 ha sido de 1.542, situándose en el segundo cuartil de la categoría *OPTICS* (34 de 83).

En este primer artículo presentamos un nuevo elemento difractivo que combina las PZF con PZ cuadradas, obteniendo lo que llamamos Placas Zonales Fractales Cuadradas (PZFC). Bajo iluminación plana

monocromática, estos elementos difractivos generan un conjunto de focos con forma de cruz que presentan una distribución axial autosimilar extendiendo considerablemente su profundidad de foco. Estas características otorgan a las PZFCs la posibilidad de integrarse en sistemas de alineamiento óptico tridimensional.

El **segundo artículo** que se presenta en esta Tesis se titula "Cantor dust zone plates" [Ferrando13a]. Este artículo fue publicado en la revista Optics Express en 2013. El factor de impacto en el año 2013 fue de 3.525, situándose en el primer decil de la categoría *OPTICS* (8 de 83).

En este trabajo se presenta un elemento difractivo basado en una estructura fractal bidimensional: una criba de fotones fractal con geometría cuadrada. El diseño de esta criba de fotones esta basado en el fractal de Cantor extendido a dos dimensiones, también conocido como polvo de Cantor. El dispositivo presentado genera, bajo la iluminación de un haz plano monocromático, un conjunto de focos con forma de cruz, que extienden la profundidad de foco, similares a los generados por la PZFC, pero con dos principales ventajas: En primer lugar, este elemento es mas fácil de fabricar, ya que puede construirse como una placa en la que se realizan perforaciones. Además, si analizamos la irradiancia vemos que en este tipo de estructura se apodizan los altos ordenes de difracción, consiguiendo así una mayor eficiencia.

El **tercer artículo** titulado "Twin axial vortices generated by Fibonacci lenses" [Calatayud13b] fue publicado, al igual que el segundo artículo, en Optics Express en el año 2013. Además, por las aportaciones de este trabajo al campo de las trampas ópticas, este artículo fue elegido posteriormente para ser publicado también en la revista Virtual Journal for Biomedical Optics (Volume 8, Issue 5, "Optical Traps, Manipulation, and Tracking").

En este trabajo se presenta un nuevo elemento difractivo que, combinando la bifocalidad de las lentes de Fibonacci y la capacidad para formar vórtices que tienen las máscaras con gradiente de fase azimutal, genera un par de vórtices sobre el eje óptico con interesantes aplicacio-

nes en el campo de las trampas ópticas.

El **cuarto artículo** fue publicado en IEEE Photonics Journal en 2014 con el titulo "Imaging properties of kinoform Fibonacci lenses" [Ferrando14b]. Esta revista tiene un factor de impacto para 2014 de 2.209, situándose en el segundo cuartil de la categoría *OPTICS* (22 de 87) y en el primer cuartil de la categoría *ENGINEERING, ELECTRICAL & ELECTRONIC* (49 de 249).

En este trabajo se presenta una nueva lente difractiva tipo kinoform basada en la secuencia de Fibonacci y se estudian sus propiedades de focalización y formación de imágenes. Con este nuevo diseño se obtiene una lente bifocal con una eficiencia mayor respecto a la PZ de Fibonacci binaria de fase.

El **quinto artículo** titulado "3D printed diffractive Terahertz lenses" [Furlan16] ha sido publicado en Optics Letters en el año 2016. Esta revista tiene un factor de impacto de 3.040 para el año 2015, situándose en el primer cuartil de la categoría *OPTICS* (15 de 90). Además, este artículo se encuentra entre los mas descargados de la revista en el mes de su publicación (abril de 2016).

En este trabajo se presentan las primeras lentes difractivas para el rango de los Terahercios fabricadas mediante técnicas de impresión 3D. Tras el estudio de las características ópticas para diferentes materiales disponibles, se han diseñado y construido PZs binarias de fase basadas en las secuencias fractal de Cantor y Fibonacci, además de las PZs periódicas equivalentes. Tambien se han comprobado experimentalmente sus propiedades de focalización bajo iluminación plana monocromática en el rango de los THz.

El **sexto artículo** titulado "Bifocal focusing and imaging properties of Thue–Morse zone plates" [Ferrando15d] ha sido publicado en Optics Express el año 2015. El factor de impacto de esta revista en 2015 fue de 3.148, situándose en el primer cuartil de la categoría *OPTICS* (14 de 90).

En este artículo se presenta el diseño y caracterización de una placa zonal de amplitud basada en la serie de Thue–Morse. Se analizan

sus propiedades ópticas bajo iluminación policromática, tanto teórica como experimentalmente. La transmitancia de esta placa zonal ha sido simulada en un montaje basado en una pantalla de cristal líquido y también construida mediante el proceso de fotolitografía. Tras los análisis concluimos que este elemento presenta bifocalidad con una alta profundidad de foco y una considerable reducción de la aberración cromática.

Tras la recopilación de artículos, el **capítulo 3** presenta una breve discusión acerca de los principales resultados obtenidos mientras que en el **capítulo 4** se presentan las conclusiones finales de la Tesis así como el cumplimiento de los objetivos planteados y las futuras lineas de trabajo.

Capítulo 2

Publicaciones

2.1 Fractal square zone plates

Optics Communications

Volume 286, 1 January 2013, Pages 42–45

Fractal square zone plates

A. Calatayud[a], V. Ferrando[a, b], F. Giménez[c], W.D. Furlan[b], G. Saavedra[b], J.A. Monsoriu[a],

[a] Centro de Tecnologías Físicas, Universitat Politècnica de València, E-46022 Valencia, Spain
[b] Departamento de Óptica, Universitat de València, E-46100 Burjasstot (Valencia), Spain
[c] I.U. Matemática Pura y Aplicada, Universitat Politècnica de València, E-46022 Valencia, Spain

Received 23 April 2012, Accepted 1 September 2012, Available online 21 September 2012

Show less

doi:10.1016/j.optcom.2012.09.002

Abstract

In this paper we present a novel family of zone plates with a fractal distribution of square zones. The focusing properties of these fractal diffractive lenses coined fractal square zone plates are analytically studied and the influence of the fractality is investigated. It is shown that under monochromatic illumination a fractal square zone plate gives rise a focal volume containing a delimited sequence of two-arms-cross pattern that are axially distributed according to the self-similarity of the lens.

Fractal square zone plates

Arnau Calatayud,[1] Vicente Ferrando,[1,2] Fernando Giménez,[3] Walter D. Furlan,[2] Genaro Saavedra,[2] and Juan A. Monsoriu[1,*]

[1]Centro de Tecnologías Físicas, Universitat Politècnica de València, 46022 Valencia, Spain.
[2]Departamento de Óptica, Universitat de València, 46100 Burjassot, Spain.
[3]I.U. Matemática Pura y Aplicada, Universitat Politècnica de València, 46022 Valencia, Spain.
*jmonsori@fis.upv.es

Optics Communications **286**, 42–45 (2013).

Abstract In this paper we present a novel family of zone plates with a fractal distribution of square zones. The focusing properties of these fractal diffractive lenses coined fractal square zone plates are analytically studied and the influence of the fractality is investigated. It is shown that under monochromatic illumination a fractal square zone plate gives rise a focal volume containing a delimited sequence of two-arms-cross pattern that are axially distributed according to the self-similarity of the lens.

Introduction

Diffractive optics has found a great number of new applications in the last few years, satisfying the increasing demand of more compact, light-weight, and cost-effective optical systems and components. With the rapid development of photonic technology, a wide range of applications arises also in areas where conventional refractive optics do not provide good solutions or where it is even impossible to use it, as for example, in some branches of Ophthalmology [Davison06], in THz Imaging [Wang02], and in X-ray Microscopy [Wang03]. Furthermore, with the availability of spatial light modulators technology, variable geometry of generated wavefronts becomes possible and DOEs can be recorded in real-time in recyclable recording media. This speeds up the development of new ideas in science and technology as cost-efficient

rapid prototyping of DOEs and also in real time applications. Following this trend, a few years ago, we presented fractal zone plates (FZPs) [Saavedra03] as new promising diffractive lenses with interesting focusing [Monsoriu04] and imaging properties [Furlan07]. A FZP is characterized by its fractal profile along the square of the radial coordinate. The main feature of a FZP arises from its ability to produce multiple foci distributed in a fractal way along the optical axis reproducing the self-similarity of the FZP itself.

Square zone plates (SZPs) [Janicijevic82, Alda09a] are another kind of promising diffractive optical elements which are the result of the combination of two linear Fresnel zone plates [Hart66]. Thus, its resulting structure presents alternate transparent and opaque square zones with side length $\sqrt{j}b$, where b is the side length of the first zone and j is the number of the zone. Under a monochromatic plane wave illumination this configuration produces a focalization pattern with a cross-like irradiance distribution. SZPs have exhibited applications in precision alignment systems [Herrmannsfeldt68], in infrared antennas [González04] and more recently have been combined with spiral phase masks for generating hollow beams [Zhang10].

In this work we introduce the concept of Fractal Square Zone Plates (FSZP), i.e. zone plates with a fractal distribution of square zones. Some practical considerations about the design of this type of SZP are investigated, taking into account the physical limits imposed by the different construction parameters. Finally, the influence on the axial and transverse irradiance produced by the fractality of these lenses is numerically evaluated and compared with the response of conventional SZPs.

FSZPs design

Our proposal for a FSZP is based on the triadic Cantor set shown in Fig. 2.1.1(a). The first step in the construction procedure consists in defining a straight-line segment of unit length called initiator (stage $S = 0$). Next, at stage $S = 1$, the generator of the set is constructed by dividing the segment in three equal parts of length $1/3$ and removing the central one. Following this procedure in subsequent stages $S = 1, 3, \ldots$ is easy to see that, in general, at stage S there are 2^S segments (each one of length 3^{-S}) separated by $2^S - 1$ gaps. In Fig. 2.1.1(a), only the four first stages are shown for clarity. Note that

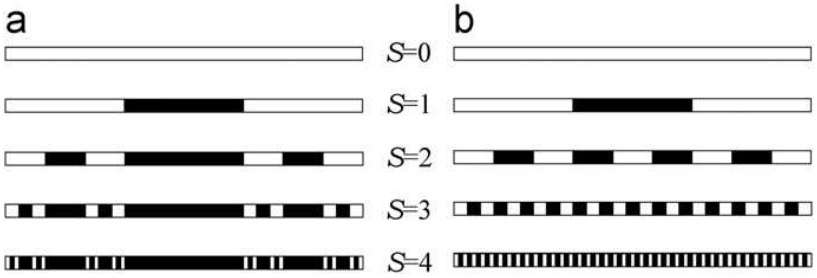

Figure 2.1.1: Comparison between (a) the triadic Cantor set and (b) the equivalent periodic structure generated at different stages S.

the S-th stage of the Cantor set can be interpreted as a quasiperiodic distribution of segments which can be obtained by removing some segments in the finite periodic distribution as shown in Fig. 2.1.1(b). This periodic distribution at stage S has $(3^S+1)/2$ segments with $(3^S-1)/2$ gaps being the total number of elements (segment + gaps) $N=3^S$.

It is interesting, for our purposes, to note that triadic Cantor set in Fig. 2.1.1(a) can also codified using an array of binary elements [Maciá12]. The generating array for $S=1$ is $\{101\}$, where "1" represent a white segment and "0" a black segment in Fig. 2.1.1. The Cantor array is generated recursively by replacing $\{1\}$ by $\{101\}$ and $\{0\}$ by $\{000\}$ at each stage of the construction of the fractal structure. Then, the corresponding array at $S=2$ would be $\{101000101\}$ and the equivalent periodic array $\{101010101\}$.

A FSZP can be constructed in a similar way to a SZP; i.e., as a sequence of square zones with side length $\sqrt{j}b$ but defining the transmittance t_j of the j-th zone as the j-th element of the fractal binary array where $t_j=1$ for transparent zones and $t_j=0$ for opaque zones. The resulting structure for $S=3$ is shown in Fig. 2.1.2(a) and Fig. 2.1.2(b) shows the equivalent SZP with the same focal length. Note that a FSZP can be considered as a SZP but with some missing clear square zones.

In mathematical terms, the transmittance function for both kinds of lenses

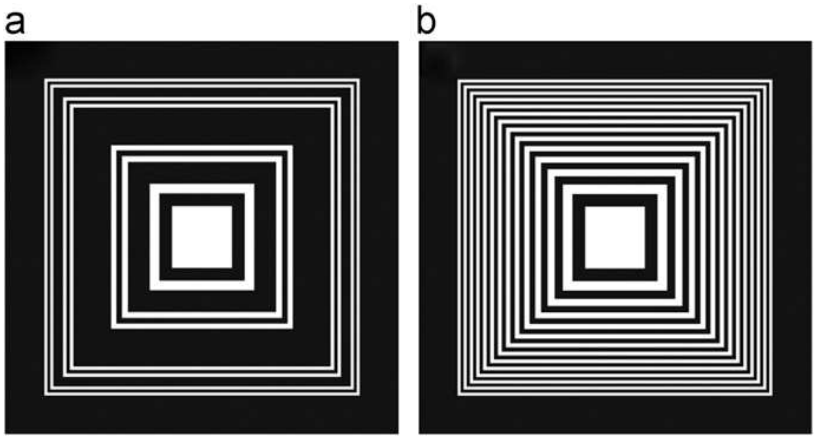

Figure 2.1.2: Comparison between (a) a FSZP and (b) the equivalent SZP ($S = 3$).

can be written with the same mathematical expression,

$$p(x,y) = \sum_{j=1}^{N} t_j \left[\text{rect}\left(\frac{x}{a\sqrt{j/N}} \right) \text{rect}\left(\frac{y}{a\sqrt{j/N}} \right) - \text{rect}\left(\frac{x}{a\sqrt{(j-1)/N}} \right) \text{rect}\left(\frac{y}{a\sqrt{(j-1)/N}} \right) \right], \qquad (2.1.1)$$

where N is the total number of zones and the length of the outer zone is $2a$.

Focusing properties of FSZPs

Let us consider the irradiance provided by a square pupil of length $2a$, and amplitude transmittance $p(x,y)$, when it is illuminated by a monochromatic plane wave of wavelength λ. Within the Fresnel approximation the diffracted field at a given point (x,y,z), where z is the axial distance from the pupil plane, can be expressed by

$$I(x,y,z) = \frac{1}{\lambda^2 z^2} \left| \iint_{-\infty}^{\infty} p(x_0,y_0) e^{\frac{-i\pi}{\lambda z}\left(x_0^2+y_0^2\right)} e^{\frac{i2\pi}{\lambda z}(xx_0+yy_0)} dx_0 dy_0 \right|^2. \qquad (2.1.2)$$

If the transmittance of the pupil is defined in terms of the normalized variables, $\{\bar{x}_0,\bar{y}_0\}=\{x_0/a,y_0/a\}$, then the irradiance can be re-written as

$$I(\bar{x},\bar{y},u)=4u^2\left|\iint_{-1}^{1}q(\bar{x}_0,\bar{y}_0)e^{-i2\pi u\left(\bar{x}_0^2+\bar{y}_0^2\right)}e^{i2\pi u(2\bar{x}\bar{x}_0+2\bar{y}\bar{y}_0)}d\bar{x}_0d\bar{y}_0\right|^2, \quad (2.1.3)$$

where $q(\bar{x}_0,\bar{y}_0)=p(a\bar{x}_0,a\bar{y}_0)$, $u=a^2/2\lambda z$ is the reduced axial coordinate, and $\{\bar{x},\bar{y}\}$=$\{x/a,y/a\}$ are the normalized transverse coordinates.

If we consider the diffracting square aperture of transmittance (2.1.1) in the above equation we obtain the analytical expression of the irradiance:

$$\begin{aligned}I(\bar{x},\bar{y},u)=&\frac{1}{16}\left|\sum_{j=1}^{N}t_j\left\{\left(\mathrm{erf}\left[(1+i)\sqrt{\pi u}\left(\sqrt{j/N}+\bar{x}\right)\right]\right.\right.\right.\\&+\mathrm{erf}\left[(1+i)\sqrt{\pi u}\left(\sqrt{j/N}-\bar{x}\right)\right]\Big)\\&\times\left(\mathrm{erf}\left[(1+i)\sqrt{\pi u}\left(\sqrt{j/N}+\bar{y}\right)\right]\right)\\&+\mathrm{erf}\left[(1+i)\sqrt{\pi u}\left(\sqrt{j/N}-\bar{y}\right)\right]\Big)\\&-\left(\mathrm{erf}\left[(1+i)\sqrt{\pi u}\left(\sqrt{(j-1)/N}+\bar{x}\right)\right]\right.\\&+\mathrm{erf}\left[(1+i)\sqrt{\pi u}\left(\sqrt{(j-1)/N}-\bar{x}\right)\right]\Big)\\&\times\left(\mathrm{erf}\left[(1+i)\sqrt{\pi u}\left(\sqrt{(j-1)/N}+\bar{y}\right)\right]\right.\\&\left.\left.\left.+\mathrm{erf}\left[(1+i)\sqrt{\pi u}\left(\sqrt{(j-1)/N}-\bar{y}\right)\right]\right)\right\}\right|^2, \qquad (2.1.4)\end{aligned}$$

where $\mathrm{erf}(x)$ is the error function of the argument x. If we focus our attention to the values that the irradiance takes along the optical axis, Eq. (2.1.4) becomes:

$$I(0,0,u)=\left|\sum_{j=1}^{N}t_j\left(\mathrm{erf}^2\left[(1+i)\sqrt{\pi u}\sqrt{j/N}\right]-\mathrm{erf}^2\left[(1+i)\sqrt{\pi u}\sqrt{(j-1)/N}\right]\right)\right|^2. \quad (2.1.5)$$

The axial irradiance of FSZPs computed for different stages of growth S is shown in Fig. 2.1.3. The irradiance of the associated SZPs is shown in

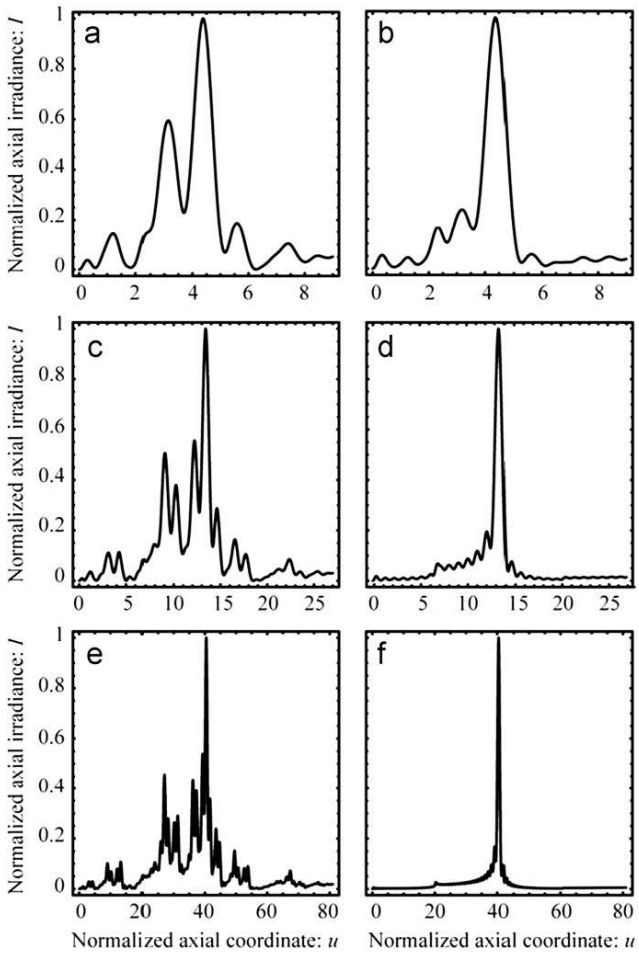

Figure 2.1.3: Normalized irradiance vs. the axial coordinate u obtained for a FSZP (left part) and its associated SZP (right part) at three stages of growth, $S = 2$ (upper part), $S = 3$ (middle part), and $S = 4$ (lower part).

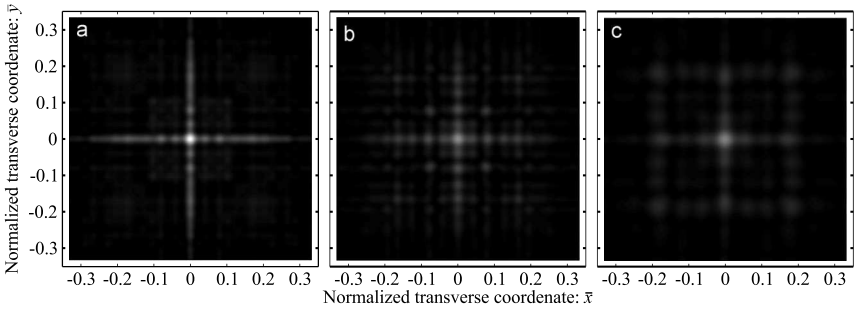

Figure 2.1.4: Transverse diffraction patterns of a SFZP with $S = 3$ at (a) the main focus located at $u = 13.40$, and two subsidiary foci located at (b) $u = 12.20$ and (c) $u = 9.05$.

the same figure for comparison. Note that the scale for the axial coordinate in each step is a magnified version of the one in the previous step by a factor $\gamma = 3$. It can be seen that the axial positions of the central lobes of the main foci coincide with those of the associated SZP. Interestingly, the irradiance produced by the FSZPs have fractal properties. In fact, the three patterns in the left part of Fig. 2.1.3 are self-similar, i.e., the axial irradiance distribution corresponding to a given FSZP of order $S = 4$ is a modulated version of the irradiance distribution corresponding to the FSZP of order $S = 3$. The same happens for $S = 3$ and $S = 2$. This means that the axial irradiance generated by a FSZP is self-similar, as it is the FSZP itself.

The distribution of the diffracted energy, not only in the optical axis but over the whole transverse plane is of interest for the prediction of the applications capabilities of FSZPs. Thus, a two-dimensional analysis of the diffracted intensities is required. Eq. (2.1.4) has been used to calculate the evolution of the diffraction patterns for a FSZP from near field to far field. Of particular interest are the intensities at transverse planes corresponding to the different maxima of the axial irradiance. Fig. 2.1.4 shows the result obtained for $S = 3$ at the main focus located at $u = 13.40$ and two subsidiary foci located at $u = 12.20$, and $u = 9.05$. Intensities are normalized to the maximum value obtained at the main focus.

It is shown that under monochromatic illumination a FSZP gives a main

focal volume containing a two-arms-cross pattern which, at this plane, is similar to that obtained with the associated SZP (not shown). However, it can be noted that the secondary maxima at $u = 12.20$, and $u = 9.05$ preserves the crossed shape, and this behavior can be interpreted as an extension of depth of focus. In fact, the intensity given by the associated SZP at these planes is almost zero.

Conclusions

A new family of diffractive lenses, coined "Fractal Square Zone Plates", has been introduced. It is shown that the distribution of square zones of theses fractal lenses is obtained through the triadic Cantor set. The focusing properties of FSZPs have been analyzed and compared with those corresponding to a conventional SZP. Under monochromatic illumination FSZPs produces a focal volume containing a delimited sequence of two-arms-cross pattern that are axially distributed according to the self-similarity of the lens. One potential application of these new designs of square lenses with increased depth of focus is its integration in three-dimensional optical alignment systems. Other polygonal Fresnel zone plates [Alda08, Alda09b] with fractal structure are currently under study.

Acknowledgements

We acknowledge the financial support from Ministerio de Ciencia e Innovacion (grants FIS2011-23175 and TRA2009-0215), Generalitat Valenciana (grant PROMETEO2009-077), and Universitat Politecnica de Valencia (grant PAID-05-11), Spain.

Referencias

[Alda08] J. Alda y G. Boreman, "Optimization of polygonal fresnel zone plates", *Microwave and Optical Technology Letters* **50**, 536–541 (2008).

[Alda09a] J. Alda y F. J. González, "Polygonal Fresnel zone plates", *Journal of Optics A: Pure and Applied Optics* **11**, 085707 (2009).

[Alda09b] J. Alda, J. M. Rico-García, F. J. Salgado-Remacha y L. M. Sanchez-Brea, "Diffractive performance of square Fresnel zone plates", *Optics Communications* **282**, 3402–3407 (2009).

[Davison06] J. A. Davison y M. J. Simpson, "History and development of the apodized diffractive intraocular lens", *Journal of cataract and refractive surgery* **32**, 849–858 (2006).

[Furlan07] W. D. Furlan, G. Saavedra y J. A. Monsoriu, "White-light imaging with fractal zone plates", *Optics Letters* **32**, 2109–2111 (2007).

[González04] F. J. González, J. Alda, B. Ilic y G. D. Boreman, "Infrared Antennas Coupled to Lithographic Fresnel Zone Plate Lenses", *Applied Optics* **43**, 6067–6073 (2004).

[Hart66] H. E. Hart, J. B. Scrandis, R. Mark y R. D. Hatcher, "Diffraction Characteristics of a Linear Zone Plate", *Journal of the Optical Society of America* **56**, 1018–1023 (1966).

[Herrmannsfeldt68] W. B. Herrmannsfeldt, M. J. Lee, J. J. Spranza y K. R. Trigger, "Precision Alignment Using a System of Large Rectangular Fresnel Lenses", *Applied Optics* **7**, 995–1005 (1968).

[Janicijevic82] L. J. Janicijevic, "Diffraction characteristics of square zone plates", *Journal of Optics* **13**, 199–206 (1982).

[Maciá12] E. Maciá, "Exploiting aperiodic designs in nanophotonic devices", *Reports on Progress in Physics* **75**, 036502 (2012).

[Monsoriu04] J. A. Monsoriu, G. Saavedra y W. D. Furlan, "Fractal zone plates with variable lacunarity", *Optics Express* **12**, 4227–4234 (2004).

[Saavedra03] G. Saavedra, W. D. Furlan y J. A. Monsoriu, "Fractal zone plates", *Optics Letters* **28**, 971–973 (2003).

[Wang02] S. Wang, X. C. Zhang, M. P. Maley, M. F. Hundley, L. N. Bulaevskii, A. E. Koshelev y A. J. Taylor, "Terahertz Tomographic Imaging With a Fresnel Lens", *Optics and Photonics News* **13**, 58–58 (2002).

[Wang03] Y. Wang, W. Yun y C. Jacobsen, "Achromatic Fresnel optics for wideband extreme-ultraviolet and X-ray imaging", *Nature* **424**, 50–53 (2003).

[Zhang10] B. Zhang y D. Zhao, "Square Fresnel zone plate with spiral phase for generating zero axial irradiance", *Optics Letters* **35**, 1488–1490 (2010).

2.2 Cantor dust zone plates

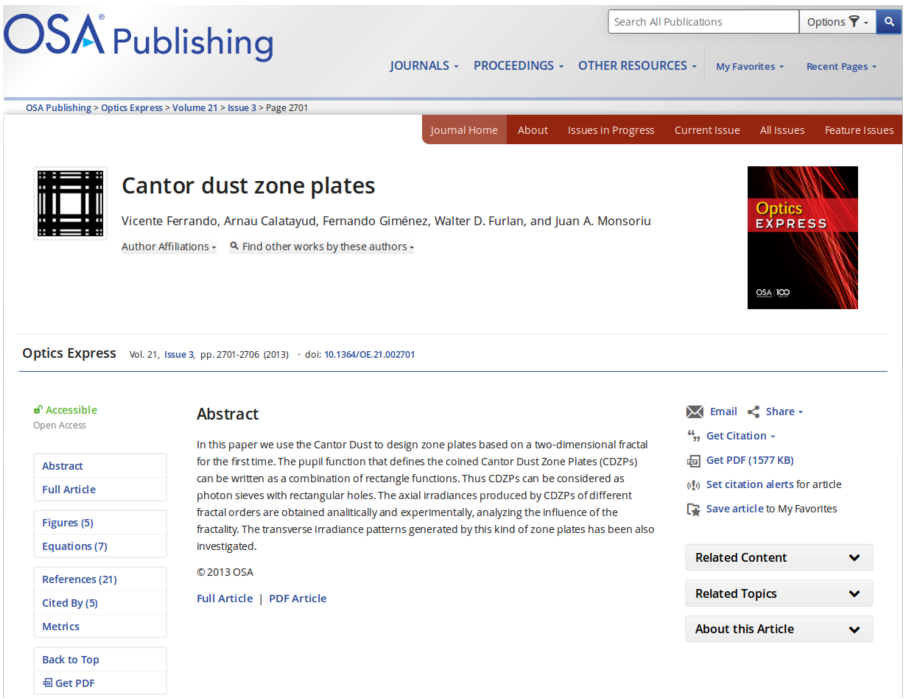

Cantor dust zone plates

Vicente Ferrando,[1,2] Arnau Calatayud,[1] Fernando Giménez,[3]
Walter D. Furlan,[2] and Juan A. Monsoriu[1,*]

[1]Centro de Tecnologías Físicas, Universitat Politècnica de València, 46022 Valencia, Spain.
[2]Departamento de Óptica, Universitat de València, 46100 Burjassot, Spain.
[3]I.U. Matemática Pura y Aplicada, Universitat Politècnica de València, 46022 Valencia, Spain.
*jmonsori@fis.upv.es

Optics Express **21**, 2701–2706 (2013).

Abstract In this paper we use the Cantor Dust to design zone plates based on a two-dimensional fractal for the first time. The pupil function that defines the coined Cantor Dust Zone Plates (CDZPs) can be written as a combination of rectangle functions. Thus CDZPs can be considered as photon sieves with rectangular holes. The axial irradiances produced by CDZPs of different fractal orders are obtained analitically and experimentally, analyzing the influence of the fractality. The transverse irradiance patterns generated by this kind of zone plates has been also investigated.

Introduction

A renewed interest in focusing diffractive optical elements has been experienced by the scientific community in the last years because these elements are essential in image forming setups not only used in the visible range, but also in THz optics [Siemion12] or in X-ray microscopy [Sakdinawat07]. Following this trend, our group introduced a new type of image-forming structure: the Fractal Zone Plate (FZP) [Saavedra03] which is based on the one-dimensional Cantor Set. It has been proved theoretically [Saavedra03] and experimentally [Davis04] that under monochromatic plane wave illumination, a FZP produces multiple foci along the optical axis. The internal structure of

each focus exhibits a characteristic fractal structure that reproduces the self-similarity of the originating FZP. The number of foci and their relative amplitude can be modified with the FZP design [Monsoriu04, Hai-Tao05]. It has been shown that this property can be profited in image forming systems to obtain an enhancement of the depth of field [Furlan07, Ge12].

Square zone plates (SZPs) [Janicijevic82, Alda09a] are another kind of interesting diffractive optical elements which can be obtained as the combination of two linear Fresnel zone plates and produces a focalization pattern with a cross-like irradiance distribution. Based on the SZP, Fractal Rectangular Zone Plates (FSZPs), i.e., zone plates with a fractal distribution of square zones, have been recently introduced providing a main focal volume containing a self-similar sequence of cross-shaped patterns [Calatayud13a].

On the other hand, a Photon Sieve (PS) [Kipp01,Cao02] is another promising diffractive optical element that is based on a classical Fresnel zone plate. It is constructed by substitution of the transparent areas in it by a great number of non overlapping circular holes of different sizes. PSs have been proposed for hard-x-ray focusing, in the high energy region above 20 keV [Xie10] and also used in two-dimensional hard-x-ray differential-interference-contrast imaging [Xie12]. In addition, they have been recently employed in prototypes of primary lenses for lightweight space telescopes [Andersen10]. The principal characteristic of a PS is that it improves the resolution of a conventional zone plate. Moreover, when a fractal distribution of holes is considered an extended depth of field is also obtained [Giménez06, Giménez07].

In this work we present the Cantor Dust Zone Plate (CDZP) as combination of the concepts of FSZP and PS. We have replaced the transparent square zones of a FSZP by a set of rectangular holes spatially distributed according to a two dimensional fractal known as Cantor Dust. To our knowledge, CDZPs are the first family of diffractive lenses designed with a two-dimensional fractal, improving the performance of FSZPs mainly on two aspects: 1) A CDZP has not connected regions so it can be fabricated in a single surface without any substrate. 2) The distribution of holes produces the apodization that improves the diffraction efficiency of a FSZP.

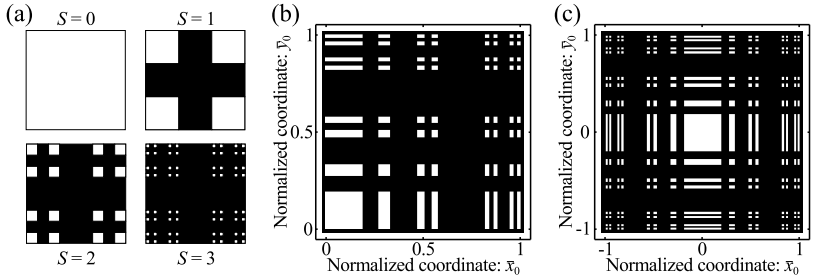

Figure 2.2.1: (a) Geometrical construction of the Cantor Dust distribution up to third order. (b) Cantor dust varying the distribution sides quadratically with respect to the transverse coordinates. (c) Pupil function $q(\bar{x}_0, \bar{y}_0)$ —Eq. (2.2.2)— obtained from the order $S = 3$ Cantor Dust distribution.

Cantor dust zone plate design

A CDZP is based on a 2D fractal which is geometrically constructed as shown in Fig. 2.2.1(a). Starting from two elements, $S = 0$ and $S = 1$, called the initiator and the generator respectively, the next higher order elements $S = 2, 3...$ are constructed sequentially by replacing every white square in the previous stage by the generator ($S = 1$). Mathematically the fractal Cantor Dust distribution can be generated by using an array of binary elements. Starting from the 1×1 array seed, $t_0 = [1]$, the next higher fractal order is constructed by applying to each element the following transformation rules:

$$[1] \rightarrow \begin{bmatrix} 1 & 0 & 1 \\ 0 & 0 & 0 \\ 1 & 0 & 1 \end{bmatrix} \qquad \text{and} \qquad [0] \rightarrow \begin{bmatrix} 0 & 0 & 0 \\ 0 & 0 & 0 \\ 0 & 0 & 0 \end{bmatrix} . \tag{2.2.1}$$

After an arbitrary number of iterations, S, a binary array, t_S, is obtained with $3^S \times 3^S$ elements. The array elements of t_S will be referred as $t_{Sjj'}$, where j and j' take values from 1 to 3^S. With this encoding, "1" represents a white square and "0" represents a black one.

From this geometrical representation, a CDZP can be constructed as a photon sieve constituted by an array of rectangular transparent holes, white squares, distributed along the squared transverse coordinates —see Fig. 2.2.1(b)—. Then, to obtain the corresponding pupil function two reflection

(mirror) symmetries are applied being the mirror lines the coordinate axes —see Fig. 2.2.1(c)—. Note that a CDZP can be considered as a FSZP [Calatayud13a] where the square rings are replaced by a set of rectangular holes. Mathematically, the pupil function which represents a CDZP can be written as:

$$q(\bar{x}_0,\bar{y}_0)=\sum_{j=1}^{N}\sum_{j'=1}^{N} t_{Sjj'}RECT_j(\bar{x}_0)RECT_{j'}(\bar{y}_0)\,, \tag{2.2.2}$$

where $N=3^S$, $\{\bar{x}_0,\bar{y}_0\}=\left\{\frac{x_0}{a},\frac{y_0}{a}\right\}$ (being a the half-width of the zone plate and $\{x_0,y_0\}$ the cartesian coordinates at the pupil plane), and $RECT_j(x)$ is defined as

$$RECT_j(x)=\left[rect\left(\sqrt{\frac{N}{j}}\,x\right)-rect\left(\sqrt{\frac{N}{j-1}}\,x\right)\right]. \tag{2.2.3}$$

In Eq. 2.2.3, $rect(x)$ is the rectangle function which takes the value 1 for $|x|\leq 1$ and 0 elsewhere. Thus, Fig. 2.2.1(c) shows a CDZP pupil of order $S=3$ in normalized coordinates.

Focusing properties

Under a monochromatic plane wave illumination, the diffracted irradiance patterns produced by a CDZP can be expressed (applying the Fresnel approximation) as:

$$I(\bar{x},\bar{y},u)=4u^2\left|\int_{-1}^{1}\int_{-1}^{1} q(\bar{x}_0,\bar{y}_0)\exp\left\{-2\pi iu\left[\left(\bar{x}_0^2+\bar{y}_0^2\right)-\left(2\bar{x}\bar{x}_0+2\bar{y}\bar{y}_0\right)\right]\right\}d\bar{x}_0d\bar{y}_0\right|^2, \tag{2.2.4}$$

where $u=a^2/2\lambda z$ is the normalized axial coordinate and $\{\bar{x},\bar{y}\}=\left\{\frac{x}{a},\frac{y}{a}\right\}$ are the normalized transverse coordinates. From the pupil function $q(\bar{x}_0,\bar{y}_0)$, defined in Eq. (2.2.2), it is easy to obtain the irradiance of a CDZP analytically:

$$I(\bar{x},\bar{y},u)=\frac{1}{16}\left|\sum_{j}^{N}\left\{\left[ERF_j(\bar{x},u)-ERF_{j-1}(\bar{x},u)\right]\times\sum_{j'}^{N}t_{Sjj'}\left[ERF_{j'}(\bar{y},u)-ERF_{j'-1}(\bar{y},u)\right]\right\}\right|^2, \tag{2.2.5}$$

where

$$ERF_j(x,u)=Erf\left[(1+i)\sqrt{\pi u}\left(\sqrt{\frac{j}{N}}+x\right)\right]+Erf\left[(1+i)\sqrt{\pi u}\left(\sqrt{\frac{j}{N}}-x\right)\right],$$

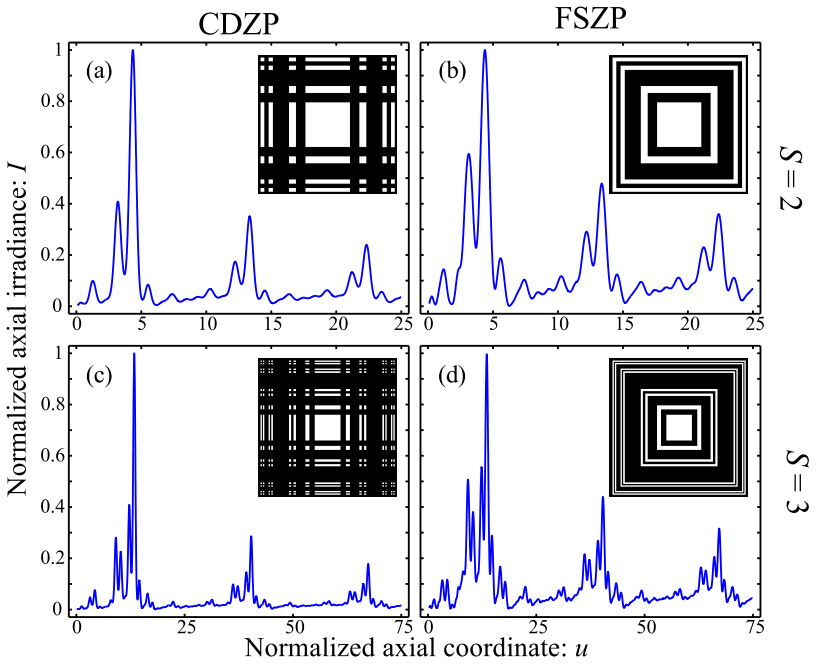

Figure 2.2.2: Normalized axial irradiance for the CDZP and its associated FSZP.

being $Erf[x] = 2\pi^{-1/2}\int_0^x \exp(-t^2)dt$ the error function. The irradiance along the optical axis, $\{\bar{x},\bar{y}\} = \{0,0\}$, Eq. (2.2.5) is:

$$I(0,0,u) = \left| \sum_j^N t_{Sjj} \left\{ Erf\left[(1+i)\sqrt{\pi u}\sqrt{\frac{j}{N}}\right] - Erf\left[(1+i)\sqrt{\pi u}\sqrt{\frac{j-1}{N}}\right] \right\} \right|^4 . \tag{2.2.6}$$

To compare the performance of a CDZP with the associated FSZP we used Eq. (2.2.6) to compute the axial irradiances. The result for $S = 2$ and $S = 3$ up to third order foci is shown in Fig. 2.2.2. It can be seen that CDZPs preserves the characteristic self-similar behavior of a FSZP with the foci located at the same positions because the axial patterns for $S = 3$ are a modulated version of that for $S = 2$. However, the secondary foci of CDZP are apodized with respect to FSZP ones. It can be also observed that the apodization is enhaced for higher fractal orders improving the diffraction efficiency.

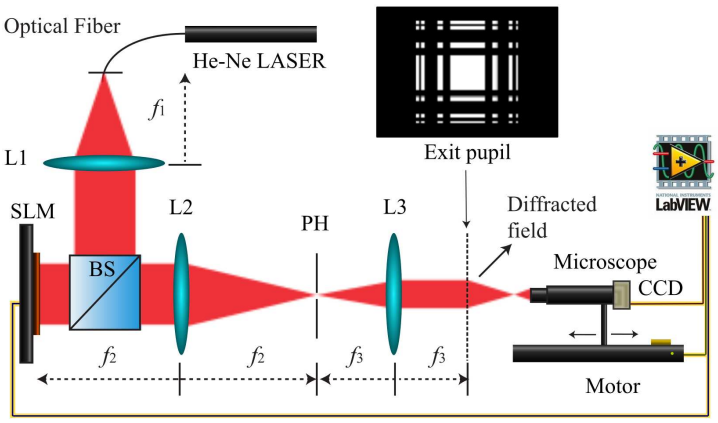

Figure 2.2.3: Scheme of the experimental setup used for the simulation of the lenses.

Experimental results

The performance of different CDZPs have been tested experimentally with a programmable Liquid Crystal on Silicon SLM (Holoeye PLUTO, 8-bit gray-level, pixel size $d = 8\,\mu$m and resolution equal to 1920×1080) operating in phase-only modulation mode. The SLM was calibrated for a 2π phase shift at $\lambda = 633\,$nm. The experimental setup is sketched in Fig. 2.2.3. A collimated beam (He-Ne Laser $\lambda = 633\,$nm) impinges onto the SLM, in which the CDZP is programed adding a linear phase grating to avoid the noise originated by the specular reflection (zero order diffraction) and the pixelated structure of the SLM (higher diffraction orders). This linear phase is compensated by tilting the SLM slightly and a pin-hole (PH) filter all diffraction orders except the order $+1$. Then at lens L3 focal plane (exit pupil) is a rescaled image of the desired lens pupile. The diffracted field is captured and registered with a microscope (4x Zeiss Plan-Apochromat objective) attached to a CCD camera (EO-1312M 1/2" CCD Monochrome USB Camera, 8-bit gray-level, pixel pitch of $4.65\,\mu$m and 1280×1024 pixels). The microscope and the CCD are mounted on a translation stage (Thorlabs LTS 300, Range: 300 mm and $5\,\mu$m precision) along the optical axis. The programming of the SLM, movements of the translation stage, the image recording and analysis is fully automatized by means of a LabVIEW program.

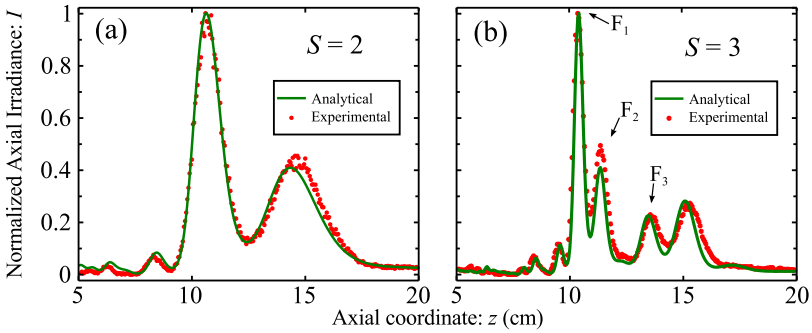

Figure 2.2.4: a) Analytical (green) and experimental (red) irradiances provided by different fractal order CDZPs (first order focus) for $S = 2$. b) Same as in Fig. 2.2.4(b) for $S = 3$; F_1, F_2, F_3 are three different maxima of the compound first order focus. (see Fig. 2.2.5)

The experimental and the analytical axial irradiances are shown together in Fig. 2.2.4 for comparison. We have taken $a = 0.75\,\text{mm}$ and $1.31\,\text{mm}$ for $S = 2$ and $S = 3$ respectively in order to fix the main focus at the same position in both cases.

The distribution of the diffracted pattern over the whole transverse plane is of interest for the prediction of applications capabilities of CDZPs. Thus, a two-dimensional analysis of the diffracted irradiances is required. Equation (2.2.5) has been used to calculate the evolution of the diffraction patterns provided by a CDZP from near field to far field. Of particular interest are the irradiance patterns in the transverse planes which correspond to the different maxima of the axial irradiance.

In Fig. 2.2.4 the experimental transverse irradiances obtained at the main focus ($z = 10.4\,\text{cm}$) and at two subsidiary foci ($z = 11.3\,\text{cm}$ and $z = 13.6\,\text{cm}$) can be compared with the analytical results calculated using Eq. (2.2.5) for the order $S = 3$. In all cases, the irradiance has been normalized to its own maximum value. In spite of that the experimental images are affected by noise and by the aberrations of both, L3 and the microscope objective, a very good agreement with the numerical simulation is obtained. A characteristic two-arms-cross pattern at the main focus, extended to the subsidiary foci, can also be observed, so this behavior can be interpreted as an extension of depth of

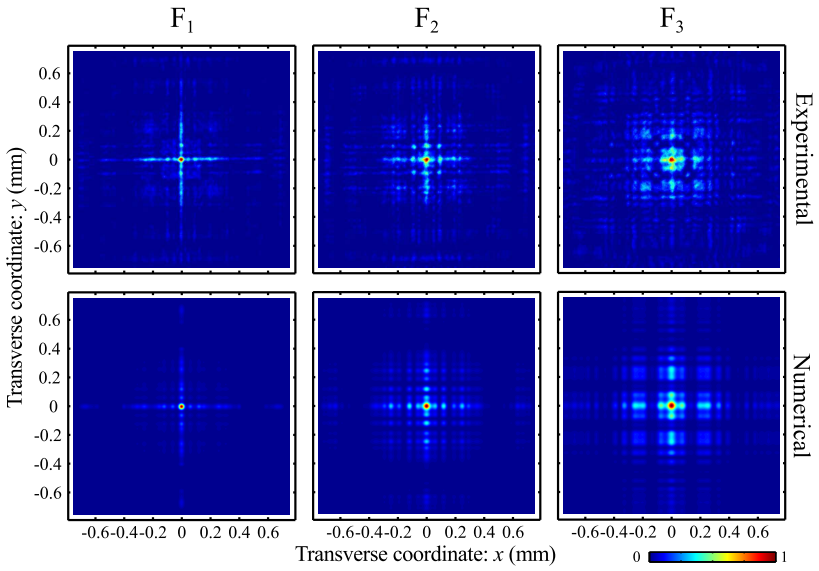

Figure 2.2.5: Experimental transverse irradiance (top) compared with the analytically obtained irradiance (bottom) for a fractal order $S = 3$ CDZP. Transversal planes belong to the first order focus shown in Fig. 2.2.4(b) located at $z = 10.4\,\text{cm}$ and two secondary foci at $z = 11.3\,\text{cm}$ and $z = 13.6$ cm.

focus.

Conclusions

A new fractal diffractive optical element a CDZP is proposed. The focusing properties of this novel kind of lenses are analytically and experimentally investigated. The axial irradiances provided by these elements have been computed for different fractal stages obtaining a self-similar behavior. Moreover, under a monochromatic illumination, a CDZP gives rise a focal volume containing a delimited sequence of two-arms-cross patterns which are axially distributed according to the self-similarity of the lens. One potential application of CDZP is to generate a reference pattern in optical alignment and calibration of 3D systems. A spiral phase mask superposed to the CDZP pupil function — Eq. (2.2.2)— can be used for generating hollow rectangular beams [Zhang10].

Moreover, CDZP could be applied in THz communications given that Fresnel zone plates have been proved to be valuable elements for improving the performance in infrared antennas [González04]. On the other hand, its cross-shaped focal pattern and its enhanced focal depth could be also helpful to perform parallel photopolymerisation in three-dimensional microstructure fabrication [Kelemen07]

Acknowledgements

We acknowledge the financial support from Ministerio de Ciencia e Innovación (grants FIS2011-23175 and TRA2009-0215), Generalitat Valenciana (grant PROMETEO2009-077), and Universitat Politècnica de València (PAID-05-11), Spain.

Referencias

[Alda09a] J. Alda y F. J. González, "Polygonal Fresnel zone plates", *Journal of Optics A: Pure and Applied Optics* **11**, 085707 (2009).

[Andersen10] G. Andersen, "Membrane photon sieve telescopes", *Applied Optics* **49**, 6391–6394 (2010).

[Calatayud13a] A. Calatayud, V. Ferrando, F. Giménez, W. D. Furlan, G. Saavedra y J. A. Monsoriu, "Fractal square zone plates", *Optics Communications* **286**, 42–45 (2013).

[Cao02] Q. Cao y J. Jahns, "Focusing analysis of the pinhole photon sieve: individual far-field model", *Journal of the Optical Society of America A* **19**, 2387–2393 (2002).

[Davis04] J. A. Davis, L. Ramirez, J. A. Rodrigo, T. Alieva y M. L. Calvo, "Focusing properties of fractal zone plates: experimental implementation with a liquid-crystal display", *Optics Letters* **29**, 1321–1323 (2004).

[Furlan07] W. D. Furlan, G. Saavedra y J. A. Monsoriu, "White-light imaging with fractal zone plates", *Optics Letters* **32**, 2109–2111 (2007).

[Ge12] X. Ge, Z. Wang, K. Gao, D. Wang, Z. Z. Z. Wu, J. Chen, Z. Pan, K. Zhang, Y. Hong, P. Zhu y Z. Z. Z. Wu, "Use of fractal zone plates for transmission X-ray microscopy", *Analytical and bioanalytical chemistry* **404**, 1303–1309 (2012).

[Giménez06] F. Giménez, J. A. Monsoriu, W. D. Furlan y A. Pons, "Fractal photon sieve", *Optics Express* **14**, 11958–11963 (2006).

[Giménez07] F. Giménez, W. D. Furlan y J. A. Monsoriu, "Lacunar fractal photon sieves", *Optics Communications* **277**, 1–4 (2007).

[González04] F. J. González, J. Alda, B. Ilic y G. D. Boreman, "Infrared Antennas Coupled to Lithographic Fresnel Zone Plate Lenses", *Applied Optics* **43**, 6067–6073 (2004).

[Hai-Tao05] D. Hai-Tao, W. Xin y X. Ke-Shu, "Focusing Properties of Fractal Zone Plates with Variable Lacunarity: Experimental Studies Based on Liquid Crystal on Silicon", *Chinese Physics Letters* **22**, 2851–2854 (2005).

[Janicijevic82] L. J. Janicijevic, "Diffraction characteristics of square zone plates", *Journal of Optics* **13**, 199–206 (1982).

[Kelemen07] L. Kelemen, S. Valkai y P. Ormos, "Parallel photopolymerisation with complex light patterns generated by diffractive optical elements", *Optics Express* **15**, 14488–14497 (2007).

[Kipp01] L. Kipp, M. Skibowski, R. L. Johnson, R. Berndt, R. Adelung, S. Harm y R. Seemann, "Sharper images by focusing soft X-rays with photon sieves", *Nature* **414**, 184–188 (2001).

[Monsoriu04] J. A. Monsoriu, G. Saavedra y W. D. Furlan, "Fractal zone plates with variable lacunarity", *Optics Express* **12**, 4227–4234 (2004).

[Saavedra03] G. Saavedra, W. D. Furlan y J. A. Monsoriu, "Fractal zone plates", *Optics Letters* **28**, 971–973 (2003).

[Sakdinawat07] A. Sakdinawat y Y. Liu, "Soft-x-ray microscopy using spiral zone plates", *Optics Letters* **32**, 2635–2637 (2007).

[Siemion12] A. Siemion, A. Siemion, M. Makowski, J. Suszek, J. Bomba, A. Czerwinski, F. Garet, J.-L. Coutaz y M. Sypek, "Diffractive paper lens for terahertz optics", *Optics Letters* **37**, 4320–4322 (2012).

[Xie10] C. Xie, X. Zhu, H. Li, L. Shi y Y. Wang, "Feasibility study of hard-x-ray nanofocusing above 20 keV using compound photon sieves", *Optics Letters* **35**, 4048–4050 (2010).

[Xie12] C. Xie, X. Zhu, H. Li, L. Shi, Y. Hua y M. Liu, "Toward two-dimensional nanometer resolution hard X-ray differential-interference-contrast imaging using modified photon sieves", *Optics Letters* **37**, 749–751 (2012).

[Zhang10] B. Zhang y D. Zhao, "Square Fresnel zone plate with spiral phase for generating zero axial irradiance", *Optics Letters* **35**, 1488–1490 (2010).

2.3 Twin axial vortices generated by Fibonacci lenses

Twin axial vortices generated by Fibonacci lenses

Arnau Calatayud,[1] Vicente Ferrando,[1,2] Laura Remón,[1]
Walter D. Furlan,[2] and Juan A. Monsoriu[1,*]

[1]Centro de Tecnologías Físicas, Universitat Politècnica de València, 46022 Valencia, Spain.
[2]Departamento de Óptica, Universitat de València, 46100 Burjassot, Spain.
*jmonsori@fis.upv.es

Optics Express **21**, 10234-10239 (2013).

Abstract Optical vortex beams, generated by Diffractive Optical Elements (DOEs), are capable of creating optical traps and other multifunctional micromanipulators for very specific tasks in the microscopic scale. Using the Fibonacci sequence, we have discovered a new family of DOEs that inherently behave as bifocal vortex lenses, and where the ratio of the two focal distances approaches the golden mean. The disctintive optical properties of these Fibonacci vortex lenses are experimentally demonstrated. We believe that the versatility and potential scalability of these lenses may allow for new applications in micro and nanophotonics.

Introduction

In photonics technology, Diffrative Optical Elements (DOEs) have found a large number of new aplications in many different areas, covering the whole electromagnetic spectrum from X-ray Microscopy [Sakdinawat07], to THz Imaging [Siemion12]. Difractive lenses such as conventional Fresnel zone plates, are essential in many focusing and image forming systems but they have inherent limitations. Fractal zone plates are a new type of multifocal diffractive lenses that have been proposed to overcome some of these limitations, mainly under polychromatic illumination [Saavedra03, Davis06]. In fact, it was shown that these lenses, generated with the fractal Cantor set have

an improved behavior, especially under wide band illumination [Furlan07].

DOEs have been also designed to generate optical vortices. Optical vortices are high value optical traps because in addition to trap microparticles they are capable to set these particles into rotation due to its inherent orbital angular moment [Roux04, Gbur06]. These special optical beams have been used, for exemple, as actuators and testers in micromechanical systems [Bishop03]. Arrays of optical vortices have shown the ability to assemble and drive mesoscopic optical pumps in microfluidic systems [Ladavac04].

Among the several methods that have been proposed for optical vortices generation, spiral phase plates [Lee04] stands out, mainly because they provide high energy efficiency. Spiral phase plates have been recently combined with Fractal Zone Plates to produce a sequence of focused optical vortices along the propagation direction [Tao06, Furlan09].

In this work we present the Fibonacci Vortex Lenses (FVLs), which are able to generate simultaneously two optical vortices along the axial coordinate whose diametres are related by the golden mean. These new type of DOEs are constructed using the Fibonacci sequence [Monsoriu10, Monsoriu13] along the squared radial coordinate. This sequence has been also employed in the development of different photonic devices [Maciá12], such as multilayers and linear gratings [Sah95], circular gratings [Gao11], spiral zone plates [Dai12].

Fibonacci vortex lenses design

A FVL is defined as a pure phase diffractive element whose phase distribution is given by $\Phi_{FVL}(\zeta,\theta_0) = mod_{2\pi}[\Phi_a(\theta_0)+\Phi_j(\zeta)]$. It combines the azimuthal phase variation that characerizes a vortex lens, i.e. $\Phi_a = m\theta_0$, where m is a non zero integer called the topological charge [Dai12] and θ_0 is the azimuthal angle about the optical axis at the pupil plane, with the radial phase distribution that is generated through the Fibonacci sequence in the following way:

Starting with two elements (seeds) $F_0 = 0$ and $F_1 = 1$, the Fibonacci numbers, $F_j = \{0,1,1,2,3,\ 5,8,13,21,\ldots\}$, are obtained by the sequential application of the following rule: $F_{j+1} = F_j + F_{j-1}$, $(j = 0,1,2,\ldots)$. The golden mean, or golden ratio, is defined as the limit of the ratio of two consecutive

Fibonacci numbers:

$$\varphi = \lim_{j\to\infty} F_j/F_{j-1} = \left(1+\sqrt{5}\right)/2\,. \tag{2.3.1}$$

Based on the Fibonacci numbers, a binary aperiodic Fibonacci sequence can also be generated with two seed elements, as for exemple, $S_1 = \{A\}$ and $S_0 = \{B\}$. Then, next order of the sequence is obtained simply as the concatenation of the two previous ones: $S_{j+1} = \{S_j S_{j-1}\}$ for $j \geq 1$. Therefore, $S_2 = \{AB\}$, $S_3 = \{ABA\}$, $S_4 = \{ABAAB\}$, $S_5 = \{ABAABABA\}$, etc. Note that, in each sequence, two succesive "B" are separated by either, one or two "A", and that the total number of elements of the order j sequence is F_{j+1}, which results from the sum of F_j elements "A", plus F_{j-1} elements "B". Each of these sequences can be used to define the binary generating function for the radial phase distribution of the FVL. For our purpose, the generating function, $\Phi_j(\zeta)$, is defined in the domain $[0,1]$, and this interval is partitioned in F_{j+1} sub-intervals of length $d = 1/F_{j+1}$. Then, the value that the function $\Phi_j(\zeta)$ takes at the k^{th} sub-interval will be 0 or π if the value of the k^{th} element of the S_j sequence, S_{jk}, is "A" or "B", respectively. Next, from a particular generating function $\Phi_j(\zeta)$, the radial part of the transmittance of the corresponding binary pure-phase FVL is obtained as $q(\zeta) = \exp[i\Phi_j(\zeta)]$, after performing the following coordinate transformation: $\zeta = (r/a)^2$, being r the radial coordinate of the lens, and a its maximum value. Typical examples of FVLs are shown in Fig. 2.3.1. For comparison, a conventional vortex lenses based on Fresnel zone plates are represented in the same figure. The corresponding Fresnel zone plates can be considered periodic structures along the square radial coordinate ζ having the same number of elements, F_{j+1}, with period $p = 2d$, but where the position of some zones with different phase have been interchanged. Fibonacci sequences are apediodic, but they have two incommensurable periods [Maciá12]. It is easy to show that, according to our nomenclature, these periods are related to the period of the equivalent zone plate throught $p_1 = 1/F_{j-1} \approx 0.5\,(\varphi+1)\,p$ and $p_2 = 1/F_j \approx 0.5\,\varphi\,p$. Thus, a FVL with $m = 0$ can be understood as two Fresnel zone plates interlaced.

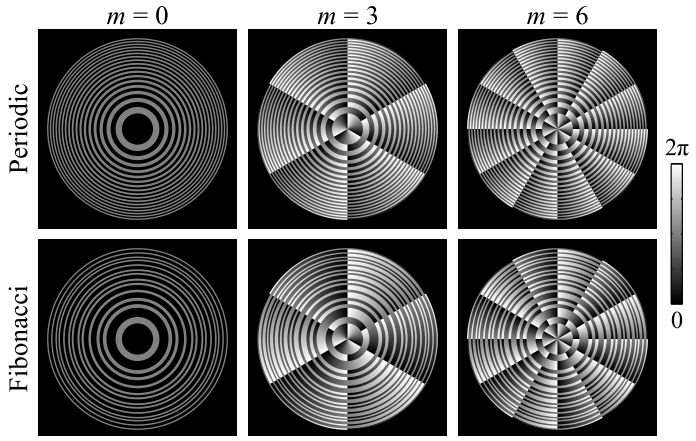

Figure 2.3.1: Bottom: Phase distributions of FVLs based on the Fibonacci sequence S_8, with different topological charges. Top: The equivalent periodic lenses with the same number of zones.

Focusing properties

To study the focusing properties of FVLs we have computed the irradiance provided by the transmittance of this lens, $t(\zeta,\theta_0) = q(\zeta)\exp[im\theta_0]$, when it is illuminated by a plane wave of wavelength λ. Within the Fresnel approximation the irradiance function is given by:

$$I(u,v,\theta) = u^2 \left| \int_0^1 \int_0^{2\pi} t(\zeta,\theta_0) \exp(-i2\pi u\zeta) \exp\left[i4\pi uv\zeta^{1/2}\cos(\theta-\theta_0)\right] d\zeta d\theta_0 \right|^2, \tag{2.3.2}$$

where $u = a^2/2\lambda z$ is the dimensionless reduced axial coordinate [Saavedra03] and $v = r/a$ is the normalized transverse coordinate. Note that the reduced axial coordinate contains the full dependende of the irradiance with λ. Replacing $t(\zeta,\theta_0)$ and taking into account that

$$\int_0^{2\pi} \exp(im\theta_0) \exp\left[i4\pi uv\zeta^{1/2}\cos(\theta-\theta_0)\right] d\theta_0 = 2\pi \exp\left[im\left(\theta+\frac{\pi}{2}\right)\right] J_m\left(4\pi uv\zeta^{1/2}\right), \tag{2.3.3}$$

Eq. (2.3.2) is reduced to

$$I(u,v) = 4\pi^2 u^2 \left| \int_0^1 q(\zeta) \exp(-i2\pi u\zeta) J_m\left(4\pi uv\zeta^{1/2}\right) d\zeta \right|^2, \tag{2.3.4}$$

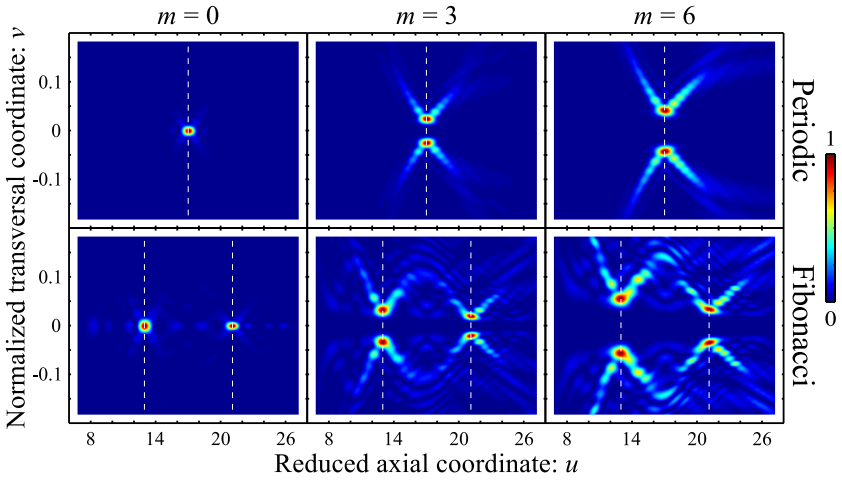

Figure 2.3.2: Evolution of the transverse irradiance for S_8 based FVLs with different topological charges and their periodic equivalent lenses.

being $J_m()$ the Bessel function of the first kind of order m.

By using Eq. (2.3.4) we have computed the irradiances provided by the lenses shown in Fig. 2.3.1. The integrals were numerically evaluated applying the Simpson's rule using a step length $1/2000$. The result is shown in Fig. 2.3.2. It can be seen that FVLs produce a twin foci whose positions are given by the Fibonacci numbers. In this case, for S_8 FVLs, the first focus is located at $u_1 = 13 = F_{j-1} = 1/p_1$ and the other one at $u_2 = 21 = F_j = 1/p_2$. Thus, the ratio of the focal distances satisfies $u_2/u_1 \approx \varphi$. Note also that, for non-null values of the topological charge, each focus is a vortex, thus, in general, a pair of doughnut shaped foci is generated by a FVL. Comparing the diffraction patterns provided by FVLs with different topological charges it can be verified that the diameter of the doughnuts increases with the topological charge as those produced by conventional vortex lenses [Swartzlander01, Curtis03].

Experimental results

For the experimental study of the properties of FVLs, we implemented the experimental setup shown in Fig 2.3.3. The proposed lenses were recorded

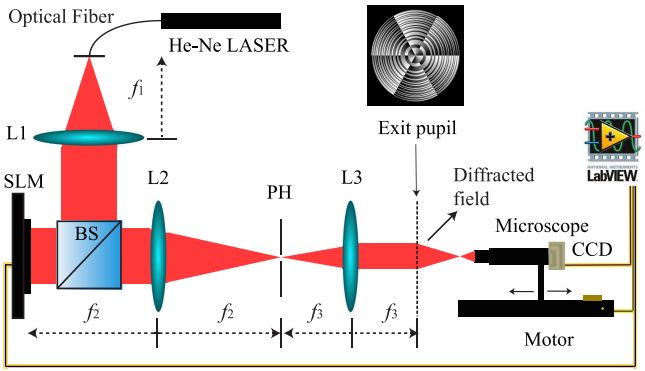

Figure 2.3.3: Experimental setup used for studying the focusing properties of FVLs.

on a Liquid Crystal in a Silicon SLM (Holoeye PLUTO, 8-bit gray-level, pixel size $8\,\mu$m and resolution equal to 1920×1080 pixels), calibrated for a 2π phase shift at $\lambda = 633$ nm operating in phase-only modulation mode. The procedure to compensate the wavefront distorsions caused by the lack of flatness of the SLM and the other optical components was detailed elsewhere [Calatayud12b]. In addition to the diffractive lenses, a linear phase carrier was modulated on the SLM to avoid the noise originated by the specular reflection (zero order diffraction) and the pixelated structure of the SLM (higher diffraction orders). This linear phase is compensated by tilting the SLM and a pin-hole (PH) is used to filter all diffraction orders except the first one. Then at the L3 lens focal plane (exit pupil) a rescaled image of the desired lens pupil is achieved. A collimated beam (He-Ne Laser $\lambda = 633$ nm) impinges onto the SLM and the diffracted field is captured and registered with a microscope (10x Zeiss Plan-Apochromat objective) attached to a CCD camera (EO-1312M 1/2" CCD Monochrome USB Camera, 8-bit gray-level, pixel pitch of $4.65\,\mu$m and 1280×1024 pixels). The microscope and the CCD are mounted on a translation stage (Thorlabs LTS 300, Range: 300 mm and $5\,\mu$m precision) along the optical axis.

The experimental and computed irradiances produced by a S_8 FVL with topological charge $m = 6$ along the optical axis (using the dimensionless reduced axial coordinate) are shown in Fig. 2.3.4. As predicted by the theoretical analysis, the axial localization of the focal rings depends on the Fibonacci

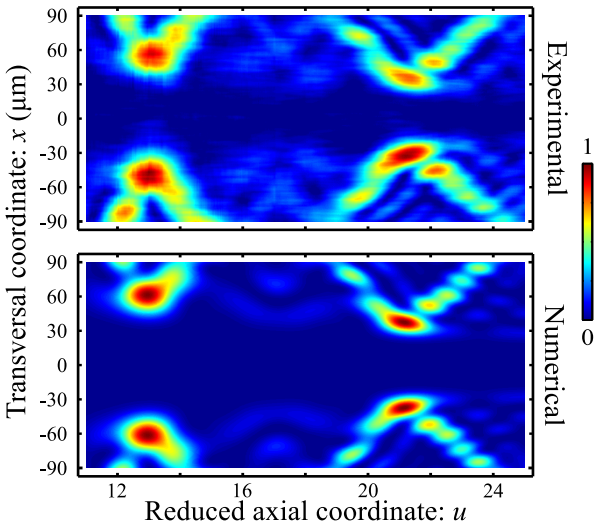

Figure 2.3.4: Experimental and computed transverse irradiance evolution along the optical axis provided by the S_8 FVL with $m = 6$ and $a = 1.1\,\text{mm}$.

numbers F_j and F_{j-1}, and such focal distances satisfy the following relationship: $f_1/f_2 = F_j/F_{j-1} \approx \varphi$.

Figure 2.3.5 shows the experimental and the numerically simulated transverse irradiance at the focal planes for the same FVL. Interestingly, the diameter of the focal rings, Δ, which also depends on the topological charge of the FVL, satisfies a similar rule i.e. $\Delta_1/\Delta_2 \approx \varphi$ (see Fig. 2.3.5). Thus, FVLs are capable of generating twin axial vortices with different, but perfectly established, diameter of the central core.

Conclusions

Sumarizing, a new type of bifocal vortex lenses has been introduced, whose design is based on the Fiboonacci sequence. It was found that a FVL produces a twin optical vortices along the axial coordinate. The positions of both foci depend on the two incommensurable periods of the Fibonacci sequence in which the FVL is based on. The radii of these twin vortices increase with the topological charge of the vortex lens, but always their ratio approaches the

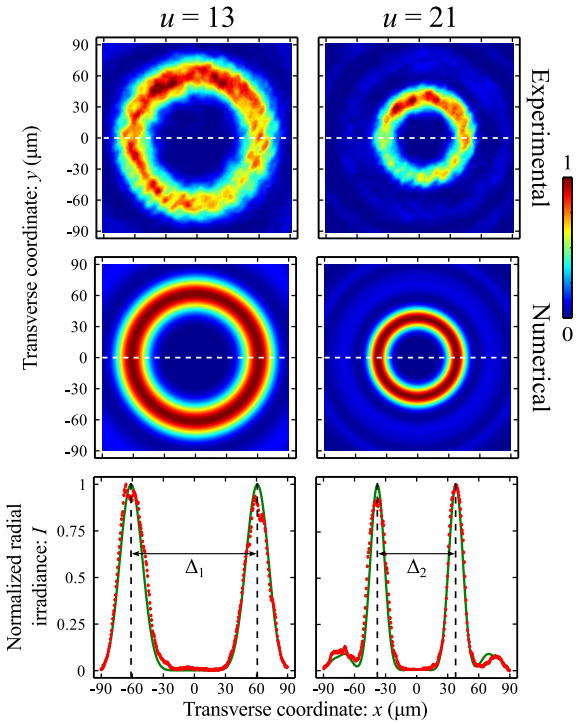

Figure 2.3.5: Experimental and numerical transverse irradiance at the focal planes provided by the S_8 based on FVL with $m = 6$ and $a = 1.1$ mm. The intensity profiles along the white, dotted lines are plotted (bottom) together with the numerical results for comparison.

golden mean. The 3D distribution of the diffracted field provided by FVLs has been tested experimentally using a SLM. An excellent agreement between the experimental results and the theoretical predictions has been demonstrated.

Acknowledgments

We acknowledge the financial support from Ministerio de Economía y Competitividad (grant FIS2011-23175), Generalitat Valenciana (grant PROMETEO2009-077), and Universitat Politècnica de València (SP20120569),

Spain. L.R. acknowledges a fellowship of "Fundación CajaMurcia", Spain.

Referencias

[Bishop03] A. Bishop, T. Nieminen, N. Heckenberg y H. Rubinsztein-Dunlop, "Optical application and measurement of torque on microparticles of isotropic nonabsorbing material", *Physical Review A* **68**, 033802 (2003).

[Calatayud12b] A. Calatayud, J. A. Rodrigo, L. Remón, W. D. Furlan, G. Cristóbal, J. A. Monsoriu, J. A. Rodrigo Martín-Romo, L. Remón, W. D. Furlan, G. Cristóbal, J. A. Monsoriu, J. A. Rodrigo Martín-Romo, L. Remón y G. Cristóbal, "Experimental generation and characterization of devil's vortex-lenses", *Applied Physics B* **106**, 915–919 (2012).

[Curtis03] J. E. Curtis y D. G. Grier, "Structure of Optical Vortices", *Physical Review Letters* **90**, 133901 (2003).

[Dai12] H. T. Dai, Y. J. Liu y X. W. Sun, "The focusing property of the spiral Fibonacci zone plate", S. Jiang, M. J. F. Digonnet y J. C. Dries, eds., "SPIE, Optical Components and Materials IX", tomo 8257, 82570T1–82570T7 (2012).

[Davis06] J. A. Davis, S. P. Sigarlaki, J. M. Craven y M. L. Calvo, "Fourier series analysis of fractal lenses: theory and experiments with a liquid-crystal display", *Applied optics* **45**, 1187–1192 (2006).

[Furlan07] W. D. Furlan, G. Saavedra y J. A. Monsoriu, "White-light imaging with fractal zone plates", *Optics Letters* **32**, 2109–2111 (2007).

[Furlan09] W. D. Furlan, F. Giménez, A. Calatayud y J. A. Monsoriu, "Devil's vortex-lenses", *Optics Express* **17**, 21891–21896 (2009).

[Gao11] N. Gao, Y. Zhang y C. Xie, "Circular Fibonacci gratings", *Applied Optics* **50**, G142–G148 (2011).

[Gbur06] G. Gbur y T. D. Visser, "Phase singularities and coherence vortices in linear optical systems", *Optics Communications* **259**, 428–435 (2006).

[Ladavac04] K. Ladavac y D. G. Grier, "Microoptomechanical pumps assembled and driven by holographic optical vortex arrays", *Optics Express* **12**, 1144–1149 (2004).

[Lee04] W. M. Lee, X.-C. Yuan y W. C. Cheong, "Optical vortex beam shaping by use of highly efficient irregular spiral phase plates for optical micromanipulation", *Optics Letters* **29**, 1796–1798 (2004).

[Maciá12] E. Maciá, "Exploiting aperiodic designs in nanophotonic devices", *Reports on Progress in Physics* **75**, 036502 (2012).

[Monsoriu10] J. A. Monsoriu, A. Calatayud, L. Remón, W. D. Furlan, G. Saavedra y P. Andrés, "Zone Plates Generated with the Fibonacci Sequence", "Proceedings of EOS Topical Meeting on Diffractive Optics", 151–152 (2010).

[Monsoriu13] J. A. Monsoriu, A. Calatayud, L. Remón, W. D. Furlan, G. Saavedra y P. Andrés, "Bifocal Fibonacci diffractive lenses", *IEEE Photonics Journal* **5**, 3400106 (2013).

[Roux04] F. S. Roux, "Distribution of angular momentum and vortex morphology in optical beams", *Optics Communications* **242**, 45–55 (2004).

[Saavedra03] G. Saavedra, W. D. Furlan y J. A. Monsoriu, "Fractal zone plates", *Optics Letters* **28**, 971–973 (2003).

[Sah95] Y. Sah y G. S. Ranganath, "Optical diffraction in some Fibonacci structures", *Optics Communications* **114**, 18–24 (1995).

[Sakdinawat07] A. Sakdinawat y Y. Liu, "Soft-x-ray microscopy using spiral zone plates", *Optics Letters* **32**, 2635–2637 (2007).

[Siemion12] A. Siemion, A. Siemion, M. Makowski, J. Suszek, J. Bomba, A. Czerwinski, F. Garet, J.-L. Coutaz y M. Sypek, "Diffractive paper lens for terahertz optics", *Optics Letters* **37**, 4320–4322 (2012).

[Swartzlander01] J. Swartzlander, "Peering into darkness with a vortex spatial filter", *Optics Letters* **26**, 497–499 (2001).

[Tao06] S. H. Tao, X.-C. Yuan, J. Lin y R. E. Burge, "Sequence of focused optical vortices generated by a spiral fractal zone plate", *Applied Physics Letters* **89**, 031105 (2006).

2.4 Imaging properties of kinoform Fibonacci lenses

Imaging Properties of Kinoform Fibonacci Lenses

6 Author(s)

V. Ferrando ; Centro de Tecnol. Fisicas, Univ. Politec. de Vale`ncia, Valencia, Spain ; A. Calatayud ; P. Andrés ; R. Torroba

more authors

In this paper, we present a new kind of bifocal kinoform lenses in which the phase distribution is based on the Fibonacci sequence. The focusing properties of these DOEs coined Kinoform Fibonacci lenses (KFLs) are analytically studied and compared with binary-phase Fibonacci lenses (FLs). It is shown that, under monochromatic illumination, a KFL drives most of the incoming light into two single foci, improving in this way the efficiency of the FLs. We have also implemented these lenses with a spatial light modulator. The first images obtained with this type of lenses are presented and evaluated.

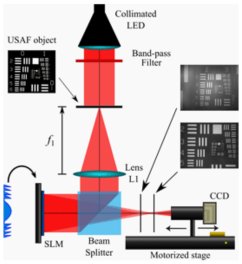

Imaging properties of Kinoform Fibonacci lenses.

Published in:
IEEE Photonics Journal (Volume:6 , Issue: 1)

Article#:
6500106

ISSN :
1943-0655

INSPEC Accession Number:
14110336

DOI:
10.1109/JPHOT.2014.2304560

Date of Publication :
04 February 2014

Date of Current Version :
20 February 2014

Issue Date :
Feb. 2014

Sponsored by :
IEEE Photonics Society

Publisher:
IEEE

Imaging properties of Kinoform Fibonacci Lenses

Vicente Ferrando,[1,2] Arnau Calatayud,[1] Pedro Andrés,[2] Roberto Torroba,[3] Walter D. Furlan[2] and Juan A. Monsoriu[1,*]

[1]Centro de Tecnologías Físicas, Universitat Politècnica de València, E-46022 Valencia, Spain.
[2]Departamento de Óptica, Universitat de València, E-46100 Burjassot, Spain.
[3]Centro de Investigaciones Ópticas (CONICET La Plata-CIC) and UID OPTIMO, Facultad de Ingeniería, Universidad Nacional de La Plata, P.O. Box 3 C.P 1897, La Plata, Argentina
*jmonsori@fis.upv.es

IEEE Photonics Journal **6**, 6500106 (2014).

Abstract In this paper we present a new kind of bifocal kinoform lenses in which the phase distribution is based on the Fibonacci sequence. The focusing properties of these DOEs coined Kinoform Fibonacci Lenses (KFLs) are analytically studied and compared with binary phase Fibonacci Lenses (FLs). It is shown that under monochromatic illumination a KFL drives most of the incoming light into two single foci, improving in this way the efficiency of the FLs. We have also implemented these lenses with a spatial light modulator. The first images obtained with this type of lenses are presented and evaluated.

Over the last decades the role of aperiodic order (order without periodicity [Maciá06]) in nature has been deserved a growing interest by the scientific community. In fact, the observation of nature has allowed scientists to perceive different kinds of morphological orders, being the Fibonacci sequence, one of the most recurrent mathematical fitting models. It is well known that the ratio of two consecutive elements of the Fibonacci sequence approaches asymptotically an irrational number known as the golden mean and that this number is frequently associated with some subjective concepts such as equilibrium, or harmony. Fibonacci series and the golden mean can be found profusely in nature, from the helical arrangement of seeds and leaves of plants [Fleming02]

to all dynamical systems exhibiting the period-doubling route to chaos [Linage06]. Artificial Fibonacci patterns also appear on core/shell structures constructed through stress-driven self assembly induced by cooling [Li05], and the golden mean has recently been found in the fine structure of spin dynamics around critical points in quantum phase transitions [Coldea10], just to name a few. Photonics is a potential field of applications for novel devices designed and constructed using the Fibonacci sequence [Maciá12]. Supported in part by the enormous progress in technology development in this area, quantum cascade lasers based on a Fibonacci distributed feedback sequence [Mahler10], and Fibonacci arrays of nanoparticles that produce quasi-periodic distribution of plasmon modes [Dallapiccola08], have been recently proposed. Following this trend, our group has recently proposed the Fibonacci Lenses (FLs) [Monsoriu13], which are diffractive lenses constructed using the Fibonacci sequence.

A FL is a binary lens that, like a conventional Fresnel zone plate, produces intensity maxima along the optical axis at odd fractions of its main focal distance. However, in this case each focus is axially doubled. These twin foci are located one in front and one behind the focus of an equivalent Fresnel zone plate of the same number of zones. The axial positions of this foci are given by the Fibonacci numbers, being the golden mean the ratio of the two FL focal distances. Moreover, we found that the golden mean is also the responsible of the energetic balance of both foci and also of their axial and transverse resolution. Inspired on FLs we recently proposed a new type of bifocal vortex lenses, the Fibonacci Vortex Lenses (FVLs) [Calatayud13b], that produce a twin optical vortices along the axial coordinate. The positions of these vortices depend on the two incommensurable periods of the Fibonacci sequence in which the FVL is based on. The radii of these twin vortices increase with the topological charge of the vortex lens and their ratio is the golden mean. Although the binary FL and FVL are effective in controlling the luminous intensity, their diffraction efficiency is relatively low.

Since the diffraction efficiency of Diffractive Optical Elements (DOEs) is crucial for certain practical applications, in this work we introduce the concept of Kinoform Fibonacci Lenses (KFLs), i.e., blazed zone plates with a radial structure based on the Fibonacci sequence. KFLs design is formally presented in this paper and an analytical expression for the phase profile is derived.

As blazed DOEs, KFLs drive most of the incoming light into a splitted main focus, improving in this way the efficiency of FLs. This fact is demonstrated theoretically by means of the Modulation Transfer Function (MTF) and experimentally in an image forming experiment.

Kinoform Fibonacci lenses design

A KFL is defined as a pure phase diffractive element whose radial phase distribution is obtained from the Fibonacci sequence as follows: Starting with two elements (seeds) $F_0 = 0$ and $F_1 = 1$, the Fibonacci numbers, $F_j = \{0,1,1,2,3,5,8,13,21,\ldots\}$, are obtained by the sequential application of the iterative rule $F_{j+1} = F_j + F_{j-1}$, $(j = 1,2,\ldots)$. The golden mean, or golden ratio, is defined as the limit of two consecutive Fibonacci numbers: $\varphi = \lim_{j\to\infty} F_j/F_{j-1} = \left(1+\sqrt{5}\right)/2$.

In a similar way, a binary aperiodic Fibonacci sequence can also be deterministically generated with two seed elements, as for exemple, $S_1 = \{A\}$ and $S_0 = \{B\}$ and the succesive elements of the sequence are obtained simply as the concatenation of the two previous ones: $S_{j+1} = \{S_j S_{j-1}\}$ for $j \geq 1$. In this way, $S_2 = \{AB\}$, $S_3 = \{ABA\}$, $S_4 = \{ABAAB\}$, $S_5 = \{ABAABABA\}$, and so on. Note that, in any given sequence of order S_j, two succesive "B" are separated by either, one or two "A", and that the total number of elements F_{j+1}, results from the sum of F_j elements "A", and F_{j-1} elements "B". In the design of a KFL each element of the Fibonacci sequence can be used to define the generating function, $\Phi(\zeta)$, for the radial phase distribution of the lens: With compact support in the interval [0,1], $\Phi(\zeta)$ is defined with a linear variation between $\Phi = 0$ and $\Phi = 2\pi$ at each subinterval $\{AB\}$ of the sequence, being $\Phi = 0$ otherwise (see Fig. 2.4.1(a). Thus, the generating function of the radial phase for the j^{th} order KFL can be written analytically as

$$\Phi_j^{KFL}(\zeta) = -\frac{2\pi}{2d_j}\sum_{i=1}^{F_{j-1}} \mathrm{rect}\left(\frac{\zeta-\zeta_{i,j}}{2d_j}\right)(d_j+\zeta_{i,j}-\zeta)\,, \qquad (2.4.1)$$

where $d_j = 1/F_{j+1}$, $\zeta = r^2/a^2$ is the normalized radial coordinate, and $\zeta_{i,j}$ is the position for the i^{th} element "B" of the sequence. This position can be obtained as $\zeta_{i,j} = (\lfloor(\varphi+1)\,i\rfloor - 1)\cdot d_j$, being $\lfloor x\rfloor$ the floor function of x [Redish90].

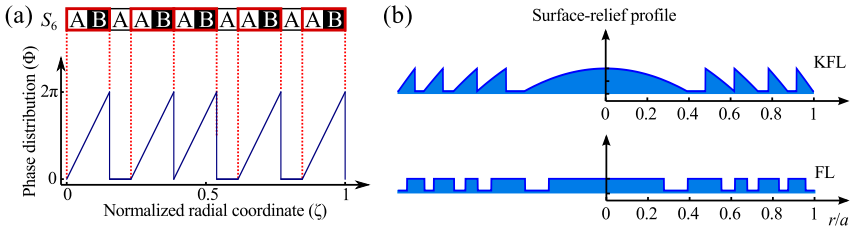

Figure 2.4.1: (a) Phase profile of the S_6 based KFL represented against a squared radial coordinate. (b) KFL and FL surface-relief profiles generated from a Fibonacci sequence of order $j = 6$.

For example, applying Eq. (2.4.1), the generating function of the radial phase for $j = 6$ order is given by:

$$\begin{aligned}\Phi_6^{KFL}(\zeta) \quad = \quad & -\pi(2-13\zeta)\text{rect}\left[\frac{(\zeta-1/13)}{2/13}\right] - \pi(5-13\zeta)\text{rect}\left[\frac{(\zeta-4/13)}{2/13}\right] \\ & -\pi(7-13\zeta)\text{rect}\left[\frac{(\zeta-6/13)}{2/13}\right] - \pi(10-13\zeta)\text{rect}\left[\frac{(\zeta-9/13)}{2/13}\right] \\ & -\pi(13-13\zeta)\text{rect}\left[\frac{(\zeta-12/13)}{2/13}\right] .\end{aligned} \tag{2.4.2}$$

The profile of the KFL generated by Eq. (2.4.2) is represented in Fig. 2.4.1(b). For comparison the radial profile of a FL of the same focal distance is represented in the same figure. As can be seen obtaining the phase of a KFL from the phase of FL is not a trivial task as it is for a Kinoform Fresnel lens from a binary phase Fresnel lens. As it was not previously reported, the generating function of the radial phase corresponding to a FL, Φ_j^{FL}, is defined here for completeness:

$$\Phi_j^{FL}(\zeta) = \pi \sum_{i=1}^{F_{j-1}} \text{rect}\left(\frac{\zeta - \zeta_{i,j} - \frac{d_j}{2}}{d_j}\right) . \tag{2.4.3}$$

Focusing and imaging properties

To evaluate the focusing properties of the KFLs it is of interest to compute the axial irradiance provided by these lenses normally illuminated by a plane

wave of wavelength λ. Within the Fresnel aproximation the axial irradiance function is given by

$$I(u) = 4\pi u^2 \left| \int_0^1 t(\zeta) \exp(-2\pi i u \zeta) d\zeta \right|^2 , \qquad (2.4.4)$$

where $u = a^2/2\lambda z$ is the reduced axial coordinate, a is the lens radi, $t(\zeta) = \exp[i\Phi(\zeta)]$ is the transmitance function, being $\Phi_j(\zeta)$ the phase of the lens. By using the Eq. (2.4.4) we have computed the axial irradiances provided by KFLs of order S_8 and S_{10} and for comparison pourposes those corresponding to FLs of the same orders. The results are shown in Fig. 2.4.2.

As can be seen the KFLs drive most of the incoming light into two single foci located at $u_1 \simeq F_{j-1}$ and $u_2 \simeq F_j$, being the ratio of the focal distances $u_2/u_1 \simeq \varphi$. On the other hand, as shown in [Monsoriu13], FLs provide multiple diffraction orders due to the binary nature of the structure. Each order presents two diffraction peaks, due to its quasiperiodic distribution of zones with two inconmensurable periods. The first order foci of the FL coincide with the foci of the KFL, but their relative intensity is 60 % lower.

The performance of a KFL as an image forming device is analyzed in the spatial-frequency domain by calculation of the MTFs at the two focal planes (see Fig. 2.4.3). To that end, a MATLAB algorithm has been employed for numerically evaluating the autocorrelation function of the generalized pupil function represented in a 1001×1001 matrix. As can be seen, in a similar fashion to the effect of the kinoform profile on the axial irradiance, the MTFs reveal the improved performance of a KFL provided by the blazed profile, especially in the mid-low range of frequencies.

We have experimentally tested the imaging capabilities of KFLs and FLs of the same main focal distances. A schematic illustration of the experimental setup if shown in Fig. 2.4.4(a). The diffractive lenses were implemented on a Liquid Crystal in a Silicon SLM (Holoeye PLUTO, 8-bit gray-level, pixel size $8\,\mu$m, and resolution 1920×1080 pixels), calibrated for a 2π phase shift at $\lambda = 633$ nm and operating in phase-only modulation mode. The illumination system consists of a red collimated LED (Mounted High-Power LED, red 625 nm, 1000 mA) and a band-pass filter ($\lambda = 632.8 \pm 0.6$ nm). A test object (the 1951 USAF resolution test chart) was mounted at the focal plane of achromatic Badal Lens, L_1, (focal length: 160 mm). The images produced

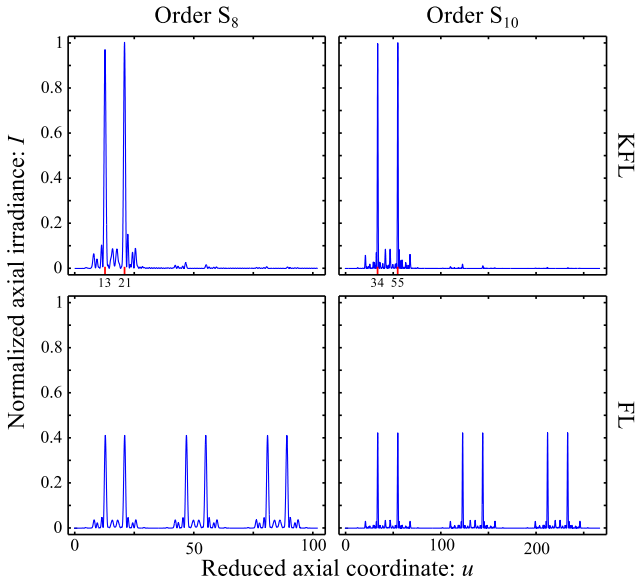

Figure 2.4.2: Normalized axial irradiances provided by FLs and KFLs of orders S_8 and S_{10}.

by the diffractive lenses were captured and registered with a CCD camera (8 bit gray-level, pixel pitch of $3.75\,\mu$m, and 1280×960 pixels) mounted on a translation stage (Thorlabs LTS 300; range: 300 mm; precision: $5\,\mu$m) along the optical axis. The images produced by a KFL and a FL at both focal planes are shown in Fig. 2.4.4(b). A profile of the irradiance, measured along a single element of the image of the test is shown in Fig. 2.4.4(c). As can be seen, the images provided by the KFL have higher contrast, C, than those provided by the FL of the same order ($C_{FL}/C_{KFL} \approx 0.6641$). On the other hand it can be observed that, as expected, the relative size of the images at both planes also are related by the golden ratio. In fact in Fig. 2.4.4(b) the relative sizes of the segments a and b satisfy $a/b \approx \varphi$.

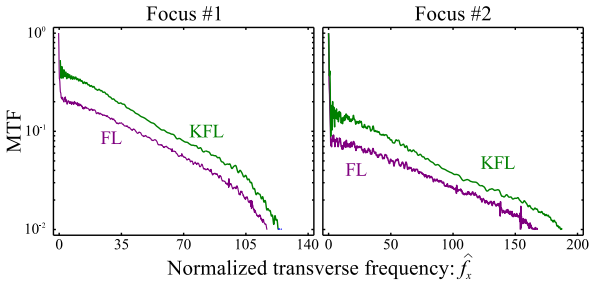

Figure 2.4.3: MTFs at both foci of KFL and FL of the same order (S_{10}).

Conclusions

We have presented a novel design of Fibonacci lenses with improved focusing and imaging capabilities. These lenses have a blazed profile whose analytical expression has been deduced. KFLs present two single foci, being the golden mean, the ratio of the two focal distances. The higher quality of the images produced by KFLs are demonstrated theoretically and experimentally. On the one hand, the MTFs obtained for KFLs display superior performance over the MTFs obtained for FLs. Moreover, the first images produced by these kind of lenses are reported. Due to their exclusive properties, we believe that KFLs could be of benefit in several potential applications for instance, in optical trapping, in optical micromachining, and in confocal microscopy. In particular, we suggest that the bifocal structure of a KFL can find applications in Ophthalmology to design intraocular or contact lenses for the correction of presbyopia. Additionally, the concept of FKL can be easily extended to other geometries, like square zone plates [Calatayud13a]. For different applications further resolution improvements can be obtained by using higher Fibonacci orders in the lens design and/or by combining two or more Fibonacci orders in a single lens [Giménez10].

Acknowledgments

We acknowledge the financial support from Ministerio de Economía y Competitividad (grant FIS2011-23175), Generalitat Valenciana (grant PROMETEO2009-077), and Universitat Politècnica de València (INNOVA

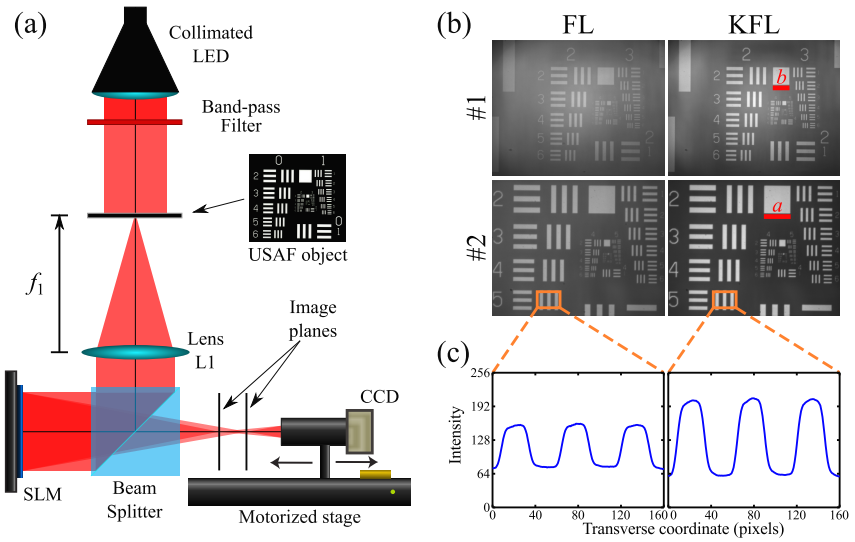

Figure 2.4.4: (a) Experimental setup employed for recording the images produced by KFLs and FLs. (b) Images of the USAF object produced by a KFL and a FL of order S_{10} at focus #1 and focus #2. (c) Profiles of the irradiances obtained at focus #2 of both for the vertical 2-4 group images.

SP20120569), Spain. R. T. also acknowledges financial support from the following grants: CONICET No. 0863/09 and No. 0549/12 (Argentina), Facultad de Ingeniería, Universidad Nacional de La Plata No. 11/I168 (Argentina).

Referencias

[Calatayud13a] A. Calatayud, V. Ferrando, F. Giménez, W. D. Furlan, G. Saavedra y J. A. Monsoriu, "Fractal square zone plates", *Optics Communications* **286**, 42–45 (2013).

[Calatayud13b] A. Calatayud, V. Ferrando, L. Remón, W. D. Furlan y J. A. Monsoriu, "Twin axial vortices generated by Fibonacci lenses", *Optics Express* **21**, 10234–10239 (2013).

[Coldea10] R. Coldea, D. A. Tennant, E. M. Wheeler, E. Wawrzynska, D. Prabhakaran, M. Telling, K. Habicht, P. Smeibidl y K. Kiefer, "Quantum criticality in an Ising chain: experimental evidence for emergent E8 symmetry", *Science* **327**, 177–180 (2010).

[Dallapiccola08] R. Dallapiccola, A. Gopinath, F. Stellacci y L. Dal Negro, "Quasi-periodic distribution of plasmon modes in two-dimensional Fibonacci arrays of metal nanoparticles", *Optics Express* **16**, 5544–5555 (2008).

[Fleming02] A. J. Fleming, "Plant mathematics and Fibonacci's flowers", *Nature* **418**, 723 (2002).

[Giménez10] F. Giménez, W. D. Furlan, A. Calatayud y J. A. Monsoriu, "Multifractal zone plates", *Journal of the Optical Society of America A* **27**, 1851–1855 (2010).

[Li05] C. Li, X. Zhang y Z. Cao, "Triangular and Fibonacci number patterns driven by stress on core/shell microstructures", *Science (New York, N.Y.)* **309**, 909–911 (2005).

[Linage06] G. Linage, F. Montoya, A. Sarmiento, K. Showalter y P. Parmananda, "Fibonacci order in the period-doubling cascade to chaos", *Physics Letters A* **359**, 638–639 (2006).

[Maciá06] E. Maciá, "The role of aperiodic order in science and technology", *Reports on Progress in Physics* **69**, 397–441 (2006).

[Maciá12] E. Maciá, "Exploiting aperiodic designs in nanophotonic devices", *Reports on Progress in Physics* **75**, 036502 (2012).

[Mahler10] L. Mahler, A. Tredicucci, F. Beltram, C. Walther, J. Faist, H. E. Beere, D. A. Ritchie y D. S. Wiersma, "Quasi-periodic distributed feedback laser", *Nature Photonics* **4**, 165–169 (2010).

[Monsoriu13] J. A. Monsoriu, A. Calatayud, L. Remón, W. D. Furlan, G. Saavedra y P. Andrés, "Bifocal Fibonacci diffractive lenses", *IEEE Photonics Journal* **5**, 3400106 (2013).

[Redish90] K. A. Redish y W. F. Smyth, "Closed form expressions for the iterated floor function", *Discrete Mathematics* **91**, 317–321 (1990).

2.5 3D printed diffractive terahertz lenses

3D printed diffractive terahertz lenses

Walter D. Furlan,[1,*] Vicente Ferrando,[1,2] Juan A. Monsoriu,[2] Przemysław Zagrajek,[3] Elżbieta Czerwińska,[3] and Mieczysław Szustakowski[3]

[1]Departamento de Óptica y Optometría y Ciencias de la Visión, Universitat de València, 46100 Burjassot, Spain.
[2]Centro de Tecnologías Físicas, Universitat Politècnica de València, 46022 Valencia, Spain.
[3]Institute of Optoelectronics, Military University of Technology, Warsaw, Poland
*walter.furlan@uv.es

Optics Letters **41**, 1748-1751 (2016).

Abstract A 3D printer was used to realize custom made diffractive THz lenses. After testing several materials, phase binary lenses with periodic and aperiodic radial profiles were designed and constructed in polyamide material to work at 0.625 THz. The non conventional focusing properties of such lenses were assessed by computing and measuring their axial point spread function (PSF). Our results demonstrate that inexpensive 3D printed THz diffractive lenses can be reliably used in focusing and imaging THz systems. Diffractive THz lenses with unpreceded features such as extended depth of focus or bifocalization have been demonstrated.

Many applications of THz radiation such as THz imaging or THz spectroscopy require passive devices for guiding and manipulating this type of radiation, including filters [Wilk09], waveguides [Astley10], waveplates [Scherger11c], and lenses [Scherger11a, Scherger11b]. Several polymers with low absorbance and dispersion [Podzorov08] are used to obtain THz lenses, and consequently, the variety of commercially available THz lenses is increasing. However, in many cases custom-made THz lenses with a special design are required. Individual refractive THz lenses are mainly manufactured from bulk polymers by milling, turning, or compression molding of polymer powders [Scherger11b]. In particular for geometrically complex lenses, this

requires high effort and sometimes results in an unwanted waste of material.

In THz setups, beam shaping optical elements are very important in almost every application. Mirrors and lenses should allow improved sensitivity of detection, what is crucial in this range of the electromagnetic radiation, where there is a lack of high power sources and sensitive detectors. Therefore, as happens in the visible range, THz technology could benefit from novel diffractive structures with unique properties designed for special applications. In fact, some diffractive THz optical elements have been proposed [Wang02, Yu09, Goldsmith92, Wiltse05] and their assessment indicates that the performance of diffractive THz lenses is comparable, or even better, than that obtained with their refractive homologous. Additionally, diffractive lenses can be fabricated with high numerical aperture [Siemion12] and allow for linear and compact setups. However, customized diffractive lenses made by conventional techniques such as reactive ion etching [Agafonov13] or lathe turning [Walsby02] are not widely available, because their construction consists of several steps and requires specialized equipment. In this regard, Komlenok, et al [Komlenok15] demonstrated the possibility of fabricating a silicon multilevel THz diffractive optical element, constructed by means of laser ablation process.

Very recently, 3D printing technology has begun to be employed to construct spherical [Busch14], aspherical [Squires14], and hyperbolic lenses [Suszek15] for THz and sub-THz radiation range. In an effort to provide rapid and low cost solutions of complex THz lenses in this letter we propose the use of 3D printing technology for constructing non-conventional, fractal [Saavedra03] and Fibonacci [Monsoriu13], THz binary diffractive lenses. The performance of these prototypes was numerically evaluated and experimentally tested.

Several 3D printing materials including Nylon Polyamide (PA6) and Acrylonitrile-Butadiene-Styrene (ABS) with two different densities were tested. In particular, we measured their absorption coefficient and refractive index in the $0.1 - 2.0\,\mathrm{THz}$ frequency range, using Time Domain Spectroscopy (TDS) [Lee09]. A commercial equipment, TPS Spectra 3000 (Teraview Ltd, Cambridge, UK) was used to this end. During the measurement two spectrograms were obtained: a reference spectrogram, to take into account the influence of the setup, and a spectrogram of the investigated material using

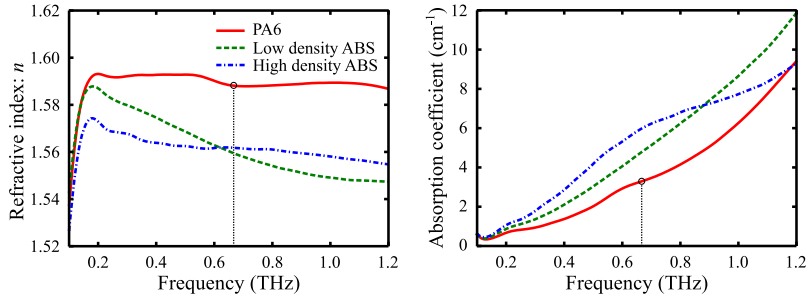

Figure 2.5.1: Refractive index of various materials obtained in the TDS system.

a probe of constant thickness. The transmission type measurement, executed in the time domain, provided the phase difference of the radiation passing through the sample φ_s and the reference setup φ_r ,then, the refractive index as a function of frequency, ν, was calculated in terms the sample thickness, d, as: [Han01, Hangyo02, Naftaly07]

$$n(\nu) = 1 + c\left(\varphi_s(\nu) - \varphi_r(\nu)\right)/(2\pi\nu d)\,. \tag{2.5.1}$$

The results are presented in Fig. 2.5.1. Prototypes of diffractive lenses were constructed in these materials to select the one that presented the highest fidelity compared to the original design PA 6 with a refractive index $n = 1.59$ and absorption coefficient $3.09\,\mathrm{cm}^{-1}$ at $0.625\,\mathrm{THz}$ was selected for the realization of the lenses. Unless this material was previously characterized by using a THz time-domain spectrometry in the frequency range $2-15\,\mathrm{THz}$ [D'Angelo14],to the best of our knowledge, to date PA6 has not been measured for lower frequencies neither used to construct diffractive lenses.

In designing THz diffractive lenses we followed the procedure described in detail in Refs. [Saavedra03] and [Monsoriu13]. In this case the fractal zone plate was based on a triadic Cantor set for stage 2, and the Fibonacci zone plate was based on the Fibonacci sequence of order 5. Figure 2.5.2 shows the experimental models which were designed using a browser-based CAD software (Tinkercad.com), and constructed with a 0.3 mm spatial resolution by an online 3D printing service (i.materialise, Leuven, Belgium), which were made from a polyamide granular powder by selective laser sintering technique.

The diameter of the Fresnel and fractal lenses was 4.62 cm, having both the main focal distance (first diffraction order) $f = 12.35$ cm. The bifocal Fibonacci lens diameter was 4.94 cm, with focal distances $f_1 = 12.9$ cm and $f_2 = 20.0$ cm. All lenses had the same base layer thickness: 1 mm, and grooves height: 0.4 mm; which has been calculated to provide alternating zones with a 0 and π phase delay for the design frequency: 625 GHz.

Using the nonparaxial scalar diffraction theory the axial irradiance provided by these lenses of a given radius a was numerically evaluated as:

$$I(z) = \left| \int_0^1 \exp[i\pi\phi(\zeta)] \cdot \frac{\exp\left[\frac{2\pi i a}{\lambda}\sqrt{\zeta + \left(\frac{z}{a}\right)^2}\right]}{\sqrt{\zeta + \left(\frac{z}{a}\right)^2}} d\zeta \right|^2 , \qquad (2.5.2)$$

where λ is the wavelength, z is the propagated distance, and $\phi(\zeta)$ defines the phase distribution of the studied lens represented in terms of the square normalized radial coordinate, $\zeta = (r/a)^2$. The phase function $\phi(\zeta)$ for Fresnel lenses can be written as a Ronchi-type periodic binary function with period p

$$\phi(\zeta) = \phi_{\mathrm{F}}(\zeta, p) = \mathrm{rect}[\zeta - 0.5] \cdot \mathrm{rect}\left[\frac{\mathrm{mod}[\zeta + 0.5p - 1, p]}{p}\right] , \qquad (2.5.3)$$

where $p = 2/9$ for the Fresnel lens shown in Fig. 2.5.2(a) and the function $\mathrm{mod}[x, y]$ gives the remainder on division of x by y. The corresponding phase function $\phi(\zeta)$ for triadic Cantor lenses developed up to a certain growing stage S can be written as the above periodic function as

$$\phi(\zeta) = \phi_{\mathrm{Frac}}(\zeta, S) = \prod_{i=0}^{S} \phi_{\mathrm{F}}\left(\zeta, 2/3^i\right) , \qquad (2.5.4)$$

being $S = 2$ for the fractal lens shown in Fig. 2.5.2(b). In the case of a Fibonacci lens of order S, the phase function $\phi(\zeta)$ is given by

$$\phi(\zeta) = \phi_{\mathrm{Fibonacci}}(\zeta, S) = \sum_{i=0}^{F_S} \mathrm{rect}[\zeta F_{S+1} + 0.5 + \lfloor i\varphi \rfloor] , \qquad (2.5.5)$$

where F_j is the Fibonacci number of order j, φ is the golden ratio [Monsoriu13], and $\lfloor x \rfloor$ denotes the largest integer less than or equal to x. Figure 2.5.2(c) shows a Fibonacci lens of order $S = 5$.

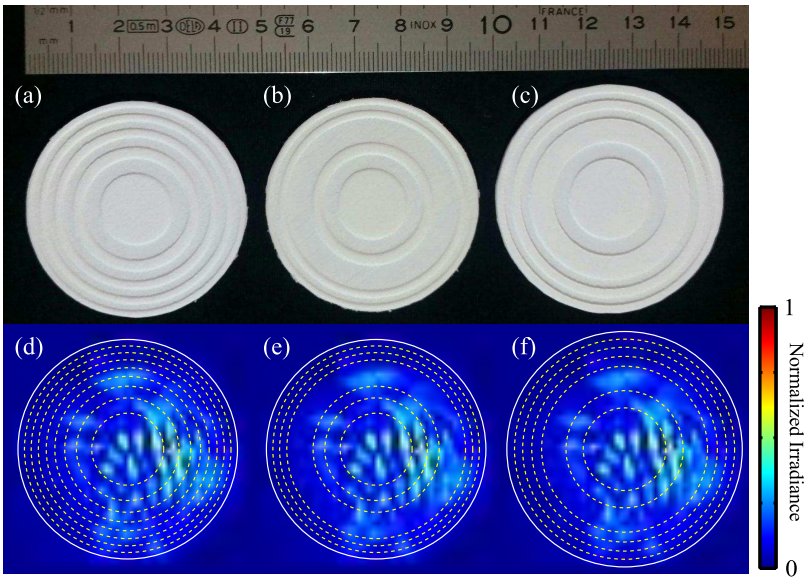

Figure 2.5.2: Experimental (a) Fresnel, (b) fractal, and (c) Fibonacci models of 3D printed THz diffractive lenses made PA6. Map of the THz irradiance measured at the plane of the lens in the experimental setup represented in Fig. 2.5.3 (dotted lines represent the phase transitions) for (d) Fresnel, (e) fractal, and (f) Fibonacci lenses.

The experimental setup for the optical characterization of the lenses is shown in Fig. 2.5.3. The axial point spread function (PSF) was measured with a 625 GHz beam provided by a VDI frequency multiplier (Virginia Diodes, Inc. Charlottesville, VA. USA). The emitter was equipped with a horn antenna which produced a divergent beam, which was focused by a high density polyethylene (HDPE) refractive lens into a pinhole (2 mm diameter). Next the beam was collimated by a second HDPE lens and directed to the investigated diffractive lens. Fig. 2.5.2(d-f) shows the local irradiance of the electromagnetic field at the plane of the lenses. The local maxima and minima of irradiance were caused by interferences during beam propagation. Besides, the main spots are not perfectly centered because, despite that the experimental setup was carefully configured to maintain the center of the beam on the optical axis, a small misalignment still remained. The focal volume was axially

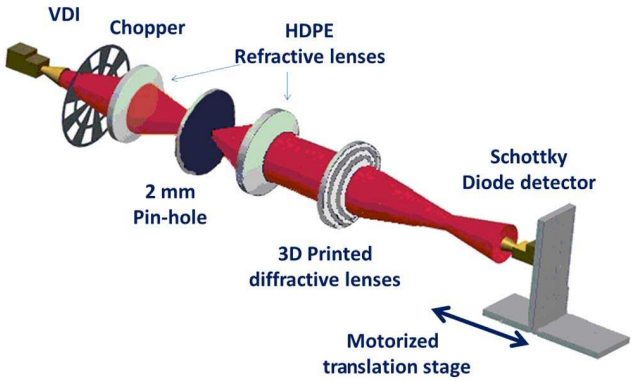

Figure 2.5.3: Scheme of the optical setup used for axial PSF measurements.

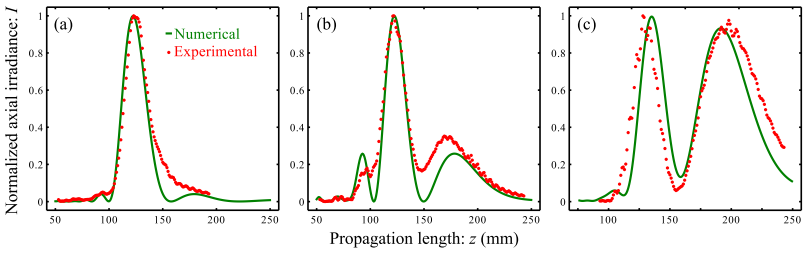

Figure 2.5.4: Numerical simulation, continuous (green) lines and experimental results (dotted) red lines provided by the 3D printed THz lenses of Fig. 2.5.2: (a) Fresnel, (b) fractal, and (c) Fibonacci.

scanned with a Schottky diode (equipped with a horn antenna) mounted on a motorized stage. Due to its finite size, the detector integrates the irradiance in an area of 2.5 mm $\times$ 2.5 mm around the optical axis.

Experimental results for the axial PSF are represented in Fig. 2.5.4 (dotted red points) together with the numerical results (continuous green lines) computed using Eqs. (2.5.2-2.5.5). As can be seen, the fractal binary lens has an extended depth of focus compared with conventional Fresnel zone plate, while Fibonacci lens splits the main focus, providing a pair of foci satisfying $f_1/f_2 \approx \varphi$. Although, the experimental results are affected by the finite size of the detector and by the inhomogeneity of the THz beam (see Fig. 2.5.2(d-f)),

a very good agreement between theory and experiment can be observed.

Summarizing, we have demonstrated the feasibility of realizing high quality THz diffractive lenses with 3D printing technology. The focusing properties of nonconventional lenses named: fractal and Fibonacci zone plates were tested using 0.625 THz beam for the first time. Using non paraxial scalar diffraction theory we have shown numerically the special performance of such lenses which were confirmed experimentally using a simple experimental THz PSF setup. We found that T-ray fractal zone binary lens have an extended depth of focus compared with Fresnel zone plate which opens the possibility to fabricate optics with low chromatic aberration for wideâband THz applications. Concerning to diffractive THz optics with extended depth of focus, Agafonov et al. [Agafonov16] recently presented interesting results of a silicon binary diffractive optical element focusing a THz laser Gaussian beam into a paraxial segment. On the other hand, a bifocal Fibonacci THz lens has been also constructed, which has potential applications in THz quality control systems or THz medical diagnosis and therapy [Liu16]. Moreover, with the advance of the 3D technology, better resolutions will allow the construction of lenses with multilevel (even kinoform) diffractive structures with improved diffraction efficiency.

Although for our investigations we have chosen a Fresnel, fractal and Fibonacci lenses of fixed focal lengths, the versatile 3D printing technology can be applied to construct lenses with different focal lengths and geometries (multiorder, elliptical, conical, etc.) and even array of lenses with any spatial distribution. Moreover, the diffraction efficiency can be increased with the number of phase levels. Work is in progress in these directions.

Funding

Ministerio de Economí a y Competitividad (MINECO) (FIS2011-23175); Generalitat Valenciana (PROMETEOII/2014/072); National Center for Research and Development in Poland (LIDER/020/319/L-5/13/NCBR/2014)

Acknowledgement

The authors thank A. Hermida for his help in the 3D printing of the prototypes.

Referencias

[Agafonov13] A. N. Agafonov, B. O. Volodkin, A. K. Kaveev, B. A. Knyazev, G. I. Kropotov, V. S. Pavelyev, V. A. Soifer, K. N. Tukmakov, E. V. Tsygankova y Y. Y. Choporova, "Silicon diffractive optical elements for high-power monochromatic terahertz radiation", *Optoelectronics, Instrumentation and Data Processing* **49**, 189–195 (2013).

[Agafonov16] A. N. Agafonov, B. O. Volodkin, D. G. Kachalov, B. A. Knyazev, G. I. Kropotov, K. N. Tukmakov, V. S. Pavelyev, D. I. Tsypishka, Y. Y. Choporova y A. K. Kaveev, "Focusing of Novosibirsk Free Electron Laser (NovoFEL) radiation into paraxial segment", *Journal of Modern Optics* **63**, 1051–1054 (2016).

[Astley10] V. Astley, J. Scheiman, R. Mendis y D. M. Mittleman, "Bending and coupling losses in terahertz wire waveguides", *Optics letters* **35**, 553–555 (2010).

[Busch14] S. F. Busch, M. Weidenbach, M. Fey, F. Schäfer, T. Probst y M. Koch, "Optical Properties of 3D Printable Plastics in the THz Regime and their Application for 3D Printed THz Optics", *Journal of Infrared, Millimeter, and Terahertz Waves* **35**, 993–997 (2014).

[D'Angelo14] F. D'Angelo, Z. Mics, M. Bonn, D. Turchinovich, F. D'Angelo, Z. Mics, M. Bonn y D. Turchinovich, "Ultra-broadband THz time-domain spectroscopy of common polymers using THz air photonics", *Optics Express* **22**, 12475–12485 (2014).

[Goldsmith92] P. F. Goldsmith y P.F. Goldsmith, "Zone plate lens antennas for millimeter and submillimeter wavelengths", "Third International Symposium on Space Terahertz Technology", 345–361 (1992).

[Han01] P. Y. Han y X.-C. Zhang, "Free-space coherent broadband terahertz time-domain spectroscopy", *Measurement Science and Technology* **12**, 1747–1756 (2001).

[Hangyo02] M. Hangyo, T. Nagashima y S. Nashima, "Spectroscopy by pulsed terahertz radiation", *Measurement Science and Technology* **13**, 1727–1738 (2002).

[Komlenok15] M. S. Komlenok, B. O. Volodkin, B. A. Knyazev, V. V. Kononenko, T. V. Kononenko, V. I. Konov, V. S. Pavelyev, V. A. Soifer, K. N. Tukmakov y Y. Y. Choporova, "Fabrication of a multilevel THz Fresnel lens by femtosecond laser ablation", *Kvant. electron.* **45**, 933–936 (2015).

[Lee09] Y.-S. Lee, *Principles of Terahertz Science and Technology*, Springer (2009).

[Liu16] W.-Q. Liu, Y.-F. Lu, G.-H. Jiao, X.-F. Chen, J.-Y. Li, S.-H. Chen, Y.-M. Dong y J.-C. Lv, "Terahertz optical properties of the cornea", *Optics Communications* **359**, 344–348 (2016).

[Monsoriu13] J. A. Monsoriu, A. Calatayud, L. Remón, W. D. Furlan, G. Saavedra y P. Andrés, "Bifocal Fibonacci diffractive lenses", *IEEE Photonics Journal* **5**, 3400106 (2013).

[Naftaly07] M. Naftaly y R. E. Miles, "Terahertz Time-Domain Spectroscopy for Material Characterization", *Proceedings of the IEEE* **95**, 1658–1665 (2007).

[Podzorov08] A. Podzorov y G. Gallot, "Low-loss polymers for terahertz applications", *Applied Optics* **47**, 3254–3257 (2008).

[Saavedra03] G. Saavedra, W. D. Furlan y J. A. Monsoriu, "Fractal zone plates", *Optics Letters* **28**, 971–973 (2003).

[Scherger11a] B. Scherger, C. Jördens y M. Koch, "Variable-focus terahertz lens", *Optics express* **19**, 4528–4535 (2011).

[Scherger11b] B. Scherger, M. Scheller, C. Jansen, M. Koch y K. Wiesauer, "Terahertz lenses made by compression molding of micropowders", *Applied optics* **50**, 2256–2262 (2011).

[Scherger11c] B. Scherger, M. Scheller, N. Vieweg, S. T. Cundiff y M. Koch, "Paper terahertz wave plates", *Optics express* **19**, 24884–24889 (2011).

[Siemion12] A. Siemion, A. Siemion, M. Makowski, J. Suszek, J. Bomba, A. Czerwinski, F. Garet, J.-L. Coutaz y M. Sypek, "Diffractive paper lens for terahertz optics", *Optics Letters* **37**, 4320–4322 (2012).

[Squires14] A. D. Squires, E. Constable y R. A. Lewis, "3D printing of aspherical terahertz lenses and diffraction gratings", "2014 39th International Conference on Infrared, Millimeter, and Terahertz waves (IRMMW-THz)", 1–2, IEEE (2014).

[Suszek15] J. Suszek, A. Siemion, M. S. Bieda, N. Blocki, D. Coquillat, G. Cywinski, E. Czerwinska, M. Doch, A. Kowalczyk, N. Palka, A. Sobczyk, P. Zagrajek, M. Zaremba, A. Kolodziejczyk, W. Knap y M. Sypek, "3-D-Printed Flat Optics for THz Linear Scanners", *IEEE Transactions on Terahertz Science and Technology* **5**, 314–316 (2015).

[Walsby02] E. D. Walsby, S. Wang, J. Xu, T. Yuan, R. J. Blaikie, S. M. Durbin, X.-C. Zhang y D. R. S. Cumming, "Multilevel silicon diffractive optics for terahertz waves", *Journal of Vacuum Science & Technology B: Microelectronics and Nanometer Structures* **20**, 2780–2783 (2002).

[Wang02] S. Wang, X. C. Zhang, M. P. Maley, M. F. Hundley, L. N. Bulaevskii, A. E. Koshelev y A. J. Taylor, "Terahertz Tomographic Imaging With a Fresnel Lens", *Optics and Photonics News* **13**, 58–58 (2002).

[Wilk09] R. Wilk, N. Vieweg, O. Kopschinski y M. Koch, "Liquid crystal based electrically switchable Bragg structure for THz waves", *Optics Express* **17**, 7377–7382 (2009).

[Wiltse05] J. C. Wiltse, "Zone plate designs for terahertz waves", R. J. Hwu, D. L. Woolard y M. J. Rosker, eds., "Defense and Security. Proceeding of SPIE Symposium", 167–179, SPIE-INT SOC OPTICAL ENGINEERING (2005).

[Yu09] Y. Yu y W. Dou, "Generation of pseudo-Bessel beams at THz frequencies by use of binary axicons", *Optics Express* **17**, 888–893 (2009).

2.6 Bifractal focusing and imaging properties of Thue–Morse Zone Plates

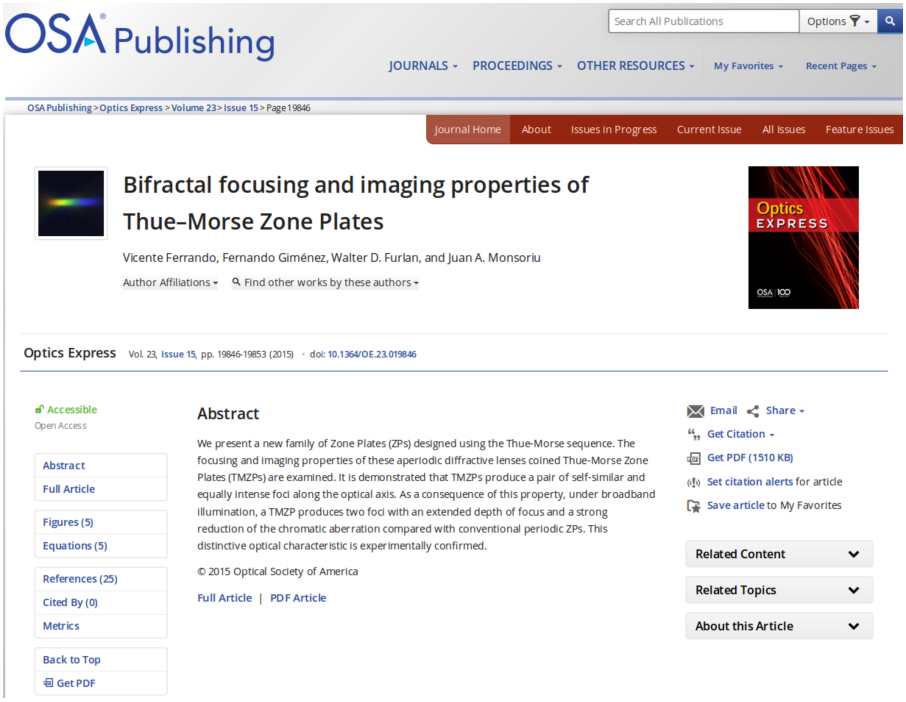

Bifractal focusing and imaging properties of Thue–Morse Zone Plates

Vicente Ferrando,[1,2] Fernando Giménez,[3] Walter D. Furlan[2] and Juan A. Monsoriu[1,*]

[1]Centro de Tecnologías Físicas, Universitat Politècnica de València, E-46022 Valencia, Spain.
[2]Departamento de Óptica, Universitat de València, E-46100 Burjassot, Spain.
[3]I.U. Matemática Pura y Aplicada, Universitat Politècnica de València, E-46022 Valencia, Spain.
*jmonsori@fis.upv.es

Optics Express **23**, 19846–19853 (2015).

Abstract We present a new family of Zone Plates (ZPs) designed using the Thue-Morse sequence. The focusing and imaging properties of these aperiodic diffractive lenses coined Thue-Morse Zone Plates (TMZPs) are examined. It is demonstrated that TMZPs produce a pair of self-similar and equally intense foci along the optical axis. As a consequence of this property, under broadband illumination, a TMZP produces two foci with an extended depth of focus and a strong reduction of the chromatic aberration compared with conventional periodic ZPs. This distinctive optical characteristic is experimentally confirmed.

Introduction

Zone Plates (ZPs) have found a great number of new applications in the last few years [Ojeda-Castañeda96], especially outside of visible range of the electromagnetic spectrum, for example, in X-ray microscopy for the observation of certain nanostructures [Wang03] and in THz optics for tomographic imaging [Wang02]. A standard ZP consist of a series of concentric circular rings of equal area, with alternating absorbing and transmitting zones. The focusing effect is created by the constructive interference of waves passing through the

transmitting zones distributed periodically along the square of the radial coordinate.

In recent years different aperiodic sequences [Maciá06] have been employed to design new types of ZPs with interesting physical properties and many potential applications. Two of them are Fractal Zone Plates [Saavedra03] and Fibonacci Zone Plates [Monsoriu13]. The former ones are characterized by its fractal structure along the square of the radial coordinate, and produce multiple foci along the optical axis which are defined by the self-similar Fourier spectrum of the fractal pupil function. It has been demonstrated these self-similar foci produce an increase of depth of field and a reduction of the chromatic aberration under wideband illumination [Furlan07]. Since their introduction, fractal ZPs have received the attention of several research groups working on different fields, for instance, X-ray microscopy [Ge14], optical tweezers [Tao13], image-forming systems [Zhang12], optical tomography [Zhang11], photon sieves [Liu09], and plasmonics [Fu08].

Fibonacci ZPs are bifocal ZPs with their foci located at certain axial positions given by the Fibonacci numbers, being the "golden mean" the ratio of the two focal distances [Monsoriu13]. Although the focusing and imaging capabilities of Fibonacci lenses have been experimentally demonstrated under monochromatic illumination [Ferrando14b], these lenses are affected by the same limitations of conventional ZPs when broadband illumination is considered, since the twin foci are not self-similar.

In this paper we present a new family of aperiodic ZPs that combine the advantages of fractal ZPs (reduction of the chromatic aberration) and Fibonacci ZPs (bifocusing along the optical axis). The new diffractive lenses are based on the deterministic Thue–Morse sequence. This sequence has been applied in several branches of Physics, as for example in the context of photonic crystals [Tsao14], quantum wells [Hsueh14], metamaterials [Monsoriu07] and graphene superlattices [Huang13]. Here we present the first diffractive lenses contructed using this formalism. We show that a ZP designed according to the Thue–Morse sequence produces two main self-similar foci along the optical axis with extended depth of focus. Therefore, TMZPs are intrinsically bifocal lenses with low chromatic aberration. These properties are theoretically investigated and experimentally demonstrated in an image forming experiment.

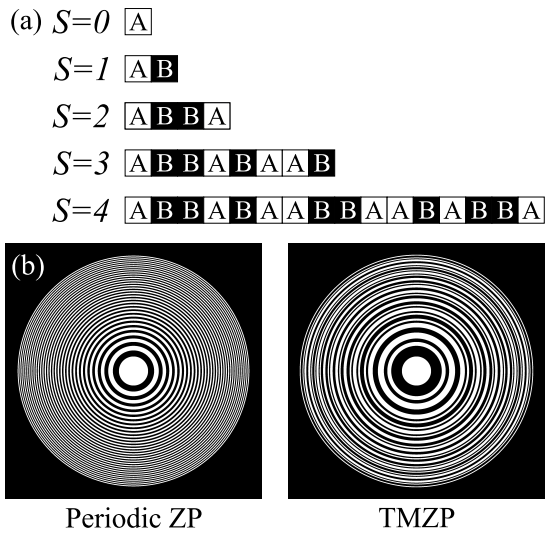

Figure 2.6.1: (a) Geometrical construction of the TM sequence up to order $S = 4$. (b) TMZP of order $S = 6$ and its equivalent periodic ZP.

Focusing properties

A ZP can be constructed starting from a 1D compact supported periodic function $q(\zeta)$, where $\zeta = (r/a)^2$ is the normalized square radial coordinate and a is the external radius of the outermost ring. In a binary ZP every pair of opaque (B) and transparent (A) annular zones constitutes a period, being the area of each period constant over all the ZP. In a similar way, a TMZP can be constructed by replacing the periodic function $q(\zeta)$ by the Thue–Morse sequence. This binary sequence with elements A and B is constructed defining a seed $D_0 = A$ and then, each element that follows the sequence is obtained by replacing A by AB and B by BA. Therefore, the first order is $D_1 = AB$ and the next orders are $D_2 = ABBA$, $D_3 = ABBABAAB$, $D_4 = ABBABAABBAABABBA$, and so on. Figure 2.6.1(a) shows the geometrical construction of the TM sequence up to order $S = 4$.

When designing TMZPs, each of these sequences can be used to define the transmission generating function $q(\zeta)$ with compact support on the interval $\zeta \in [0,1]$. This interval is partitioned in 2^S sub-intervals of length $d_S = 1/2^S$,

and the transmitance value, $t_{S,j}$, that takes at the j-th sub-interval is associated to the value of the element $D_{S,j}$, being $t_{S,j} = 1$ when $D_{S,j}$ is "*A*" and $t_{S,j} = 0$ when $D_{S,j}$ is "*B*". Figure 2.6.1(b) shows the transmitance pupil function of a TMZP of order $S = 6$ and its equivalent periodic ZP. Note that like a conventional ZP the period of a TMZP is $p_S = 2d_S$, where the position of transparent/opaque zones have been interchanged. Therefore, the width of the zones of a TMZP and its equivalent periodic ZP are the same, so both kind of lenses can be fabricated with the same technology. In mathematical terms, the transmitance function, $q(\zeta)$, for both kind of lenses can be written with the same mathematical expression

$$q(\zeta) = \sum_{j=1}^{2^S} t_{S,j} \cdot \mathrm{rect}\left[\frac{\zeta - (j-1/2)\cdot d_S}{d_S}\right]. \tag{2.6.1}$$

To evaluate the focusing properties of TMZPs we have computed the axial irradiance provided by these diffractive lenses under a monochromatic plane wave illumination, using the Fresnel approximation:

$$I(u) = 4\pi u^2 \left| \int_0^1 q(\zeta) \exp\left(-i2\pi u\zeta\right) d\zeta \right|^2, \tag{2.6.2}$$

where $u = a^2/2\lambda z$ is the reduced axial coordinate, and λ is the wavelength of the light. If we consider the pupil function of transmitance (2.6.1) in the above equation, we obtain:

$$I(u) = 4\pi^2 u^2 d_S^2 \mathrm{sinc}^2\left[d_S \cdot u\right] \left| \sum_{j=1}^{2^S} t_{S,j} e^{-i2\pi u j d_S} \right|^2. \tag{2.6.3}$$

We have computed the axial irradiance provided by TMZPs of orders $S = 4, 5$, and 6 and their equivalent periodic ZPs for comparison. The results are shown in Fig. 2.6.2. The axial irradiance distribution, represented against the normalized variable u, shows that the reordering of transparent and opaque zones of a ZP according to the Thue–Morse sequence produces a symmetrical splitting of the first order focus achieving zero axial irradiance at the foci of the equivalent periodic ZP. This zero irradiance is due to the destructive interference produced by the fields transmited by the two conjugated parts of the

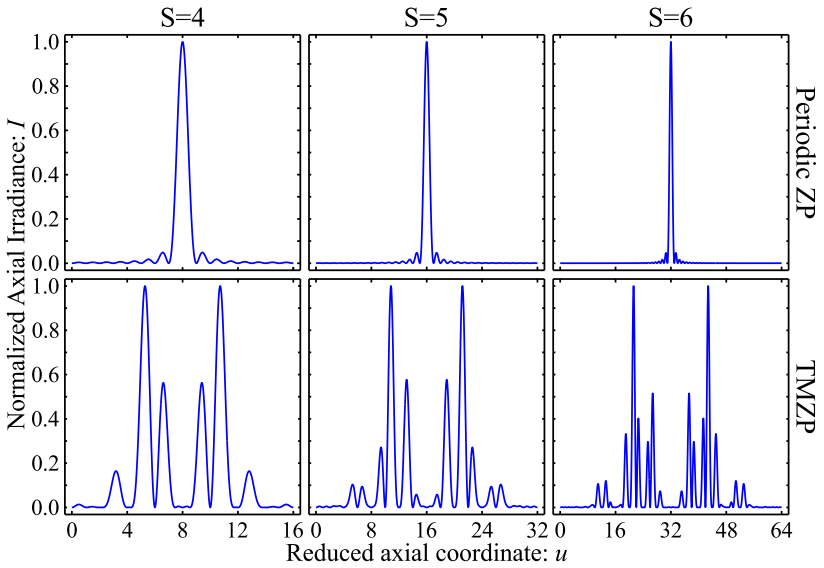

Figure 2.6.2: Normalized axial irradiance provided by TMZPs of orders $S = 4$, 5, and 6, and their respective equivalent periodic ZPs.

lens. Therefore, TMZPs are intrinsically bifocals. Interestingly, the irradiance produced by these aperiodic lenses is characterized by a sequence of subsidiary foci around each main focus following a fractal structure. In fact, the three patterns in the lower part of Fig. 2.6.2 are selfsimilar, i.e. the irradiance distribution corresponding to a TMZP of order S is a modulated version of the irradiance distribution corresponding to the previous stage, $S-1$, magnified by a factor $\gamma = 2$.

In Fig. 2.6.3(a) we have represented the axial irradiances provided by a TMZP ($S = 6$) and the equivalent periodic ZP computed for three different wavelengths in the visible range ($\lambda = 450, 550$, and $650\,$nm). The axial distance, z, has been normalized to the main focal distance, $f = \frac{a^2}{\lambda 2^S}$, of the equivalent periodic ZP at $\lambda = 550\,$nm. Note that the multiple subsidiary foci around the main foci of a TMZP overlap for different wavelengths creating a pair of foci with an extended depth of focus. Therefore, a TMZP should be less sensitive to the chromatic aberration than the equivalent periodic ZP. Next, we analyze

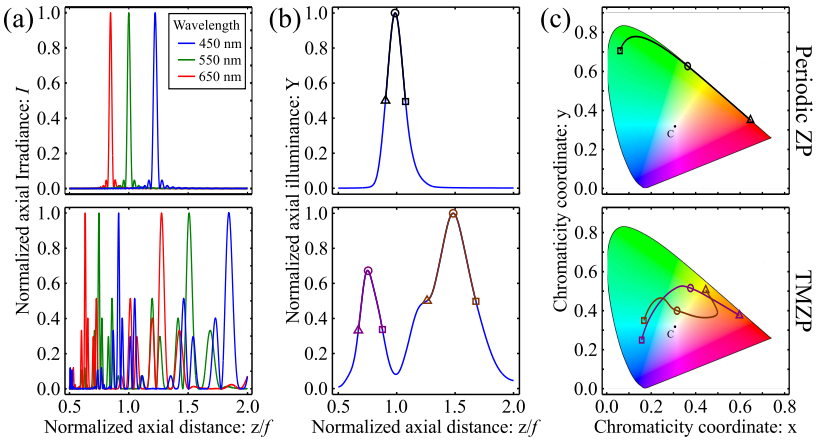

Figure 2.6.3: (a) Normalized axial irradiance for different wavelengths in the visible range, (b) Normalized axial illuminance, and (c) chromaticity of the different foci for the TMZP of order $S = 6$ and its equivalent periodic ZP.

this hypothesis.

The behavior of a TMZP under broadband illumination can be evaluated, following the conventional approach [Giménez10], in terms of the tristimulus values computed along the optical axis,

$$X(z) = \int_{\lambda_1}^{\lambda_2} I(z;\lambda) S(\lambda) \tilde{x} d\lambda \,,$$
$$Y(z) = \int_{\lambda_1}^{\lambda_2} I(z;\lambda) S(\lambda) \tilde{y} d\lambda \,,$$
$$Z(z) = \int_{\lambda_1}^{\lambda_2} I(z;\lambda) S(\lambda) \tilde{z} d\lambda \,, \qquad (2.6.4)$$

where $S(\lambda)$ is the spectral distribution of the source, $(\tilde{x}, \tilde{y}, \tilde{z})$ are the three sensitivity chromatic functions of the detector, and (λ_1,λ_2) represent the considered wavelength interval. In particular, in the assessment of visual systems $(\tilde{x}, \tilde{y}, \tilde{z})$ are usually the sensitivity functions of the human eye (CIE 1931) and the axial response is normally expressed in terms of the axial illuminance Y

and the axial chromaticity coordinates (x, y),

$$x = \frac{X}{X+Y+Z}, \qquad y = \frac{Y}{X+Y+Z}. \tag{2.6.5}$$

To compare the performance of a TMZP under polychromatic illumination we have computed Eqs. (2.6.4) and (2.6.5) for the ZPs shown in Fig. 2.6.1. We numerically computed 41 monochromatic irradiances for equally spaced wavelengths ranging from 380 to 780 nm. The standard illuminant C was used as a spectral distribution of the source. The illuminances computed for the TMZP of order $S = 6$ and its equivalent periodic ZP are shown in Fig. 2.6.3(b). The open circles in this figure represent the main foci of both ZPs, and the triangles and the squares represent the axial positions where the illuminance has decreased to a half of its maximum value. Figure 2.6.3(c) represents the chromatic coordinates of the axial irradiance around the main foci of the lenses. In this figure, the circles, triangles, and squares represent the chromatic coordinates at the axial points shown in Fig. 2.6.3(b). Note that the curves that reveal the chromatic content of each polichromatic focus of the TMZP are closer to the point representing the white illuminant, than the curve corresponding to the equivalent periodic ZP. Therefore the chromatic aberration of the TMZP is lower than the chromatic aberration of the equivalent binary Fresnel zone plate.

Experimental characterization

We have experimentally tested the polychromatic focusing properties of a TMZP developed in the presvious section. A schematic illustration of the experimental setup is shown in Fig. 2.6.4. The ZPs were implemented on a Liquid Crystal in a Silicon SLM (Holoeye PLUTO, 8-bit gray-level, pixel size $8\,\mu$m, and resolution 1920×1080 pixels), operating in amplitude mode, calibrated for different wavelengths in the visible range. The illumination system consisted of a Cold-White collimated LED (Mounted High-Power LED, CW, 1000 mA) and CRI VariSpec Liquid Crystal Tunable Filter (LCTF). This filter allows us to select a wavelength in the visible range with a bandwith of 10 nm. A pin-hole with a diameter of $150\,\mu$m was located at the focal plane of the achromatic Badal lens, L1 (focal length 160 mm). The images produced by the diffractive lenses were captured and registered with a CCD camera

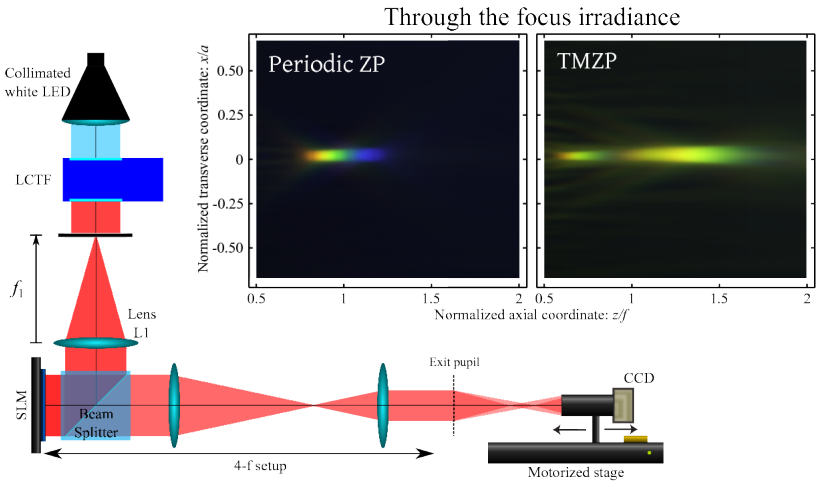

Figure 2.6.4: Scheme of the experimental setup and the polychromatic PSFs provided by the simulated TMZP of order $S = 6$ and its equivalent periodic ZP.

(8 bit gray-level, pixel pitch of $3.75\,\mu$m, and 1280×960 pixels) mounted on a translation stage (Thorlabs LTS 300; range 300 mm; precision $5\,\mu$m) along the optical axis. The images were captured at 248 axial positions for 58 wavelengths of visible light. Using Eq. (2.6.4) and transforming the tristimulus values XYZ to RGB coordinates [Pascale03], the polychromatic PSFs were obtained. Figure 2.6.4 shows the resulting polychromatic PSFs for a TMZP of order $S = 6$ and its equivalent periodic ZP with a focal distance $f = 100$ mm. As expected, the periodic ZP provides a single foci with high chromatic aberration, while the TMZP provides a pair of foci with enhanced focal depth and reduced chromatic aberration.

We have also tested the image forming capabilities of TMZPs under white-light illumination. In this case the binary diffractive lenses were printed on graphic films (standard polyester films) using a photoplotter with 2400 lpi resolution. We have generated a TMZP with 128 zones ($S = 7$) with $a = 3$ mm (main focal distances $f_{TM1} = 188$ mm and $f_{TM2} = 96$ mm for a design wavelength $\lambda = 550$ nm). Its equivalent periodic ZP with the same number of zones (focal distance $f_0 = 126$ mm for $\lambda = 550$ nm) was also constructed to compare their performances. In our experiment we considered a conventio-

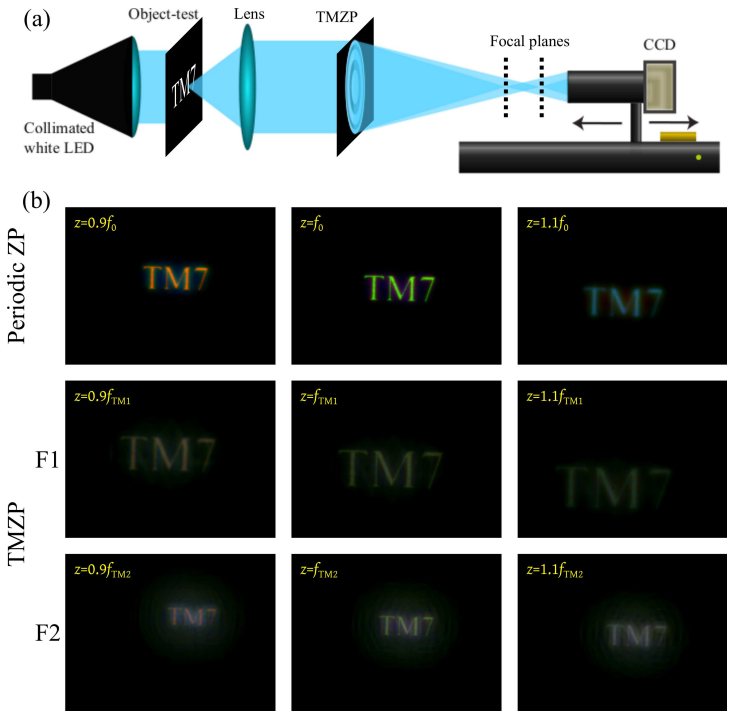

Figure 2.6.5: Captured RGB images provided by the printed TMZP of order S_7 and its equivalent periodic ZP. The images are captured at the focal length which corresponds to every focus and around these focal planes ($\pm 10\,\%$)

nal image forming arrangement as shown in Fig. 2.6.5(a). A polychromatic light source (a cold-white LED) was employed. The object-test (binary letters "TM7") was located at the object focal plane of the achromatic lens, so the image was formed at the focal image plane of the diffractive lens. The images were captured with a CMOS Camera (EO-5012C 1/2" CMOS RGB, pixel pitch of $4.4\,\mu$m). Figure 2.6.5 shows the images provided by the TMZP and by the equivalent periodic ZP at the main focal planes for the design wavelength. To obtain defocused images, the distance from the diffractive lens to the CMOS Camera was varied $\pm 10\,\%$ around the focal planes. It can be seen that the TMZP provides a pair of images with a reduced chromatic aberration

compared with the image provided by the periodic ZP, even at the main focal planes.

Conclusions

A new type of aperiodic ZPs based on the Thue-Morse sequence has been presented with interesting focusing and imaging capabilities. We have shown that a TMZP produces two self-similar foci situated symmetrically along the optical axis, one at each side of the focus of the equivalent periodic ZP of the same number of zones. As an image forming device under white light illumination, a TMZP produces a pair of images with an extended depth of field and a strong reduction in the chromatic aberration due to its bifractal focusing behavior. Therefore, TMZPs could be profitable across a broad range of applications where conventional periodic and Fractal zone plates [Furlan07] are currently applied including: spectral domain OCT [Zhang11], X-ray microscopy [Ge14, Ge12], design of artificial compound eyes [Keum13], among others [Tao13, Verma13, Gao13, Liu14]. Other potential application of these aperiodic lenses will require no absortion losses and improved diffraction efficiency, as for example, bifocal intraocular or contact lens for the correction of presbyopia. To improve the diffraction efficiency of the TMZP here presented the equivalent pure phase diffractive lenses with a blazed profile are currently under study.

Acknowledgements

This work was supported by the Ministerio de Economía y Competividad (grant FIS2011-23175) and by Generalitat Valenciana (PROMETEOII/2014/072), Spain.

Referencias

[Ferrando14b] V. Ferrando, A. Calatayud, P. Andrés, R. Torroba, W. D. Furlan y J. A. Monsoriu, “Imaging Properties of Kinoform Fibonacci Lenses”, *IEEE Photonics Journal* **6**, 6500106 (2014).

[Fu08] Y. Fu, W. Zhou y L. Lim, "Propagation properties of plasmonic micro-zone plates with and without fractals", *Applied Physics B* **90**, 421–425 (2008).

[Furlan07] W. D. Furlan, G. Saavedra y J. A. Monsoriu, "White-light imaging with fractal zone plates", *Optics Letters* **32**, 2109–2111 (2007).

[Gao13] N. Gao, H. Li, X. Zhu, Y. Hua y C. Xie, "Quasi-periodic gratings: diffraction orders accelerate along curves", *Optics letters* **38**, 2829–2831 (2013).

[Ge12] X. Ge, Z. Wang, K. Gao, D. Wang, Z. Z. Z. Wu, J. Chen, Z. Pan, K. Zhang, Y. Hong, P. Zhu y Z. Z. Z. Wu, "Use of fractal zone plates for transmission X-ray microscopy", *Analytical and bioanalytical chemistry* **404**, 1303–1309 (2012).

[Ge14] X. Ge, Z. Wang, K. Gao, D. Wang, Z. Wu, J. Chen, K. Zhang, Y. Hong, P. Zhu y Z. Wu, "Effects of the condenser fractal zone plate in a transmission X-ray microscope", *Radiation Physics and Chemistry* **95**, 424–427 (2014).

[Giménez10] F. Giménez, W. D. Furlan, A. Calatayud y J. A. Monsoriu, "Multifractal zone plates", *Journal of the Optical Society of America A* **27**, 1851–1855 (2010).

[Hsueh14] W. J. Hsueh, C. H. Chang y C. T. Lin, "Exciton photoluminescence in resonant quasi-periodic Thue-Morse quantum wells", *Optics letters* **39**, 489–492 (2014).

[Huang13] H. Huang, D. Liu, H. Zhang y X. Kong, "Electronic transport and shot noise in Thue-Morse sequence graphene superlattice", *Journal of Applied Physics* **113**, 043702 (2013).

[Keum13] D. Keum y K.-H. Jeong, "Artificial compound eye with fractal zone plate arrays", "2013 International Conference on Optical MEMS and Nanophotonics (OMN)", 31–32, IEEE (2013).

[Liu09] Y. J. Liu, H. T. Dai, X. W. Sun y T. J. Huang, "Electrically switchable phase-type fractal zone plates and fractal photon sieves", *Optics Express* **17**, 12418 (2009).

[Liu14] Y. J. Liu, H. Liu, E. S. P. Leong, C. C. Chum y J. H. Teng, "Fractal Holey Metal Microlenses with Significantly Suppressed Side Lobes and High-Order Diffractions in Focusing", *Advanced Optical Materials* **2**, 487–492 (2014).

[Maciá06] E. Maciá, "The role of aperiodic order in science and technology", *Reports on Progress in Physics* **69**, 397–441 (2006).

[Monsoriu07] J. A. Monsoriu, R. A. Depine y E. Silvestre, "Non-Bragg band gaps in 1D metamaterial aperiodic multilayers", *Journal of the European Optical Society: Rapid Publications* **2**, 07002(1–5) (2007).

[Monsoriu13] J. A. Monsoriu, A. Calatayud, L. Remón, W. D. Furlan, G. Saavedra y P. Andrés, "Bifocal Fibonacci diffractive lenses", *IEEE Photonics Journal* **5**, 3400106 (2013).

[Ojeda-Castañeda96] J. Ojeda-Castañeda y C. Gómez-Reino, *Selected papers on zone plates*, tomo MS128, SPIE Optical Engineering Press, Washington (1996).

[Pascale03] D. Pascale, *A Review of RGB Color Spaces ...from xyY to R'G'B*, The BabelColor Company, Montreal(Canada) (2003).

[Saavedra03] G. Saavedra, W. D. Furlan y J. A. Monsoriu, "Fractal zone plates", *Optics Letters* **28**, 971–973 (2003).

[Tao13] S. H. Tao, B. C. Yang, H. Xia y W. X. Yu, "Tailorable three-dimensional distribution of laser foci based on customized fractal zone plates", *Laser Physics Letters* **10**, 035003 (2013).

[Tsao14] C. W. Tsao, Y. H. Cheng y W. J. Hsueh, "Localized modes in one-dimensional symmetric Thue-Morse quasicrystals", *Optics express* **22**, 24378–24383 (2014).

[Verma13] R. Verma, M. K. Sharma, V. Banerjee y P. Senthilkumaran, "Robustness of Cantor diffractals", *Optics express* **21**, 7951–7956 (2013).

[Wang02] S. Wang, X. C. Zhang, M. P. Maley, M. F. Hundley, L. N. Bulaevskii, A. E. Koshelev y A. J. Taylor, "Terahertz Tomographic Imaging With a Fresnel Lens", *Optics and Photonics News* **13**, 58–58 (2002).

[Wang03] Y. Wang, W. Yun y C. Jacobsen, "Achromatic Fresnel optics for wideband extreme-ultraviolet and X-ray imaging", *Nature* **424**, 50–53 (2003).

[Zhang11] Q. Q. Zhang, J. G. Wang, M. W. Wang, J. Bu, S. W. Zhu, R. Wang, B. Z. Gao y X.-C. X.-C. Yuan, "A modified fractal zone plate with extended depth of focus in spectral domain optical coherence tomography", *Journal of Optics* **13**, 055301 (2011).

[Zhang12] Q. Zhang, J. Wang, M. Wang, J. Bu, S. Zhu, B. Z. Gao y X. Yuan, "Depth of focus enhancement of a modified imaging quasi-fractal zone plate", *Optics and laser technology* **44**, 2140–2144 (2012).

Capítulo 3

Discusión general de los resultados

En este capítulo se hace una puesta en común de los resultados presentados en los artículos del capítulo anterior. Cabe mencionar que los principales resultados alcanzados tras varios años de investigación, son la elaboración de la presente Tesis Doctoral y la publicación de los artículos que la componen en revistas científicas indexadas en el JRC.

Como se ha visto a lo largo del presente documento, esta Tesis Doctoral profundiza en el estudio de EODs cuyo diseño esta basado en las series de Cantor, Fibonacci y Thue–Morse. En particular, el trabajo se centra en el diseño y caracterización de nuevas placas zonales binarias tanto de amplitud como de fase y tambien tipo kinoform que aprovechan las propiedades que otorga la implementación de estas secuencias aperiódicas en su diseño.

Tras el estudio realizado aplicando estas series a algunos tipos de EODs vemos que cada una de ellas aporta unas propiedades ópticas especificas al elemento periódico equivalente y que, en función del objetivo perseguido, son capaces de superar ciertas limitaciones inherentes al diseño periódico.

Considerando el aumento de la profundidad de foco de las placas

zonales fractales (Fig. 1.2) [Remón13b] y teniendo en cuenta el perfil de focalización en forma de cruz que producen las placas zonales con geometría cuadrada, en los artículos "Fractal square zone plate" [Calatayud13a] y "Cantor dust zone plate" [Ferrando13a] se han presentado dos nuevos EODs que, bajo iluminación plana monocromática, producen un patrón que puede utilizarse, entre otras aplicaciones, como referencia en la alineación de sistemas ópticos 3D.

Para las placas zonales fractales cuadradas se observa una profundidad de foco extendida con respecto a la placa zonal equivalente periódica. Este aumento, producido por la distribución fractal introducida en el diseño de este elemento, da lugar a un perfil de focalización autosimilar, en el que al aumentar el orden de la secuencia fractal la energía de cada uno de los focos se distribuye en un conjunto de focos secundarios. Además, se ha comprobado que este elemento produce una serie de focos en forma de cruz centrados a lo largo del eje óptico (Fig. 2.1.4).

La eficiencia de estas placas zonales ha sido mejorada mediante la aplicación de una variante de la misma secuencia fractal, el polvo de Cantor, a un EOD del tipo criba de fotones [Ferrando13a, Ferrando12a, Furlan12]. Con este nuevo diseño de apodizan los órdenes de difracción secundarios (Fig. 2.2.2) y se simplifica la construcción de este elemento, ya que consiste en un conjunto de agujeros perforados sobre una base opaca. Además, sus propiedades de focalización han sido contrastadas experimentalmente mediante un sistema basado en un modulador espacial de luz de cristal líquido (Figs. 2.2.3 y 2.2.4). Mas aún, la corrección de aberraciones de este sistema mediante un sensor frente de onda del tipo Hartmann-Shack ha dado lugar a numerosas contribuciones [Calatayud12a, Ferrando13c, Ferrando14e, Remón15, Ferrando16b, Ferrando16a].

En cuanto a la serie de Fibonacci, se ha aprovechado la bifocalidad que presenta (Fig. 1.4) en dos tipos de EOD: una lente vórtice [Calatayud13b, Ferrando13b] y una lente kinoform [Ferrando14b].

Estudiando la lente vórtice de Fibonacci observamos que esta pre-

senta dos vórtices a lo largo del eje óptico cuyas posiciones y proporciones son definidas por la distribución de Fibonacci. Mediante la carga topológica, podemos modificar el diámetro de los vórtices, pero entre ellos se mantiene la proporción áurea debido a que su distancia focal relativa también mantiene dicha proporción (Fig. 2.3.5). Las propiedades de focalización de esta lente han sido contrastadas experimentalmente mediante el sistema basado en el modulador espacial de luz de cristal líquido.

La lente kinoform de Fibonacci ha sido diseñada de forma que las zonas con gradiente de fase siguen la secuencia de Fibonacci. Se ha comprobado que esta lente mejora la eficiencia de difracción respecto a la placa zonal equivalente mediante la eliminación de los altos órdenes de difracción. De esta forma, la lente genera solo un par de focos cuyas distancias a la lente mantienen la proporción áurea. Tras comparar las capacidades de formación de imágenes de ambos elementos, tanto numérica como experimentalmente, se observa que la lente kinoform de Fibonacci presenta mejor calidad y mayor contraste en ambas posiciones focales (Figs. 2.4.3 y 2.4.4).

Además, se han estudiado placas zonales basadas en las series de *m*-Bonacci [Furlan14b, Ferrando15c] como generalización de las estructuras basadas en la serie de Fibonacci y se han estudiado otros elementos fotónicos difractivos, como las apilaciones multicapa, cuyos diseños estan basados en la secuencia de Fibonacci [Ferrando14d].

Tras la aplicación de las series fractal y Fibonacci a diferentes tipos de EOD en el rango visible, el siguiente paso es el diseño de PZs basadas en estas series que trabajan en otro rango espectral. Se han estudiado las propiedades de focalizacion y formación de imágenes en el rango de los Terahercios para diferentes placas zonales basadas en las secuencias de Cantor [Furlan13, Furlan14a] y Fibonacci [Furlan15b]. En el artículo "3D printed diffractive terahertz lenses" [Furlan16] se presentan placas zonales de fase basadas en las series de Fibonacci, Cantor y su equivalente periódica construidas mediante impresión 3D y diseñadas para trabajar en el rango de los THz (Fig. 2.5.2). Para las

tres lentes construidas se obtienen experimentalmente las propiedades de focalización y se comparan satisfactoriamente con las calculados mediante las ecuaciones de propagación no paraxial. Por una parte, para la placa zonal fractal observamos un aumento de la profundidad de foco, mientras que para la placa zonal de Fibonacci destaca su bifocalidad (Fig. 2.5.4).

Extendiendo el estudio a otras sequencias aperiódicas se ha diseñado una placa zonal de amplitud basada en la serie de Thue–Morse [Ferrando14a, Ferrando15b], la cual ha sido aplicada al diseño de fibras de cristal fotónico [Ferrando12b, Ferrando15a]. Analizando la irradiancia producida por la placa zonal de Thue–Morse observamos que el foco difractivo se desdobla en dos grandes grupos de focos secundarios. Aprovechando la extensión de foco producida por esta placa zonal, en el artículo [Ferrando15d] estudiamos su comportamiento bajo iluminación policromática para comprobar que reduce la aberración cromática respecto a su equivalente periódica. Además, obtenemos de forma experimental las propiedades de focalización de la lente mediante simulación en el sistema SLM de cristal líquido y construida mediante fotolitografía sobre papel de acetato. De esta forma comprobamos el aumento en la profundidad de foco y la reducción de la aberración cromática de este EOD con respecto a su equivalente periódica cuando actúan como elementos formadores de imagen.

Además, a lo largo del trabajo de investigación se han desarrollado herramientas para facilitar el estudio de las redes aperiodicas que posteriormente han sido aplicadas a la docencia [Ferrando14c], así como dispositivos sensores basados en el mecanismo de la difracción [Avella-Oliver15].

Capítulo 4

Conclusiones

En este capítulo de conclusiones se analiza el nivel de cumplimento de los objetivos de investigación planteados en la introducción. También se recopilan las principales conclusiones alcanzadas, se exponen cuáles son las aportaciones más relevantes del trabajo y se proponen varias líneas futuras de trabajo.

4.1 Cumplimiento de los objetivos

El primer objetivo, que consiste en el *Diseño y caracterización de un elemento óptico difractivo multifocal con geometría cuadrada que genere un patrón de referencia aplicable al alineamiento y calibración de sistemas ópticos tridimensionales*, ha sido alcanzado con los EODs presentados en los artículos 1 y 2. Estos elementos difractivos de geometría cuadrada presentan un patrón de focalización en forma de cruz con gran profundidad de foco.

El segundo objetivo, *Diseño y caracterización de un elemento óptico difractivo que genere secuencias de vórtices a lo largo del eje óptico, susceptibles de ser utilizadas como trampas ópticas*, se ha logra-

do con la publicación en el artículo 3 de una lente vórtice basada en la secuencia de Fibonacci que genera un par de vórtices distribuidos axialmente.

El tercer objetivo que consiste en la *Optimización de la eficiencia de difracción de una lente difractiva bifocal basada en la secuencia de Fibonacci mediante un diseño de tipo kinoform* se consiguió mediante la lente diseñada y caracterizada en el artículo 4. Las propiedades de esta lente han sido comprobadas teórica y experimentalmente, llegando a comprobarse la mejora de la calidad de imagen producida con respecto a su lente de Fibonacci equivalente binaria de fase invertida.

En cuanto al objetivo de *Extender la aplicabilidad de las estructuras basadas en secuencias aperiódicas a otro rango del espectro electromagnético*, se ha cumplido con el trabajo presentado en el artículo 5 en el que se diseñan y construyen lentes aperiódicas que trabajan en el rango de los THz. Además, para la construcción de las lentes se a utilizado una tecnología de bajo coste que esta en proceso de expansión, la impresión 3D.

En cuanto al *Estudio de las propiedades multifocales de las estructuras difractivas basadas la secuencia aperiódica de Thue-Morse*, en el artículo 6 se diseña y caracteriza la placa zonal basada en la secuencia de Thue–Morse. El estudio se centra en las propiedades policromáticas de este elemento difractivo, ya que combinando la bifocalidad y la extensión de foco que produce se consigue una interesante reducción de la aberración cromática que comprobamos experimentalmente utilizando esta placa zonal como elemento formador de imágenes bajo iluminación blanca.

4.2 Aportaciones realizadas

Tras comprobar que los objetivos planteados han sido plenamente alcanzados como resultado de la investigación presentada en esta Tesis Doctoral, vamos a resumir cuales han sido las principales aportaciones a la literatura existente en el campo de los EODs basados en las series fractal de Cantor, Fibonacci y Thue–Morse.

En cuanto a los EODs basado en la serie fractal de Cantor, se han diseñado y caracterizado nuevas placas zonales y cribas de fotones con geometría cuadrada que presentan un aumento en la profundidad de foco que confiere a estos elementos la capacidad de generar un patrón de referencia aprovechable en la alineación de sistemas ópticos 3D.

Como EODs basados en la serie de Fibonacci, se han diseñado dos elementos de diferente tipo: una lente vórtice que genera un par de vórtices a lo largo del eje óptico, y una lente kinoform bifocal cuya calidad de imágenes ha sido comprobada experimentalmente.

Además, se han construido las primeras lentes difractivas aperiódicas en el rango de los THz obtenidas mediante técnicas de impresión 3D y se han comprobado experimentalmente sus propiedades de focalización.

Finalmente, se ha introducido una nueva secuencia aperiódica al diseño de placas zonales, la serie de Thue–Morse, cuyas propiedades cromáticas han sido estudiadas, ya que este elemento produce un perfil de irradiancia axial bifocal y con un gran aumento de la profundidad de foco. Tras estudiar estas propiedades, las placas zonales se han construido mediante fotolitografía y se ha comprobado experimentalmente la bifocalidad y reducción de la aberración cromática.

4.3 Lineas de investigación futuras

Finalmente, se plantean varios caminos por los que seguir investigando en relación a los contenidos de esta Tesis:

Por una parte, se puede extender la aplicabilidad de algunos elementos presentados sustituyendo la serie aperiódica aplicada en el diseño. De esta forma, un elemento que se pretende estudiar es el Polvo de Fibonacci en el que se combinan placas zonales de geometría cuadrada basadas en la serie de Fibonacci. Según los resultados preliminares se obtendrá un elemento que produce dos focos en forma de cruz distribuidos axialmente. Esta distribución de irradiancia genera dos planos de referencia que podrian facilitar el alineamiento de sistemas ópticos.

Por otra parte, se pretende extender el estudio a otras secuencias aperiódicas, como las funciones de Walsh [Furlan15a], Period-doubling, Silver mean, Bronze mean, Copper mean, Nickel mean, Rudin-Saphiro, Paper folding, ... También resultara interesante la combinación de varias de estas series para generar nuevas secuencias aperiódicas, como las secuencias de Fibonacci-Cantor, en las que se alterna la aplicación de las reglas de iteración de las series de Fibonacci y Cantor, produciendo nuevas e interesantes distribuciones de irradiancia.

Bibliografía general

[Agafonov13] A. N. Agafonov, B. O. Volodkin, A. K. Kaveev, B. A. Knyazev, G. I. Kropotov, V. S. Pavelyev, V. A. Soifer, K. N. Tukmakov, E. V. Tsygankova y Y. Y. Choporova, "Silicon diffractive optical elements for high-power monochromatic terahertz radiation", *Optoelectronics, Instrumentation and Data Processing* **49**, 189–195 (2013).

[Agafonov16] A. N. Agafonov, B. O. Volodkin, D. G. Kachalov, B. A. Knyazev, G. I. Kropotov, K. N. Tukmakov, V. S. Pavelyev, D. I. Tsypishka, Y. Y. Choporova y A. K. Kaveev, "Focusing of Novosibirsk Free Electron Laser (NovoFEL) radiation into paraxial segment", *Journal of Modern Optics* **63**, 1051–1054 (2016).

[Alda08] J. Alda y G. Boreman, "Optimization of polygonal fresnel zone plates", *Microwave and Optical Technology Letters* **50**, 536–541 (2008).

[Alda09a] J. Alda y F. J. González, "Polygonal Fresnel zone plates", *Journal of Optics A: Pure and Applied Optics* **11**, 085707 (2009).

[Alda09b] J. Alda, J. M. Rico-García, F. J. Salgado-Remacha y L. M. Sanchez-Brea, "Diffractive performance of square Fresnel zone plates", *Optics Communications* **282**, 3402–3407 (2009).

[Andersen05] G. Andersen, "Large optical photon sieve", *Optics Letters* **30**, 2976–2978 (2005).

[Andersen10] G. Andersen, "Membrane photon sieve telescopes", *Applied Optics* **49**, 6391–6394 (2010).

[Astley10] V. Astley, J. Scheiman, R. Mendis y D. M. Mittleman, "Bending and coupling losses in terahertz wire waveguides", *Optics letters* **35**, 553–555 (2010).

[Avella-Oliver15] M. Avella-Oliver, V. Ferrando, J. A. Monsoriu, R. Puchades y Á. Maquieira, "Redes de difracción de bioreceptores para monitorizar eventos de reconocimiento molecular", "IX International Workshop on Sensors and Molecular Recognition", Valencia (2015).

[Bamberg03] J. Bamberg, G. Cairns y D. Kilminster, "The Crystallographic Restriction, Permutations, and Goldbach's Conjecture", *The American Mathematical Monthly* **110**, 202–209 (2003).

[Bishop03] A. Bishop, T. Nieminen, N. Heckenberg y H. Rubinsztein-Dunlop, "Optical application and measurement of torque on microparticles of isotropic nonabsorbing material", *Physical Review A* **68**, 033802 (2003).

[Busch14] S. F. Busch, M. Weidenbach, M. Fey, F. Schäfer, T. Probst y M. Koch, "Optical Properties of 3D

Printable Plastics in the THz Regime and their Application for 3D Printed THz Optics", *Journal of Infrared, Millimeter, and Terahertz Waves* **35**, 993–997 (2014).

[Calatayud12a] A. Calatayud, V. Ferrando, L. Remón, P. Andrés, W. D. Furlan y J. A. Monsoriu, "Caracterización experimental de lentes difractivas aperiódicas con un modulador espacial de luz", "X Reunión Nacional de Óptica", Zaragoza (2012).

[Calatayud12b] A. Calatayud, J. A. Rodrigo, L. Remón, W. D. Furlan, G. Cristóbal, J. A. Monsoriu, L. Remón, W. D. Furlan, G. Cristóbal y J. A. Monsoriu, "Experimental generation and characterization of devil's vortex-lenses", *Applied Physics B* **106**, 915–919 (2012).

[Calatayud13a] A. Calatayud, V. Ferrando, F. Giménez, W. D. Furlan, G. Saavedra y J. A. Monsoriu, "Fractal square zone plates", *Optics Communications* **286**, 42–45 (2013).

[Calatayud13b] A. Calatayud, V. Ferrando, L. Remón, W. D. Furlan y J. A. Monsoriu, "Twin axial vortices generated by Fibonacci lenses", *Optics Express* **21**, 10234–10239 (2013).

[Cao02] Q. Cao y J. Jahns, "Focusing analysis of the pinhole photon sieve: individual far-field model", *Journal of the Optical Society of America A* **19**, 2387–2393 (2002).

[Cao03] Q. Cao y J. Jahns, "Nonparaxial model for the focusing of high-numerical-aperture photon sie-

ves", *Journal of the Optical Society of America A* **20**, 1005–1012 (2003).

[Coldea10] R. Coldea, D. A. Tennant, E. M. Wheeler, E. Wawrzynska, D. Prabhakaran, M. Telling, K. Habicht, P. Smeibidl y K. Kiefer, "Quantum criticality in an Ising chain: experimental evidence for emergent E8 symmetry", *Science* **327**, 177–180 (2010).

[Curtis03] J. E. Curtis y D. G. Grier, "Structure of Optical Vortices", *Physical Review Letters* **90**, 133901 (2003).

[Dai12] H. T. Dai, Y. J. Liu y X. W. Sun, "The focusing property of the spiral Fibonacci zone plate", S. Jiang, M. J. F. Digonnet y J. C. Dries, eds., "SPIE, Optical Components and Materials IX", tomo 8257, 82570T1–82570T7 (2012).

[Dallapiccola08] R. Dallapiccola, A. Gopinath, F. Stellacci y L. Dal Negro, "Quasi-periodic distribution of plasmon modes in two-dimensional Fibonacci arrays of metal nanoparticles", *Optics Express* **16**, 5544–5555 (2008).

[D'Angelo14] F. D'Angelo, Z. Mics, M. Bonn y D. Turchinovich, "Ultra-broadband THz time-domain spectroscopy of common polymers using THz air photonics", *Optics Express* **22**, 12475–12485 (2014).

[Davis04] J. A. Davis, L. Ramirez, J. A. Rodrigo, T. Alieva y M. L. Calvo, "Focusing properties of fractal zone plates: experimental implementation with a

liquid-crystal display", *Optics Letters* **29**, 1321–1323 (2004).

[Davis06] J. A. Davis, S. P. Sigarlaki, J. M. Craven y M. L. Calvo, "Fourier series analysis of fractal lenses: theory and experiments with a liquid-crystal display", *Applied optics* **45**, 1187–1192 (2006).

[Davison06] J. A. Davison y M. J. Simpson, "History and development of the apodized diffractive intraocular lens", *Journal of cataract and refractive surgery* **32**, 849–858 (2006).

[Ferrando12a] V. Ferrando, A. Calatayud, F. Giménez, J. A. Monsoriu y W. D. Furlan, "Criba rectangular de fotones fractal", "X Reunión Nacional de Óptica", Zaragoza (2012).

[Ferrando12b] V. Ferrando, E. Silvestre, P. Andrés, W. D. Furlan y J. A. Monsoriu, "Propiedades de guiado de una fibra de cuasicristal fotónico", "X Reunión Nacional de Óptica", Zaragoza (2012).

[Ferrando13a] V. Ferrando, A. Calatayud, F. Giménez, W. D. Furlan y J. A. Monsoriu, "Cantor dust zone plates", *Optics Express* **21**, 2701–2706 (2013).

[Ferrando13b] V. Ferrando, A. Calatayud, L. Remón, A. Pons-Martí, W. D. Furlan y J. A. Monsoriu, "Lentes-Vórtice de Fibonacci", "XXXIV Reunión Bienal de la Real Sociedad Española de Física", 90–91, Valencia (2013).

[Ferrando13c] V. Ferrando, L. Remón, A. Calatayud, A. Pons-Martí, W. D. Furlan y J. A. Monsoriu, "Automatic reconstruction of the wavefront using

a Shack-Hartmann sensor", "7th International Image Processing & Wavelet on Real World Applications Conference", 110–114, Valencia (2013).

[Ferrando14a] V. Ferrando, A. Calatayud, P. Andrés, W. D. Furlan y J. A. Monsoriu, "Thue-Morse bifocal zone plate: Experimental results of imaging and focalization", "23rd Congress of the International Commission for Optics", PI E11, Santiago de Compostela (2014).

[Ferrando14b] V. Ferrando, A. Calatayud, P. Andrés, R. Torroba, W. D. Furlan y J. A. Monsoriu, "Imaging Properties of Kinoform Fibonacci Lenses", *IEEE Photonics Journal* **6**, 6500106 (2014).

[Ferrando14c] V. Ferrando, A. Calatayud, L. Remón, J. A. Monsoriu, A. Pons-Martí y W. D. Furlan, "Aperiodic Diffract: Estudio de redes difractivas", *Modelling inScience Education and Learning* **7**, 131–138 (2014).

[Ferrando14d] V. Ferrando, J. C. Castro-Palacio, B. Marí y J. A. Monsoriu, "Study on band gap structure of Fibonacci quantum superlattices by using the transfer matrix method", *Modern Physics Letters B* **28**, 1450053 (2014).

[Ferrando14e] V. Ferrando, L. Remón, A. Pons-Martí, W. D. Furlan y J. A. Monsoriu, "Nuevo software para el control de un dispositivo tipo Hartmann-Shack. Aplicaciones de uso docente en optometría", "XXXIII Congreso Internacional de Opto-

metría, Contactología y Óptica Oftálmica", Madrid (2014).

[Ferrando15a] V. Ferrando, A. Coves, P. Andres y J. A. Monsoriu, "Guiding Properties of a Photonic Quasi-Crystal Fiber Based on the ThueâMorse Sequence", *IEEE Photonics Technology Letters* **27**, 1903–1906 (2015).

[Ferrando15b] V. Ferrando, W. D. Furlan y J. A. Monsoriu, "Formación de imágenes con luz blanca mediante Placas Zonales de Thue-Morse", "XI Reunión Nacional de Óptica", 49, Salamanca (2015).

[Ferrando15c] V. Ferrando, W. D. Furlan y J. A. Monsoriu, "Lentes Kinoform diseñadas con distribuciones m-Bonacci", "XI Reunión Nacional de Óptica", 63, Salamanca (2015).

[Ferrando15d] V. Ferrando, F. Giménez, W. D. Furlan y J. A. Monsoriu, "Bifractal focusing and imaging properties of Thue-Morse Zone Plates.", *Optics express* **23**, 19846–19853 (2015).

[Ferrando16a] V. Ferrando, W. D. Furlan, L. Remón, F. Giménez y J. A. Monsoriu, "WAVEFRONT TESTER: Un nuevo laboratorio virtual para el estudio de los sensores frente de onda", *Modelling in Science Education and Learning* **9**, 121–128 (2016).

[Ferrando16b] V. Ferrando, L. Remón, A. Pons, W. D. Furlan y J. A. Monsoriu, "Wavefront sensing using a graphical user interface", *Computer Applications in Engineering Education* **24**, 255–262 (2016).

[Fleming02] A. J. Fleming, "Plant mathematics and Fibonacci's flowers", *Nature* **418**, 723 (2002).

[Fu08] Y. Fu, W. Zhou y L. Lim, "Propagation properties of plasmonic micro-zone plates with and without fractals", *Applied Physics B* **90**, 421–425 (2008).

[Furlan07] W. D. Furlan, G. Saavedra y J. A. Monsoriu, "White-light imaging with fractal zone plates", *Optics Letters* **32**, 2109–2111 (2007).

[Furlan09] W. D. Furlan, F. Giménez, A. Calatayud y J. A. Monsoriu, "Devil's vortex-lenses", *Optics Express* **17**, 21891–21896 (2009).

[Furlan12] W. D. W. Furlan, V. Ferrando, A. Calatayud, F. Giménez, J. A. J. A. Monsoriu, W. D. W. Furlan, J. A. J. A. Monsoriu, V. Ferrando, A. Calatayud, F. Giménez y J. A. J. A. Monsoriu, "Cantor dust zone plates", "32nd Progress In Electromagnetics Research Symposium", tomo 21, 645, OSA, Moscú (Rusia) (2012).

[Furlan13] W. D. Furlan, V. Ferrando, A. Calatayud y J. A. Monsoriu, "Fractal Zone Plates fot Terahertz Focusing and Imaging", "34th Progress In Electromagnetics Research Symposium", 1424–1427, Estocolmo (Suecia) (2013).

[Furlan14a] W. D. Furlan, V. Ferrando, P. Andrés y J. A. Monsoriu, "Aperiodic diffractive lenses for THz focusing and imaging with improved performance", "4th EOS Topical Meeting on Terahertz Science & Technology", Génova (Italia) (2014).

[Furlan14b] W. D. Furlan, V. Ferrando y J. A. Monsoriu, "Focusing properties of diffractive lenses constructed with the aperiodic m-bonacci sequence", "7th International Conference on Photonics, Devices and Systems", 945014, SPIE, Praga (Republica Checa) (2014).

[Furlan15a] W. D. Furlan, V. Ferrando, F. Giménez y J. A. Monsoriu, "Focusing properties of Walsh zone plates: Experimental implementation with a liquid-crystal display", "36th Progress In Electromagnetics Research Symposium", 1832, Praga (Republica Checa) (2015).

[Furlan15b] W. D. Furlan, V. Ferrando y J. A. Monsoriu, "Fibonacci diffractive lenses for THz focusing and imaging", "6th EOS Topical Meeting on Optical Microsystems", Capri (Italia) (2015).

[Furlan16] W. D. Furlan, V. Ferrando, J. A. Monsoriu, P. Zagrajek, E. Czerwińska y M. Szustakowski, "3D printed diffractive terahertz lenses", *Optics Letters* **41**, 1748–1751 (2016).

[Gao11] N. Gao, Y. Zhang y C. Xie, "Circular Fibonacci gratings", *Applied Optics* **50**, G142–G148 (2011).

[Gao13] N. Gao, H. Li, X. Zhu, Y. Hua y C. Xie, "Quasi-periodic gratings: diffraction orders accelerate along curves", *Optics letters* **38**, 2829–2831 (2013).

[Gbur06] G. Gbur y T. D. Visser, "Phase singularities and coherence vortices in linear optical systems", *Optics Communications* **259**, 428–435 (2006).

[Ge12] X. Ge, Z. Wang, K. Gao, D. Wang, Z. Wu, J. Chen, Z. Pan, K. Zhang, Y. Hong, P. Zhu y Z. Wu, "Use of fractal zone plates for transmission X-ray microscopy", *Analytical and bioanalytical chemistry* **404**, 1303–1309 (2012).

[Ge14] X. Ge, Z. Wang, K. Gao, D. Wang, Z. Wu, J. Chen, K. Zhang, Y. Hong, P. Zhu y Z. Wu, "Effects of the condenser fractal zone plate in a transmission X-ray microscope", *Radiation Physics and Chemistry* **95**, 424–427 (2014).

[Giménez06] F. Giménez, J. A. Monsoriu, W. D. Furlan y A. Pons, "Fractal photon sieve", *Optics Express* **14**, 11958–11963 (2006).

[Giménez07] F. Giménez, W. D. Furlan y J. A. Monsoriu, "Lacunar fractal photon sieves", *Optics Communications* **277**, 1–4 (2007).

[Giménez10] F. Giménez, W. D. Furlan, A. Calatayud y J. A. Monsoriu, "Multifractal zone plates", *Journal of the Optical Society of America A* **27**, 1851–1855 (2010).

[Goldsmith92] P. F. Goldsmith y P.F. Goldsmith, "Zone plate lens antennas for millimeter and submillimeter wavelengths", "Third International Symposium on Space Terahertz Technology", 345–361 (1992).

[González04] F. J. González, J. Alda, B. Ilic y G. D. Boreman, "Infrared Antennas Coupled to Lithographic Fresnel Zone Plate Lenses", *Applied Optics* **43**, 6067–6073 (2004).

[Hai-Tao05] D. Hai-Tao, W. Xin y X. Ke-Shu, "Focusing Properties of Fractal Zone Plates with Variable Lacunarity: Experimental Studies Based on Liquid Crystal on Silicon", *Chinese Physics Letters* **22**, 2851–2854 (2005).

[Han01] P. Y. Han y X.-C. Zhang, "Free-space coherent broadband terahertz time-domain spectroscopy", *Measurement Science and Technology* **12**, 1747–1756 (2001).

[Hangyo02] M. Hangyo, T. Nagashima y S. Nashima, "Spectroscopy by pulsed terahertz radiation", *Measurement Science and Technology* **13**, 1727–1738 (2002).

[Hart66] H. E. Hart, J. B. Scrandis, R. Mark y R. D. Hatcher, "Diffraction Characteristics of a Linear Zone Plate", *Journal of the Optical Society of America* **56**, 1018–1023 (1966).

[Herrmannsfeldt68] W. B. Herrmannsfeldt, M. J. Lee, J. J. Spranza y K. R. Trigger, "Precision Alignment Using a System of Large Rectangular Fresnel Lenses", *Applied Optics* **7**, 995–1005 (1968).

[Hsueh14] W. J. Hsueh, C. H. Chang y C. T. Lin, "Exciton photoluminescence in resonant quasi-periodic Thue-Morse quantum wells", *Optics letters* **39**, 489–492 (2014).

[Huang13] H. Huang, D. Liu, H. Zhang y X. Kong, "Electronic transport and shot noise in Thue-Morse sequence graphene superlattice", *Journal of Applied Physics* **113**, 043702 (2013).

[Janicijevic82] L. J. Janicijevic, "Diffraction characteristics of square zone plates", *Journal of Optics* **13**, 199–206 (1982).

[Kelemen07] L. Kelemen, S. Valkai y P. Ormos, "Parallel photopolymerisation with complex light patterns generated by diffractive optical elements", *Optics Express* **15**, 14488–14497 (2007).

[Keum13] D. Keum y K.-H. Jeong, "Artificial compound eye with fractal zone plate arrays", "2013 International Conference on Optical MEMS and Nanophotonics (OMN)", 31–32, IEEE (2013).

[Kipp01] L. Kipp, M. Skibowski, R. L. Johnson, R. Berndt, R. Adelung, S. Harm y R. Seemann, "Sharper images by focusing soft X-rays with photon sieves", *Nature* **414**, 184–188 (2001).

[Komlenok15] M. S. Komlenok, B. O. Volodkin, B. A. Knyazev, V. V. Kononenko, T. V. Kononenko, V. I. Konov, V. S. Pavelyev, V. A. Soifer, K. N. Tukmakov y Y. Y. Choporova, "Fabrication of a multilevel THz Fresnel lens by femtosecond laser ablation", *Kvant. electron.* **45**, 933–936 (2015).

[Ladavac04] K. Ladavac y D. G. Grier, "Microoptomechanical pumps assembled and driven by holographic

optical vortex arrays", *Optics Express* **12**, 1144–1149 (2004).

[Lee04] W. M. Lee, X.-C. Yuan y W. C. Cheong, "Optical vortex beam shaping by use of highly efficient irregular spiral phase plates for optical micromanipulation", *Optics Letters* **29**, 1796–1798 (2004).

[Lee09] Y.-S. Lee, *Principles of Terahertz Science and Technology*, Springer (2009).

[Li05] C. Li, X. Zhang y Z. Cao, "Triangular and Fibonacci number patterns driven by stress on core/shell microstructures", *Science (New York, N.Y.)* **309**, 909–911 (2005).

[Linage06] G. Linage, F. Montoya, A. Sarmiento, K. Showalter y P. Parmananda, "Fibonacci order in the period-doubling cascade to chaos", *Physics Letters A* **359**, 638–639 (2006).

[Liu09] Y. J. Liu, H. T. Dai, X. W. Sun y T. J. Huang, "Electrically switchable phase-type fractal zone plates and fractal photon sieves", *Optics Express* **17**, 12418 (2009).

[Liu14] Y. J. Liu, H. Liu, E. S. P. Leong, C. C. Chum y J. H. Teng, "Fractal Holey Metal Microlenses with Significantly Suppressed Side Lobes and High-Order Diffractions in Focusing", *Advanced Optical Materials* **2**, 487–492 (2014).

[Liu16] W.-Q. Liu, Y.-F. Lu, G.-H. Jiao, X.-F. Chen, J.-Y. Li, S.-H. Chen, Y.-M. Dong y J.-C. Lv, "Te-

rahertz optical properties of the cornea", *Optics Communications* **359**, 344–348 (2016).

[Maciá06] E. Maciá, "The role of aperiodic order in science and technology", *Reports on Progress in Physics* **69**, 397–441 (2006).

[Maciá12] E. Maciá, "Exploiting aperiodic designs in nanophotonic devices", *Reports on Progress in Physics* **75**, 036502 (2012).

[Mahler10] L. Mahler, A. Tredicucci, F. Beltram, C. Walther, J. Faist, H. E. Beere, D. A. Ritchie y D. S. Wiersma, "Quasi-periodic distributed feedback laser", *Nature Photonics* **4**, 165–169 (2010).

[Menon05] R. Menon, D. Gil, G. Barbastathis y H. I. Smith, "Photon-sieve lithography", *Journal of the Optical Society of America A* **22**, 342–345 (2005).

[Monsoriu03] J. A. Monsoriu, E. Silvestre, A. Ferrando, P. Andrés y J. J. Miret, "High-index-core Bragg fibers: dispersion properties", *Optics Express* **11**, 1400–1405 (2003).

[Monsoriu04] J. A. Monsoriu, G. Saavedra y W. D. Furlan, "Fractal zone plates with variable lacunarity", *Optics Express* **12**, 4227–4234 (2004).

[Monsoriu07] J. A. Monsoriu, R. A. Depine y E. Silvestre, "Non-Bragg band gaps in 1D metamaterial aperiodic multilayers", *Journal of the European Optical Society: Rapid Publications* **2**, 07002(1–5) (2007).

[Monsoriu10] J. A. Monsoriu, A. Calatayud, L. Remón, W. D. Furlan, G. Saavedra y P. Andrés, "Zone Plates Generated with the Fibonacci Sequence", "Proceedings of EOS Topical Meeting on Diffractive Optics", 151–152 (2010).

[Monsoriu13] J. A. Monsoriu, A. Calatayud, L. Remón, W. D. Furlan, G. Saavedra y P. Andrés, "Bifocal Fibonacci diffractive lenses", *IEEE Photonics Journal* **5**, 3400106 (2013).

[Naftaly07] M. Naftaly y R. E. Miles, "Terahertz Time-Domain Spectroscopy for Material Characterization", *Proceedings of the IEEE* **95**, 1658–1665 (2007).

[Ojeda-Castañeda96] J. Ojeda-Castañeda y C. Gómez-Reino, *Selected papers on zone plates*, tomo MS128, SPIE Optical Engineering Press, Washington (1996).

[Pascale03] D. Pascale, *A Review of RGB Color Spaces ...from xyY to R'G'B*, The BabelColor Company, Montreal(Canada) (2003).

[Podzorov08] A. Podzorov y G. Gallot, "Low-loss polymers for terahertz applications", *Applied Optics* **47**, 3254–3257 (2008).

[Redish90] K. A. Redish y W. F. Smyth, "Closed form expressions for the iterated floor function", *Discrete Mathematics* **91**, 317–321 (1990).

[Remón13a] L. Remón, A. Calatayud, V. Ferrando, W. D. Furlan y J. A. Monsoriu, "Chromatic behavior of multifocal intraocular lenses", "X Congreso Nacional del Color", 648–653, Valencia (2013).

[Remón13b] L. Remón, A. Calatayud, V. Ferrando, F. Giménez, W. D. Furlan y J. A. Monsoriu, "Fractal diffractive lenses", "Recent Research Development of Optics", tomo 8, 31–71, Research Signpost, Kerala (India) (2013).

[Remón15] L. Remón, V. Ferrando, L. M. Sanchez-Ruiz, E. Ballester, W. D. Furlan y J. A. Monsoriu, "Computational Fourier Optics Simulation using a virtual laboratory", "43rd Annual SEFI Conference", 56824, Orléans (Francia) (2015).

[Roux04] F. S. Roux, "Distribution of angular momentum and vortex morphology in optical beams", *Optics Communications* **242**, 45–55 (2004).

[Saavedra03] G. Saavedra, W. D. Furlan y J. A. Monsoriu, "Fractal zone plates", *Optics Letters* **28**, 971–973 (2003).

[Sah95] Y. Sah y G. S. Ranganath, "Optical diffraction in some Fibonacci structures", *Optics Communications* **114**, 18–24 (1995).

[Sakdinawat07] A. Sakdinawat y Y. Liu, "Soft-x-ray microscopy using spiral zone plates", *Optics Letters* **32**, 2635–2637 (2007).

[Scherger11a] B. Scherger, C. Jördens y M. Koch, "Variable-focus terahertz lens", *Optics express* **19**, 4528–4535 (2011).

[Scherger11b] B. Scherger, M. Scheller, C. Jansen, M. Koch y K. Wiesauer, "Terahertz lenses made by compression molding of micropowders", *Applied optics* **50**, 2256–2262 (2011).

[Scherger11c] B. Scherger, M. Scheller, N. Vieweg, S. T. Cundiff y M. Koch, “Paper terahertz wave plates”, *Optics express* **19**, 24884–24889 (2011).

[Shechtman84] D. Shechtman, I. Blech, D. Gratias y J. W. Cahn, “Metallic Phase with Long-Range Orientational Order and No Translational Symmetry”, *Physical Review Letters* **53**, 1951–1953 (1984).

[Siemion12] A. Siemion, A. Siemion, M. Makowski, J. Suszek, J. Bomba, A. Czerwinski, F. Garet, J.-L. Coutaz y M. Sypek, “Diffractive paper lens for terahertz optics”, *Optics Letters* **37**, 4320–4322 (2012).

[Squires14] A. D. Squires, E. Constable y R. A. Lewis, “3D printing of aspherical terahertz lenses and diffraction gratings”, “2014 39th International Conference on Infrared, Millimeter, and Terahertz waves (IRMMW-THz)”, 1–2, IEEE (2014).

[Suszek15] J. Suszek, A. Siemion, M. S. Bieda, N. Blocki, D. Coquillat, G. Cywinski, E. Czerwinska, M. Doch, A. Kowalczyk, N. Palka, A. Sobczyk, P. Zagrajek, M. Zaremba, A. Kolodziejczyk, W. Knap y M. Sypek, “3-D-Printed Flat Optics for THz Linear Scanners”, *IEEE Transactions on Terahertz Science and Technology* **5**, 314–316 (2015).

[Swartzlander01] J. Swartzlander, “Peering into darkness with a vortex spatial filter”, *Optics Letters* **26**, 497–499 (2001).

[Tao06] S. H. Tao, X.-C. Yuan, J. Lin y R. E. Burge, "Sequence of focused optical vortices generated by a spiral fractal zone plate", *Applied Physics Letters* **89**, 031105 (2006).

[Tao13] S. H. Tao, B. C. Yang, H. Xia y W. X. Yu, "Tailorable three-dimensional distribution of laser foci based on customized fractal zone plates", *Laser Physics Letters* **10**, 035003 (2013).

[Tsao14] C. W. Tsao, Y. H. Cheng y W. J. Hsueh, "Localized modes in one-dimensional symmetric Thue-Morse quasicrystals", *Optics express* **22**, 24378–24383 (2014).

[Verma13] R. Verma, M. K. Sharma, V. Banerjee y P. Senthilkumaran, "Robustness of Cantor diffractals", *Optics express* **21**, 7951–7956 (2013).

[Walsby02] E. D. Walsby, S. Wang, J. Xu, T. Yuan, R. J. Blaikie, S. M. Durbin, X.-C. Zhang y D. R. S. Cumming, "Multilevel silicon diffractive optics for terahertz waves", *Journal of Vacuum Science & Technology B: Microelectronics and Nanometer Structures* **20**, 2780–2783 (2002).

[Wang02] S. Wang, X. C. Zhang, M. P. Maley, M. F. Hundley, L. N. Bulaevskii, A. E. Koshelev y A. J. Taylor, "Terahertz Tomographic Imaging With a Fresnel Lens", *Optics and Photonics News* **13**, 58–58 (2002).

[Wang03] Y. Wang, W. Yun y C. Jacobsen, "Achromatic Fresnel optics for wideband extreme-ultraviolet and X-ray imaging", *Nature* **424**, 50–53 (2003).

[Wilk09] R. Wilk, N. Vieweg, O. Kopschinski y M. Koch, "Liquid crystal based electrically switchable Bragg structure for THz waves", *Optics Express* **17**, 7377–7382 (2009).

[Wiltse05] J. C. Wiltse, "Zone plate designs for terahertz waves", R. J. Hwu, D. L. Woolard y M. J. Rosker, eds., "Defense and Security. Proceeding of SPIE Symposium", 167–179, SPIE-INT SOC OPTICAL ENGINEERING (2005).

[Xie10] C. Xie, X. Zhu, H. Li, L. Shi y Y. Wang, "Feasibility study of hard-x-ray nanofocusing above 20 keV using compound photon sieves", *Optics Letters* **35**, 4048–4050 (2010).

[Xie12] C. Xie, X. Zhu, H. Li, L. Shi, Y. Hua y M. Liu, "Toward two-dimensional nanometer resolution hard X-ray differential-interference-contrast imaging using modified photon sieves", *Optics Letters* **37**, 749–751 (2012).

[Yu09] Y. Yu y W. Dou, "Generation of pseudo-Bessel beams at THz frequencies by use of binary axicons", *Optics Express* **17**, 888–893 (2009).

[Zhang10] B. Zhang y D. Zhao, "Square Fresnel zone plate with spiral phase for generating zero axial irradiance", *Optics Letters* **35**, 1488–1490 (2010).

[Zhang11] Q. Q. Zhang, J. G. Wang, M. W. Wang, J. Bu, S. W. Zhu, R. Wang, B. Z. Gao y X.-C. X.-C. Yuan, "A modified fractal zone plate with extended depth of focus in spectral domain optical

coherence tomography", *Journal of Optics* **13**, 055301 (2011).

[Zhang12] Q. Zhang, J. Wang, M. Wang, J. Bu, S. Zhu, B. Z. Gao y X. Yuan, "Depth of focus enhancement of a modified imaging quasi-fractal zone plate", *Optics and laser technology* **44**, 2140–2144 (2012).